JUNE 2020 Ph.D. in Electrical and Electronics Engineering AHMED KHALID ALI

REPUBLIC OF TURKEY

GAZİANTEP UNIVERSITY

GRADUATE SCHOOL OF NATURAL & APPLIED SCIENCES

LINEAR AND NONLINEAR CLASSIFICATION OF QUADRATURE MODULATION SIGNALS

Ph.D. THESIS

IN

ELECTRICAL AND ELECTRONICS ENGINEERING

BY

AHMED KHALID ALI

JUNE 2020

LINEAR AND NONLINEAR CLASSIFICATION OF QUADRATURE MODULATION SIGNALS

Ph.D. Thesis
in
Electrical and Electronics Engineering
Gaziantep University

Supervisor
Prof. Dr. Ergun ERÇELEBİ

by
Ahmed Khalid ALI
June 2020

I hereby declare that all information in this document has been obtained and presented in accordance with academic rules and ethical conduct. I also declare that, as required by these rules and conduct, I have fully cited and referenced all material and results that are not original to this work.

Ahmed Khalid ALI

ABSTRACT

LINEAR AND NONLINEAR CLASSIFICATION OF QUADRATURE MODULATION SIGNALS

ALI, Ahmed Khalid

Ph.D. in Electrical and Electronics Engineering

Supervisor: Prof. Dr. Ergun ERÇELEBİ

June 2020

162 Pages

Automatic modulation classification (AMC) is a form of modern technology integrated into communication receivers to automatically define the modulation type of a received signal. In this work, two new AMC algorithms based on signal feature extraction and a pattern-recognition method are introduced. First, AMC methods are summarised. Subsequently, up-to-date AMC algorithms, including their development, extracted features, their ability to recognise modulated signals, operating configurations, and some recent AMC projects are discussed from their preliminary historical development. Furthermore, state-of-the-art AMC methods are classified according to their feature-selection group, classifier structure, number of modulation signals, channel system, and simulation tool. Second, a new AMC method based on a hierarchical threshold classifier structure is presented. The proposed system comprises multiple tree-based on logarithmic thresholds. The system uses a logarithmic modification of the high-order cumulants (HOCs) of the modulated signal as discriminant features to distinguish among the different digital-modulation schemes. Moreover, the proposed system is tested for classifying QPSK and MQAM modulation types in additive white Gaussian noise (AWGN) and flat-fading environments. The simulation results demonstrate that a very good classification rate is achieved at a low SNR of 5 dB, under conditions of statistically noisy channel models. This shows the potential of the logarithmic-classifier model for application in M-QAM signal classification. Further, in this thesis, we propose the leveraging of novel higher-order spectra features (HOSF) in classification algorithms based on neural-network properties, to mitigate the modulation recognition problems specified in the M-APSK DVB-S2X modulation signals standard. The HOSF characteristics of signals are extracted under the AWGN– channel, and four individual parameters are defined for distinguishing modulation– signals from the set, {16, 32, 64}-APSK. This approach makes the recogniser more intelligent and improves its classification success rate. The results illustrate the excellent classification accuracy obtained at a low SNR of 0 dB, which demonstrates the potential of combining these proposed features with a neural-network classifier for M-APSK modulation classification. Finally, in both proposed algorithms, extensive simulations revealed that a significant improvement in classification accuracy and reduction in system complexity is achieved compared to the previously proposed systems in the literature.

Key Words: Automatic Modulation Classification (AMC), MQAM, APSKDVB-S2X standard, Radius-constellation, MLP-classifier, High Order Cumulants.

ÖZET

ÇEYREK MODÜLASYON SİNYALLERİNİN DOĞRUSAL VE DOĞRUSAL OLMAYAN SINIFLANDIRMASI

ALI, Ahmed Khalid

Doktora Tezi, Elektrik ve Elektronik Mühendisliği

Danışman: Prof. Dr. Ergun ERÇELEBİ

Haziran 2020

162 Sayfa

Otomatik modülasyon sınıflandırması (AMC), alınan bir sinyalin modülasyon tipini otomatik olarak tanımlamak için iletişim alıcılarına entegre edilmiş modern bir teknolojidir. Bu çalışmada, sinyal-özellik çıkarma ve örüntü tanıma yöntemine dayanan iki yeni AMC algoritması tanıtılmıştır.İlk olarak, AMC yöntemleri özetlenmiştir. Daha sonra, bunların gelişimi, çıkarılan özellikleri, modüle edilmiş sinyalleri tanıma yetenekleri, çalışma konfigürasyonları ve bazı yeni AMC projeleri dahil olmak üzere güncel AMC algoritmaları, ön tarihsel gelişmelerinden tartışılmaktadır. Ayrıca, en son teknolojiye sahip AMC yöntemleri, özellik seçim grubuna, sınıflandırıcı yapısına, modülasyon sinyallerinin sayısına, kanal sistemine ve simülasyon aracına göre sınıflandırılır. İkincisi, hiyerarşik eşik sınıflandırıcı yapısına dayanan yeni bir AMC yöntemi sunulmaktadır. Önerilen sistem, logaritmik eşiklere dayanan çok sayıda ağaç içerir. Sistem, farklı dijital modülasyon şemaları arasında ayrım yapmak için ayırt edici özellikler olarak modüle edilmiş sinyalin yüksek dereceli kümülanlarının (HOC) logaritmik bir modifikasyonunu kullanır. Ayrıca, önerilen sistem, ilave beyaz Gauss gürültüsü (AWGN) ve düz sönümlendirme ortamlarında QPSK ve MQAM modülasyon tiplerini sınıflandırmak için test edilmiştir. Simülasyon sonuçları, istatistiksel olarak gürültülü kanal modellerinin koşulları altında 5 dB'lik düşük bir SNR'de çok iyi bir sınıflandırma oranının elde edildiğini göstermektedir. Bu, M-QAM sinyal sınıflandırmasında uygulama için logaritmik sınıflandırıcı modelin potansiyelini gösterir. Ayrıca, bu tezde, M-APSK DVB-S2X modülasyon sinyalleri standardında belirtilen modülasyon tanıma problemlerini hafifletmek için nöral ağ özelliklerine dayanan sınıflandırma algoritmalarında yeni yüksek mertebeden spektrum özelliklerinin (HOSF) kullanılmasını öneriyoruz. Sinyallerin HOSF karakteristikleri AWGN kanalı altında çıkarılır ve modülasyon sinyalleri kümeden {16, 32, 64}-APSK ayırmak için dört ayrı parametre tanımlanır. Bu yaklaşım, tanıyıcıyı daha akıllı hale getirir ve sınıflandırma başarı oranını artırır. Sonuçlar, 0dB'nin düşük bir SNR'sinde elde edilen mükemmel sınıflandırma doğruluğunu göstermektedir; bu önerilen özelliklerin M-APSK modülasyon sınıflandırması için bir sinir ağı sınıflandırıcısı ile birleştirilme potansiyelini göstermektedir. Son olarak, önerilen her iki algoritmada da kapsamlı simülasyonlar, literatürde daha önce önerilen sistemlere kıyasla sınıflandırma doğruluğunda ve sistem karmaşıklığında azalmada önemli bir iyileşmenin sağlandığını ortaya koymuştur.

Anahtar Kelimeler: Otomatik modülasyon sınıflandırması (AMC), MQAM, APSKDVB-S2X standardı, Yarıçap-takımyıldızı, MLP-sınıflandırıcı, Yüksek mertebeden kümülatörler.

My Country, Beloved Parents.
To my great father, my mother soul
my brother, sister.

ACKNOWLEDGEMENTS

First and foremost, I am grateful for Allah that he award me patience and power to overtake all obstacles, and I arrive at this stage by his grace.

Then, I would like to express my special appreciation and all thanks giving for my supervisor, ***Prof. Dr. Ergun ERÇELEBİ***, for his helpful comments, provided all the necessary facilities for this study, also its kindness and support to complete this study, generous guidance and many insights offered during this thesis.

Special thanks are reserved Prof. Dr. İlyas EKER, Assoc. Prof. Dr. Ahmet Mete VURAL, Asst. Prof. Dr. Serkan ÖZBAY, and Asst. Prof. Dr. Abdulkerim ÖZTEKİN for serving on the committee and their contributions and suggestions to improve the quality of the thesis.

I take this opportunity to express my gratitude and my reverence for my dear parents who have nurtured me until I become a righteous and useful person. Their firm and kind-hearted personality have affected me to be steadfast and never bend to difficulty. They always let me know that they are proud of me, which motivates me to work harder and do my best.

There are lots of feelings to think, but I am sure, none what these feelings will be sufficient to thank my brother and sister, but I do not have a method, only saying all appreciation and respect for you.

TABLE OF CONTENTS

Page

LIST OF TABLES

LIST OF FIGURES

LIST OF ABBREVIATIONS

AC	Absolute Confidence
ADMI	Automatic Digital Modulation Identifier
AMC	Automatic Modulation Classification.
ANN	Artificial Neural Network
APSK	Amplitude and phase-shift keying or asymmetric phase-shift keying
ASK	Amplitude Shift Keying
AWGN	Additive White Gaussian Noise
BP	Back Propagation
BPSK	Binary Phase Shift Keying
FB	Feature-Based
FFT	Fast Fourier Transform
FSK	Frequency Shift Keying
HOC	Higher-Order Cumulants
HOM	Higher-Order Moments
KNN	K-Nearest Neighbours
LB	Likelihood-Based
LDA	Linear Discriminant Analysis
MLP	Multi-Layer Perceptron
MSE	Mean Square Error
PNN	Probability Neural Network
PSD	Power Spectral Density
PSK	Phase Shift Keying
QAM	Quadrature Amplitude Modulation

QPSK	Quadrature Phase Shift Keying
RBF	Radial Basis Function
SDR	Software-Defined Radio
SNR	Signal to Noise Ratio
SVM	Support Vector Machine
TD	Threshold Decision
WT	Wavelet Transform
M_s	Number of discrete signals (symbols)
N_b	Number of bits per symbol
f_c	Carrier frequency
W_{ij}	Weight between neuron i and neuron j
Ɛ	Learning rate
t	Output target vector. $t = (t_1 \dots t_k, \dots t_m)$

CHAPTER ONE

INTRODUCTION

1.1 Introduction

In this chapter, the fundamental concepts of automatic-modulation identification algorithms are presented. This chapter is arranged as follows. Initially, the historical scope of the work and associated applications modulation-recognition techniques are described in Section 1.1. Next, in Section 1.2, the aims and research scope of modulation recognition are presented. Section 1.3 covers the novelties and contributions of this work. Research assumptions, materials, and equipment used are highlighted in Section 1.4. Finally, the structure of the thesis and an overview of each chapter is addressed in Section 1.5.

1.2 General

The current explosion in the field of communications systems owing to rapid growth in radio-communications technology is considered to be a critical aspect in the development of a new generation of radio systems capable of recognising the modulation type of unknown communications signals. The ability to deliver sophisticated information services and systems for military applications, even in the crowded electromagnetic spectrum, is of high concern in communications for engineers. Friendly signals must be safely transmitted and received, while enemy signals should be identified, analysed, and jammed [1]. In the past seven years, several developments have been made in the field of signal-classification algorithms, especially in terms of automatic modulation classification (AMC). Currently, AMC is fast becoming a well-established area of study. The concept of AMC is based on automatically identifying the modulation scheme of a transmitted signal.

This type of identification plays an important role in modern intelligent communication systems, such as cognitive radio and radio-spectrum monitoring [2]. Furthermore, blind recognition of the modulation type of the received signal is a significant problem in commercial radio systems, especially in software-defined radio (SDR), which utilises with an assortment of communications systems. Generally, supplementary details such as baud rate, symbol rate and SNR are transmitted to permit the reconstruction of SDR signals. Blind methods could be utilised with an intelligent receiver, which leads to improved transmission efficiency by reducing the overhead. All the aforementioned applications require flexible, intelligent communication systems in which automatically recognising the modulation of received signals is a critical issue.

Figure 1.1 presents a fundamental block diagram of an AMC system. Modulation-classifier design typically includes two procedures: the appropriate selection of the signal type and a pre-processing and classification algorithm. The pre-processing operations could include (but are not confined to) performing some or all of the following processes: noise reduction, carrier frequency estimation, and symbol period, while signal power, equalisation, etc. rely on the classification algorithm selected for the next step. Various levels of accuracy are required in the pre-processing tasks; some classification algorithms demand specific estimates, while others are less sensitive to various parameters.

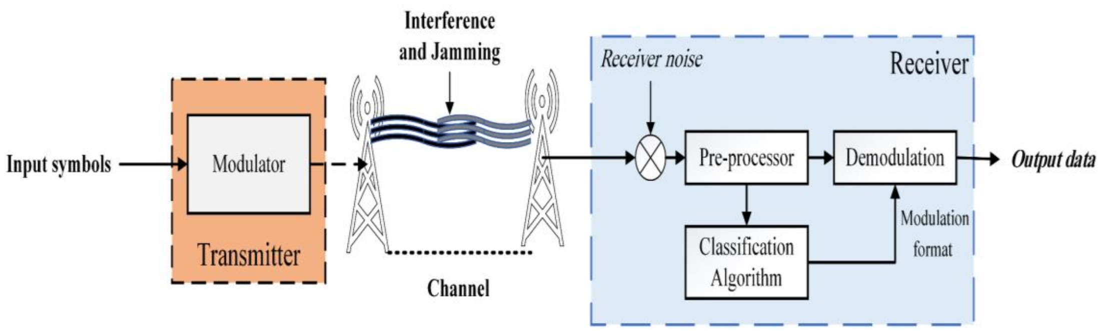

Figure 1.1 Block diagram of the AMC system model.

1.3 Background

The past four years have witnessed tremendous development in satellite-system communications, which has encouraged communication engineers to develop newer iterations of digital-modulation schemes. Recently, the DVB-S2 standard proposed a new set of modulation techniques called APSK. The DVB-S2 standard includes four modulation types – QPSK and 8PSK for non-linearized transponders, and 16APSK, 32APSK, and 64APSK for linearized transponders [3], In satellite communications, APSK is a more attractive modulation scheme than QPSK or QAM [4].

Previous studies in this field have identified two main categories of classification methods: likelihood-based (LB) and feature-based (FB) [1]. LB AMC is a multiple compound-hypothesis testing method that calculates the likelihood ratios of a selected received signal and prior defined signals. Then, it makes a decision by comparing this ratio with a threshold. This generally provides a typical solution, in the Bayesian sense, but involves significant complexity. Detailed descriptions on likelihood-based AMCs are documented in [5]. A likelihood-based classifier can provide an upper bound on the classification accuracy under a certain condition for accurate channel estimation. According to [6], and the ML method provides optimum accuracy for estimating the correct channel type. Additional literature regarding likelihood-based classifiers can be found in recent studies, such as [3,7,8]; these approaches can modify themselves to match various modulation formats and channel circumstances. Thus, their computational complexity becomes the main concern, which results in several sophisticated second-best measures designed to reduce complexity. Based on [9], the authors used the minimum-distance (MD) classifier to reduce complexity. From this viewpoint, in [10], Xu, Su, and Zhou addressed the problem of reducing complexity by storing the pre-computed values of the quantisation database to mitigate complicated operations. All the aforementioned methods succeeded in limiting complexity to various degrees, but at the penalty of some decrease in performance. The FB method has been extensively used in practical applications, and comprises two main subsystem modules: 1) feature extraction, which extracts parameters from a signal, and 2) classification, where a prediction is made. Several features have been used in previous conventional AMC methods. For example, in [11], different slices were taken from the spectral-coherence function as a feature of AMC. The features that are used most often are statistical high-order cumulants, as documented in [12–15], and high-order moments (HOMs), which process received signals differently, as addressed in [16,17]. On the other hand, features obtained from the time–frequency distribution, which comprise instantaneous amplitude, phase, and frequency [18], along with transformation features such as wavelet [19] and fast-Fourier [20] have also been used. In [21], cumulants up to the sixth order were utilised for classifying MPSK and MQAM schemes. Additionally, the researchers used the fourth-order cumulant as a feature vector for classifying digital modulation types in [22,23]. In [24], the authors utilised high-order cyclic-cumulants (CCs) obtained from received modulated signals as the features for modulation classification. In recent years, authors have used multi-cumulant-based classification to achieve improved classification accuracy for multiple-input multiple-output (MIMO) communications [25]. Numerous cumulants of various orders are chained to form multi-cumulant vectors, which are then used to classify the received signals from multiple senders. The authors of these studies guaranteed that utilising a multi-cumulant-based component vector has better performance than single-cumulant-based vectors. A novel wavelet cyclic feature (WCF) was presented in [19] to recognise BPSK, QPSK, MSK, and 2FSK. Further, the continuous wavelet transform (CWT) was utilised in [26] for template matching; this method achieved high classification accuracy at signal-to-noise ratios (SNRs) lower than 5 dB. Although this method achieved the desired results at low SNRs, it is computationally complex. Some features have commonly been suggested by researchers for supervised classification. However, some unsupervised clustering algorithms have also been suggested to investigate AMC issues. Generally, the signal-classification subsystem of the FB method recognises the correct target classes through the distinctive input features extracted from the signal. Several approaches have been utilised for the classification sub-systems in AMC. According to [26–28], the hierarchical tree, apportionment test, and machine-learning based classifiers are often utilised as classification decision-making subsystems. Among these, machine learning has been the most widely utilised option in the last decade owing to its efficient performance. In [25,27,29,30], researchers used an SVM as a classifier to distinguish various modulation types. The K-nearest neighbour (KNN) imputation method was used to address lost data in radar-signal classification as reported in [31]. Additionally, the use of an artificial neural network (ANN) was suggested in [32] and [33] to achieve modulated signal classification. Currently, deep neural networks such as sparse auto-encoders [34] and convolutional neural networks have also been applied to classify datasets [35]. From these previously published studies, it becomes evident that when designing a system to recognise digital modulation signal types automatically, certain substantial issues exist that, when properly considered, can facilitate more robust and efficient recognition. One of these problems is related to the selection of the classification method to be adopted. As mentioned above, there are some shortcomings of AMC methods, which will be described in detail in the next few chapters.

1.4 Automatic-Modulation Identification

In a conventional wireless-transmission framework, the end-modulated signal site works in conjunction with the sender site. This means that the receiver has primary knowledge regarding the modulation scheme of the transmitted signal. As modulation schemes are perpetually developing and the technology used for information transmission is becoming increasingly complex, this cooperation between the sender and receiver is becoming more and more difficult. Moreover, manual modulation classification requires experienced analysers and cannot guarantee reliable results.

To overcome this problem, the researchers in the field of signal processing have extensively studied AMC in the past five years (e.g., [1–17], [18–106], and [106–171]). In numerous cases, multiple attributes were found to solve the problems of AMC:

- Accuracy: The percentage of errors in classification is the best representation of accuracy in modulation recognition. A lower misclassification rate indicates the merit of the classifier.

- Robustness: Modulation recognition requires high success rates and recognition accuracies in different channel environments, such as Doppler-effect, multipath-fading, and AWGN-channels.

- Computationally efficient: There are two factors that affect the algorithm computational costs. An AMC algorithm that includes many signal-processing operations demands complex supporting hardware; additionally, it requires a long time to complete the recognition of modulation signals, which may make it unsuitable for applications that require real-time decisions.

In general, good modulation-classifier design is based on four factors.

1. The modulation classifier should be able to classify as many modulation types as possible. This makes a modulation classifier applicable to various signal-classification problems without requiring any changes to accommodate other communications signals.

2. The modulation classifier should provide accurate signal recognition. High success and recognition accuracy are associated with different noise levels.

3. Modulation recognisers usually have to be robust against different channel environments. Robustness could be provided by either combining both the channel-estimation algorithm and compensation mechanism within classifier system or the natural resilience of the recogniser corresponding to channel environments.

4. Efficient modulation recognisers must involve fewer mathematical operations, making them more computationally efficient. Numerous applications have strict boundaries regarding computing power, which is unsuitable for complicated algorithms.

Furthermore, some applications demand rapid classification decisions. Only a highly computationally efficient modulation recogniser could meet this demand. Subsequently, a simple and fast modulation-recogniser algorithm is in high demand. In real-time, no single recogniser can provide excellent results without any disadvantages. Hence, this study aims to develop unconventional AMC methods that surpass currently existing ones. The importance of these unconventional AMC methods is accentuated by their wide variety of applications, which require a unique set of properties of the recogniser.

1.5 Research Scope

The purpose of this dissertation is to develop algorithms for the recognition of digitally modulated signals, which involves the following:

1. Propose a novel hierarchical-tree algorithm using a pattern-recognition criterion and the statistical parameters of the modulated signals to identify the digitally modulated signals: QPSK, 8QAM, 16QAM, 32QAM, 64QAM, 128QAM, 256QAM, 512QAM, and 1024QAM.

2. Propose leveraging of novel higher-order spectra features (HOSF) in a classification algorithm based on neural-network properties to deal with the modulation-recognition problems specified in the {16, 32, and 64}-APSK DVB-S2X modulation signals standard.
3. Development of a feature-extraction method for the detected signals, which can be adapted for use with multiple hierarchical-logarithmic classifiers.
4. The identification systems proposed must be:

   - Robust against variations in the SNR.

   - Outperform the traditional feature extraction methods like the fast-Fourier transform (FFT), and classifiers like support-vector machines (SVMs) and fuzzy logic (FL), in terms of mitigating their disadvantages.

   - High probability of correct recognition.

1.5.1 Dissertation contribution and novelty

The main contributions of this dissertation are:

1. The utilisation of multiple hierarchical-logarithmic trees as classifiers for the identification of I-Q modulation signals has been presented for the first time by this dissertation, to the best of our knowledge.

2. The improvement and reduction of the distribution curve of feature extraction with properties of the natural-logarithmic and multiple-binary decision-tree classifier, creating a new classification system for 8QAM to 1024 QAM.

3. Creating a modified identification system for QPSK and MQAM through the selection of high-order statistics with a multiple-binary decision-tree classifier.

4. Identifying nine M-QAM schemes of digitally modulated signals using a logarithmic classifier, which is a higher number than that used in previous works on M-QAM-modulating signal-identification systems.

5. Develop algorithms for DVB- S2X/SH standard-specific APSK recognition based on novel key features extracted from the signal, along with the utilisation of artificial neural networks.

1.5.2 Research assumptions

This research makes the following assumptions:

1. The channel noise is modelled as additive white Gaussian noise (AWGN).

2. The AWGN power is adjusted to achieve the desired SNR level.

3. Only one signal is present in the radio-frequency environment, unless stated otherwise.

4. The SNR level is determined at the receiver input.

1.5.3 Materials and equipment

All simulated work was performed using simulation program with the Signal Processing and Communication Toolboxes. The conventional simulation program scripts were run on a laptop with a 2.3 GHz Intel® Core™ i5-4200u D-platform and Windows 10 operating systems.

1.6 Dissertation Organisation

This dissertation summarises the research on both MQAM and DVB- S2X/SH standard-specific APSK modulation classification for a transmission signal in a direct-path and multipath channel. This dissertation comprises six chapters, as follows.

- **Chapter One:** highlights extant research and primary background on the work, including its purpose, motivation, novelty, and contribution.

- **Chapter Two**: gives an overview of modulation-classifications algorithms in the literature, including likelihood-based and feature-based techniques. The objective of this chapter is to provide the reader with an introduction to the following chapters.

- **Chapter Three**: describes typical modulated-signal models and typical blocks for the AMC system. This dissertation focuses on communication-signal classifications under conventional AWGN channels. Nevertheless, in order to evaluate this work, frequency offset, phase offset, and Doppler-shift effect channels are also taken into consideration.

- **Chapter Four:** introduce the proposed systems for classification of MQAM-modulated signals, followed by describing the results, graphs, and structure of the proposed system.

- **Chapter Five:** introduce the proposed systems for the identification of DVB-S2X/SH standard-specific APSK-modulated signals, followed by showing the results, graphs, and structure of the proposed system.

- **Chapter Six:** highlight the outcomes of the study and review the benefits of the AMC algorithms proposed in Chapters 4 and 5. Furthermore, some directions for future work are given at the end of the chapter.

CHAPTER TWO

BACKGROUND ON EXISTING METHOD

2.1 Introduction

In this chapter, the background of modulation-scheme recognition methods is presented. This chapter is arranged as follows. To provide an overview of modulation, recognition methods are reviewed in Section 2.2. Subsequently, Section 2.3 summarises the details and evaluation of the methods proposed in previous works. Finally, Section 2.4 provides the conclusion on past studies and the research gap that this study is filling.

2.2 General Overview

Several methods have been developed to distinguish among modulated signals in digital communication. The primary difference between them is their classification approach. The chosen signal features and classifier attributes play a significant role in each of the presented algorithms. Most of the proposed algorithms attempt to obtain improved classification accuracy in a noisy transmission medium or a channel with a low SNR. As mentioned before, the essential concept of modulation recognition determines the scheme used for demodulating the unknown received signal [36]. If the received modulated signal is applied to an unsuitable de-modulator, to the signal may only be partially demodulated or all the data could be lost [37]. Therefore, modulated signal classification is thought to be an intermediate transaction in the process of modulated-signal determination and information extraction [38]. Practically, the modulated-signal classification is used in both military and civilian applications, such as electronic warfare, surveillance, and threat description.

Recognising the scheme of the modulated signal according to the extraction features of intercepted emitters against initially stored signal features, or partial message sorting, are the primary aspects of any surveillance method. On the other hand, some civilian applications involve signal confirmation, interference ascertainment, and spectrum management; further details are documented in [39].

Based on details reported in [1], the modulation-recognition algorithms are conventionally categorisation in two arrangements—likelihood-based (LB) strategy and feature-based (FB) strategy.

The first method depends on obtaining the likelihood function of the received modulated signal, and a decision is made by comparing among the result of the likelihood function and the constant threshold level. The ratio obtained from the LB algorithms represents the Bayesian optimum solution, which decreases the probability of incorrect classification. On the other hand, the optimal solution of this algorithm involves many mathematical operations that add complexity, and typically gives rise to sub-optimal classification accuracy. In the FB strategy, on the other hand, numerous modulated signal features are commonly used, and a decision is made according to their obtained values. Even though an FB- based strategy might not be a sufficient solution, it is commonly simple in design and has more reliable performance if carefully designed.

The primary modules of the feature-based AMC algorithm are the signal parameter-extraction module and classifier module, which chooses the correct class. The signal features are extracted in the parameter-extraction module, which plays an essential role in identifying the modulated-signal properties.

The features extracted from the modulated signal are used as inputs to the classifier to recognise the type of modulation for the unknown received signal. The compatibly between a classifier and its chosen features is the most crucial factor for obtaining the highest classification accuracy. Numerous terms are defined in the literature concerning modulation classification; for example, modulation identification, modulation recognition, and modulation distinguishing or discrimination.

2.3 Relevant Previous Work

2.3.1 FB-categories

The feature-based modulation classification method can be described according to the nature of signal features extracted. The most commonly used features are time-domain features or so-called instantaneous characteristics, transformation features, statistical and high-order statistical features, the constellation shape of the signals, and other attributes extracted from the modulated signal.

A properly designed FB algorithm could have the same performance as the LB algorithm regarding signal separation and lower computation complexity. The FB method usually has two stages: extracting features to reduce the data and decision-making to ascertain relevant features. A block diagram of the FB method is shown in Figure 2.1.

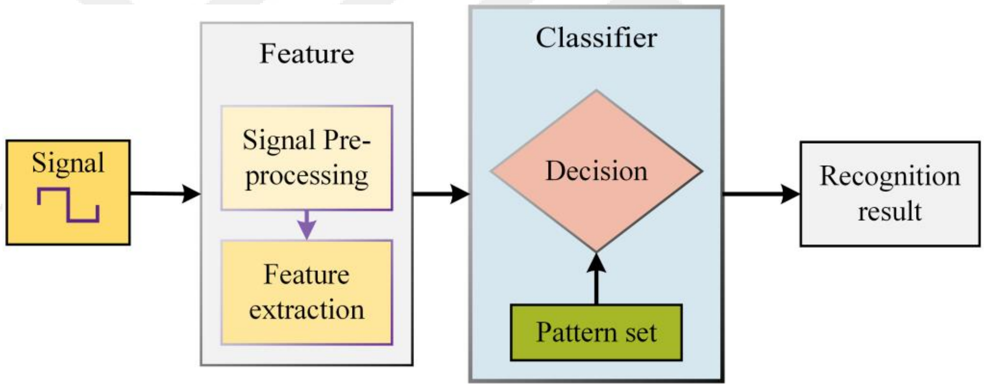

Figure 2.1 Feature-based modulation classification procedure.

The key features could be characterised as time-domain features comprising instantaneous amplitude, phase, and frequency [18,40,41]; transform-domain features, such as the wavelet transform or Fourier transform of the signals [42,43]; and the use of high-order moments (HOMs) and high-order cumulants (HOCs) as inputs to the classifier in [44]. The FB-method based on fuzzy logic is reported in [45], and constellation-shape features are additionally employed for AMCs in [46,47].

2.3.1.1 FB-instantaneous signals features

A time-domain feature of the signal has been introduced in [39]. The presented algorithm is based on the threshold-decision classifier to choose from three conventional modulation schemes (ASK, FSK, and PSK). It was claimed that all of the modulated signals had been classified with an accuracy close to 90%, at a noise ratio of 10 dB. In addition to this study, veteran researchers E. Azzouz and A. K. Nand proposed a modified version of their algorithm in [48]. It was mentioned that the presented method could recognise modulation schemes such as FSK, PSK, and QAM. The new instantaneous feature is an addition to the former features group, and it further enhances the classification accuracy, especially at SNRs below 3 dB.

As mentioned in [49], the classifications of analogue- and digital-modulation schemes (AM, DSB, LSB, USB, FM, 2ASK, 2PSK, 4PSK, 2FSK, and 4FSK) have been presented based on the extraction of the instantaneous standard deviations of the absolute values of normalised-centred, which is coupled with ANN as a classifier.

Meanwhile, in reference [50], eleven types of modulation signals (2ASK, 4ASK, 8ASK, 2PSK, 4PSK, 8PSK, 2FSK 4FSK, 8FSK, 16QAM, and 64QAM) were classified by combining a set of statistical features with a set of instantaneous features to create vector of signal features to apply as the input to the classifier. This combination improved classifier performance, increasing classification accuracy to 95% at an SNR of 0 dB. The spectral and statistical features are extracted and applied to a support vector machine (SVM) classifier to classify modulation types. In this case, the classification accuracy reaches 98.5% at SNRs below 2 dB; further details can be found in [51]. Numerous studies have utilised a set of instantaneous features, along with other features, to create a single vector of the features. In [52], a wavelet filter was applied, which improved the accuracy of recognition at low SNRs; further, three new instantaneous-information key features were presented for use as the input parameters to the classifier for recognising various schemes of digital modulation, including 2ASK, 2PSK, 2FSK, 4ASK, 4PSK, 4FSK, and 16QAM. The results showed that all interest-modulation types were recognised with a correct classification rate of 99% at an SNR of 10 dB. Although the noise ratio is lower than 5 dB, the accuracy is above 95.4% for all the interest-modulation types.

Reference [53] investigates digital signals (2ASK, 4ASK, 2PSK, 4PSK, 8PSK, 2FSK, and 4FSK) and the extraction of sets of instantaneous features. The subsequent selection of the appropriate tree structure and determination of a suitable decision threshold is also conducted on each tree node. The results obtained a successful recognition rate greater than 85% with SNR values under 10 dB.

In [54], a new method for the recognition of digital-modulation signals has been presented. The interest-signal set includes 2ASK, {2,4}-FSK, MSK, {2,4,8}-PSK, and 16QAM, which were chosen for recognition as they are the most widely used digital modulations in modern communication systems. The value of the maximum power-spectral density of the normalised-centred instantaneous amplitude of the modulated signals is used to distinguish among frequency, amplitude, and phase modulations. The architecture of the recogniser comprises 2FSK, 4FSK, and MSK on the primary stage and amplitude and phase-modulated signals (ASK, 2PSK, 4PSK, 8PSK, and 16 QAM) on the second stage. Hence, the discriminant between MFSK and MSK is based on the signal spectrum.

In [55], the feature attributes of the frequency spectrum and power spectrum are extracted by the time–frequency analysis method. Simulation results demonstrate that the neural network-integrated classifiers can be used for all types of modulation recognition; eight types of digitally modulated signals are effectively recognised, which shows that the overall recognition rate can reach 100% at an SNR of 12 dB.

According to [56], a combination of six features involves instantaneous features extracted from seven digital signals. In this work, the set of signals used are 2 ASK, 4 ASK, 2PSK, 4PSK, 2FSK, 4FSK, and OFDM. Back-propagation (BP) neural network training, based on particle swarm optimisation (PSO), is used to achieve significant improvements in signal identification. The classification algorithm presented by Cheng and Liu in [38] demonstrates optimal performance on the first category of signal features. The overall classification accuracy reached 97.54% at a noise ratio of 0 dB.

The instantaneous variations of the modulated signals such as carrier frequency, phase orientation, or amplitude are normally exploited for use in modulation classification [18,57,58]. The formulas for the instantaneous parameters are presented in Table 2.1.

Table 2.1 Mathematical representation to instantaneous features.

$$\boldsymbol{a(t)} = |Z(t)| = \sqrt{r(t)^2 + \hat{r}(t)^2}$$

$$\boldsymbol{\varphi(t)} = unwrap\left(angle\big(Z(t)\big)\right) - 2\pi f_c t$$

$$\boldsymbol{f_N} = \frac{1}{2\pi}\frac{d(arg(Z(t))}{dt}$$

Where $r(t)$ is the complex time signal, $\varphi(t)$ is the phase angle, and f_N is the normalised frequency at the carrier frequency fc.

Signal feature description	Mathematical expression
The standard deviation of the absolute value of the normalised-centred instantaneous amplitude of a modulated signal segment	$\boldsymbol{\sigma}_{\boldsymbol{aa}} = \sqrt{\frac{1}{N_s}\left[\sum_{I=1}^{N_s} a_{\boldsymbol{C_n}}(i)^2\right] - \left[\frac{1}{N_s}\sum_{I=1}^{N_s}\lvert a_{\boldsymbol{C_n}}(i)\rvert\right]^2}$ Where $\boldsymbol{a}_{\mathrm{C_n}}(i) = \boldsymbol{a_n}(i) - \mathbf{1}$, $\mathbf{a}_{\boldsymbol{n}}(i) = \frac{a(i)}{m_a}$, and $\mathrm{m_a} = \frac{1}{\mathrm{N}}\sum_{\mathrm{i=1}}^{\mathrm{N}} \mathrm{a(i)}$ is the sample mean $\mathbf{N}_{\mathrm{S}}$: Number of samples per segment in $\mathbf{a}_{\mathrm{C_n}}(i)$, which is the normalised-centred amplitude at time $\mathrm{t} = 1/\mathrm{fs}$ (i = 1, 2..., N); N: signal length sample
The standard deviation of the absolute value of the normalised-centred instantaneous amplitude in the non-weak segment of a modulated signal	$\boldsymbol{\sigma}_{\boldsymbol{a}} = \sqrt{\frac{1}{L}\left[\sum_{\boldsymbol{a_n}(i)>at_c} \boldsymbol{a}_{\boldsymbol{C_n}}(i)^2\right] - \left[\frac{1}{L}\sum_{\boldsymbol{a_n}(i)>at_c} \boldsymbol{a}_{\boldsymbol{C_n}}(i)\right]^2}$ at_c is the threshold value of the non-weak signal in $a_n(i)$, and L is the length of the non-weak values.
The standard deviation of the centred-nonlinear component of the absolute instantaneous phase in a non-weak modulated signal segment.	$\boldsymbol{\sigma}_{\boldsymbol{ap}} \sqrt{\frac{1}{L}\left[\sum_{a_n(i)>at_c} \boldsymbol{\varphi}_{\boldsymbol{N_L}}(i)^2\right] - \left[\frac{1}{L}\sum_{a_n(i)>at_c} \lvert\boldsymbol{\varphi}_{\boldsymbol{N_L}}(i)^2\rvert\right]^2}$ $\boldsymbol{\varphi}_{\mathbf{N_L}}(\mathbf{i})$: is the value of the normalised-centred component of the instantaneous phase.
The standard deviation of the centred-nonlinear component of the direct (not absolute) instantaneous phase in a non-weak modulated signal segment.	$\boldsymbol{\sigma}_{\boldsymbol{dp}} \sqrt{\frac{1}{L}\left[\sum_{a_n(i)>at_c} \boldsymbol{\varphi}_{\boldsymbol{N_L}}(i)^2\right]\left[\frac{1}{L}\sum_{a_n(i)>at_c} \boldsymbol{\varphi}_{\boldsymbol{N_L}}(i)^2\right]^2}$

The standard deviation of the absolute value of the normalised-centred instantaneous frequency of a modulated signal segment	$\boldsymbol{\sigma}_{\boldsymbol{af}} = \sqrt{\frac{1}{N_s}\left[\sum_{i=1}^{N_s} \boldsymbol{f}_N(i)^2\right] + \left[\frac{1}{N_s}\sum_{i=1}^{N_s} \lvert \boldsymbol{f}_N(i)^2 \rvert\right]^2}$ $\boldsymbol{f}_{\boldsymbol{n}}(i) = \frac{f_{m(i)}}{r_b}$, $\mathbf{m}_f = \frac{1}{N}\sum_{i=1}^{N} f(i)$, $\boldsymbol{f}_{\boldsymbol{m}}(\mathrm{i}) = \mathrm{f(i)} - m_f$ r_b is the bit rate, and $\boldsymbol{f}_{\boldsymbol{n}}(i)$ is the value of the normalised-centred instantaneous frequency.
The standard deviation of the absolute value of the normalised-centred instantaneous frequency of a non-weak modulated signal segment.	$\boldsymbol{\sigma}_{\boldsymbol{nf}} = \sqrt{\frac{1}{L}\left[\sum_{a_n(i)>at_c} \boldsymbol{f}_N(i)^2\right] + \left[\frac{1}{L}\sum_{a_n(i)>at_c} \lvert \boldsymbol{f}_N(i)^2 \rvert\right]^2}$
The kurtosis of the normalised instantaneous amplitude $\mu_{42}{}^{a}$ and frequency $\mu_{42}{}^{f}$	$\boldsymbol{\mu}_{\mathbf{42}}{}^{\boldsymbol{a}} = \frac{E(a_{\mathrm{C_n}}(i)^{\mathbf{4}})}{\{E(a_{\mathrm{C_n}}(i)^{\mathbf{2}}\}}$ $\boldsymbol{\mu}_{\mathbf{42}}{}^{\boldsymbol{f}} = \frac{E(f_{\mathrm{N}}(i)^{\mathbf{4}})}{\{E(f_N(i)^{\mathbf{2}}\}}$
The spectrum symmetry measured by the ratio S	$\mathbf{S} = \frac{\mathrm{S_L\text{-}S_u}}{\mathrm{S_L\text{-}S_u}}$ where $\mathbf{S}_L = \sum_{i=1}^{f_{C_n}} \lvert \mathrm{R(i)} \rvert^2$ $\mathbf{S}_L = \sum_{i=1}^{f_{C_n}} \lvert \mathrm{R}(\mathrm{i} + f_{cn} + 1) \rvert^2$ $f_{C_n} = \frac{f_c N_s}{f_s} - 1$ $\mathrm{R(i)} = \mathrm{FFT[r(i)]}$

It is worth mentioning that σ_{aa} and σ_a impart a variation in the amplitude of the modulated signal. Therefore, they are used for distinguishing MASK modulation schemes [59].

In [60], a symbol-shape algorithm with eight modulation signals, including 2ASK, 4ASK, 2FSK, 4FSK, 2PSK, 4PSK, 16QAM, and 32QAM, were implemented, and signals classified. The computer simulation results illustrated that the method has improved recognition performance in identifying interest-modulated signals; furthermore, the accuracy was 95% at an SNR of 5 dB. Similarly, in [61], the same method has been used to recognise both ASK- and PSK-modulated signals. Further, some studies investigated the use of these features with other parameters to recognise a set of digital-modulation signals [39,50].

In [62], an intelligent method to recognise six types of digital modulation signals has been presented. The propped scheme could recognise a set of signals (2FSK, 4FSK, 2 PSK, 8PSK, PSK, and 16 QAM); the simulation results illustrated that the correct classification rate reaches 90% at SNRs of 15 dB. Both instantaneous features, σ_{ap} and σ_{dp}, are very useful in identifying modulated signals that include a variation in phase. Hence, they have used to distinguish MFSK from 2PSK or MQAM from 16QAM [61], and to distinguish MASK from MPSK/MQAM. In [58], a modulation-recognition method has been presented. This method has used peak-spectrum estimation to determine the modulation symbols for each sample of MASK and MQAM. Simulations results demonstrated that the correct discrimination rate could reach 92% for recognising MFSK, MPSK, and MASK under noise ratios greater than 6 dB, whereas the recognition of MQAM requires a higher value of SNR, of above 15 dB. On the other hand, both variations in feature amplitude and phase would be used in the distinguishing of analogue- and digital-modulation schemes [49].

σ_{ap} and σ_{dp} were considered as input features to the binary-pattern recognition classifier in several studies, such as [59]. In [57], the application of AMC in modulated-signal sensing and the discovery of the primary user (PU) in the software-defend radio (SDR) were investigated, where twelve signals – using both digital- and analogue- modulation – were considered for classification. These interest signals included 2ASK, 4ASK, 2FSK, 2PSK, 4PSK, 16QAM, 64QAM, DSB, SSB, FM, and OFDM. The results showed that the modulated single sensing and detection method is capable of sensing and detecting all forms of PUs' modulated signals in an SDR platform. In addition, it facilitates the adoption of dynamic-spectrum access (DSA), which depends on SDR technology as an alternative radio-spectrum regulatory policy.

μ^a_{42} has been used in previous studies to separate AM from 2ASK or 4ASK, where the decision-tree algorithm was used as a classifier [59]. Similarly, μ^f_{42} has been used before to distinguish FM from 2FSK or 4FSK as well [61], [57]. Along with pattern recognition, methods such as the decision tree and artificial neural-network classifiers have been used to distinguish the spectrum symmetry of VSB and AM /MASK, LSB/USB and FM/MFSK/DSB/MPSK, and USB and LSB. Although instantaneous features are extricated, this technique is sensitive to noise and has estimation errors [62]. In [40], a blind-recognition algorithm has been developed using the instantaneous amplitude for seven modulated signals, including 4-QAM, 8-QAM, 16-QAM, 32-QAM, 64-QAM, 128-QAM, and 256-QAM. Here, the modulation order M of the QAM signal is detected according to the number of clustering centres. Four instantaneous key features, along with the power-spectral density (PSD), were used as inputs for the digital-modulation classifier, and the decision-theoretic algorithm was employed to make the identification decision, which showed that the average success rate is above 94% at a noise ratio of 10 dB [43].

2.3.1.2 FB- Transformation signals features

The maximum discrete Fourier transform of the instantaneous amplitude is calculated to recognise MFSK and MPSK/MASK. The amplitude of the former contains information, but not of the latter. Since MASK has no phase information, M-PSK and MASK are distinguished according to the variance of their absolute normalised phase [40].

In both investigations for analogue [63] and digital [61] modulation recognition, power-spectral density (PSD) was used for classifying AM, FM, USB, and LSB and M-PSK, M-FSK, M-ASK, and M-QAM, respectively. The maximum value of PSD in the normalised-centred instantaneous amplitude results from the Fourier transform are shown in Table 2.2. γ_{Max} denotes the amplitude variance and is used to distinguish between AM, FM, M-QAM, and MPSK [43]. Further, in [64], the extracted key features using PSD and instantaneous amplitude, frequency, and phase derivations are used to implement a robust AMC algorithm for classifying a set of signals, including FSK, PSK, OQPSK, QAM, along with amplitude–phase shift-keying modulations. Furthermore, this method is sufficient for recognising modulated-signal types and orders in both Gaussian and non-Gaussian environments.

A threshold was used for decision making using the above features. A simulation demonstrated that the classification accuracy is greater than 94% when the SNR is 10 dB. The maximum value of the discrete Fourier transform (DFT) Γ_k, with a magnitude to the k^{th} power, extracted from the modulated signal is shown in Table 2.2. This feature, with k=2 and k=4, has been used for classifications of modulation signals, including2PSK, 4PSK, 8PSK, 16QAM, 32QAM, and 64QAM [65]. It achieved robust performance, even when variations in carrier-frequency offset and phase offset were present.

Table 2.2 Mathematical representation of instantaneous features.

Features description	**Expression**
The maximum value of the power-spectral density (PSD) of the normalised-centred instantaneous amplitude	$\boldsymbol{\gamma}_{\mathbf{max}} = \frac{\max\left\|\mathrm{DFT}(a_{C_n}(i))\right\|^2}{N_s}$
The maximum value (DFT) with a magnitude to the power k^{th}	$\boldsymbol{\Gamma_k} = \frac{\max\left\|\mathrm{DFT}(\mathbf{a}(i)^{\mathbf{k}})\right\|^2}{N_s}$ where K=2 ,4

In the same context, the phase spectrum of 2PSK determines the number of phases used to modulate the information signal. Ordinarily, the features of the spectrum, in terms of both frequency and phase, cannot recognise all styles of modulation signals; further, performance differs from one modulation type to another. In [66], a method for modulation recognition with a new algorithm for carrier frequency estimation was introduced. This estimation method could estimate the carrier frequency accurately, with low deviation and high accuracy. Furthermore, it has a simple structure and low calculation complexity, providing sufficient results in recognising 4QAM, 16QAM, 32QAM, and 64QAM. However, it does not perform very well at low values of SNR.

On the other hand, [67] puts forth a method to recognise digitally modulated signals, including ASK, FSK2, FSK4, MSK, BPSK, QPSK, 8PSK, and 16 QAM by using an FFT extracted from the received signal. For example, if the modulation is 2FSK, two resultant frequency-spectrum peaks are obtained at the two modulation frequencies. In the case of 4-FSK, the spectrum involves four peaks, and in the case of an MFSK scheme, the spectrum content is M-Peak.

Using this procedure, the feature estimated by the ratio between the second and the third peak has been presented. The first boundary test has been conducted if the rate was more than one, i.e. if it approaches the predefined threshold. The third peak is smaller than the second peak. On the other side, the signal spectrum consists of only two peaks; therefore, in the case of any ratio below the predefined threshold, the modulated signals cannot be a BPSK scheme.

Furthermore, to recognise the signal type 4-FSK, the fourth and fifth peaks are computed first and then tested [68]. The value of this ratio would still be unity for signals that are not part of the FSK scheme. This structure has not worked well in cases of signals transmitted other than AWGN, or signals affected by any impulsive noise element.

The PSD of the normalised-centred instantaneous amplitude of the modulated signal, along with its spectrum and instantaneous phase analysis, was introduced to recognise digitally modulated signals [69]. The classification algorithm was tested to recognise digital-modulation signal content of 2ASK, 2FSK, 4FSK, MSK, 2PSK, QPSK, 8PSK, and 16QAM. They employed multipath-fading transmission to model signal propagation and correlated the signal by AWGN to obtain more realistic results to test the algorithm. The results indicate a good improvement in classification of the interest signals, even at very low values of SNR, such as 1 dB. The different nth values of the n^{th} power spectrum have computed to classification M-APSK DVB-S2X modulation signals standard. includes {16, 32, 64} -APSK [70].

Cepstral coefficients are used to recognise OFDM signals at different SNRs and in multipath channels [71]. The results of the simulation indicated that the presented method had better performance, even with noise variations and in cases of multipath channels.

A powerful algorithm for asynchronous-modulation identification without the required information about the modulated signal and transmission parameters has been presented in [72]. The extracted signal attributes are based on modulation-dependent spectral lines observed in the estimated spectra of the maximum-law transformations of modulated signals. The generation of a series of spectral lines is mapped to a series of discrete states by a vector quantizers. Subsequently, these feature vectors are classified using a separate hidden-Markov model (HMM) for each modulation scheme. The recognition results for the modulation schemes (ASK, BPSK, QPSK, 2FSK, MSK, and CW) were obtained from the computer simulation analysis. These results confirmed that the proposed algorithm has improved robustness for distinguishing a set of interest signals, but did not perform so well at identifying the orders and numbers of modulation signals types classified, which the QAM signal did not consider.

Fourier transform (FT) is a fundamental analytical technique used to investigate various signals in the frequency domain. Therefore, the FT can provide information about the spectrum of the signal, considering that the signal is stationary and its spectrum is time-invariant. For a non-stationary random variable process, the wavelet transforms (WT) is presented for investigating signals in both the time- and frequency-domains. Further, WTs have the advantage of decreasing the influence of the SNR on the modulated signal. To estimate the WT of any digital or analogue signal, the signal is passed through high-pass and low-pass filters. High-pass filters (HPFs) pass only high-frequency factors of the signal (described components of the signal), while low-pass filters (LPFs) remove the high-frequency factors of the signal and permit only low frequencies to pass (an approximation of the random signal) [14], [73]. Figure 2.2 illustrates the wavelet-decomposition process. At the first level, a modulated signal is applied to an LPF and HPF, and the approximate and detailed coefficients of the signal are computed. At the next level, the output of each filter is reapplied to the HPF and LPF, which have a cut-off frequency that differs from the cut-off frequency utilised in the first stage. The result is another estimation and detail factor for the signal. The final output of the three-level wavelet transform is defined by the sequences D1, D2, D3, and A3 [74]. A digitally modulated signal is a band-limited signal with diverse details on the same scale.

Signal features were extracted from the stage of the decomposed components and used as impute data to the classifier to distinguish the modulation levels [75].

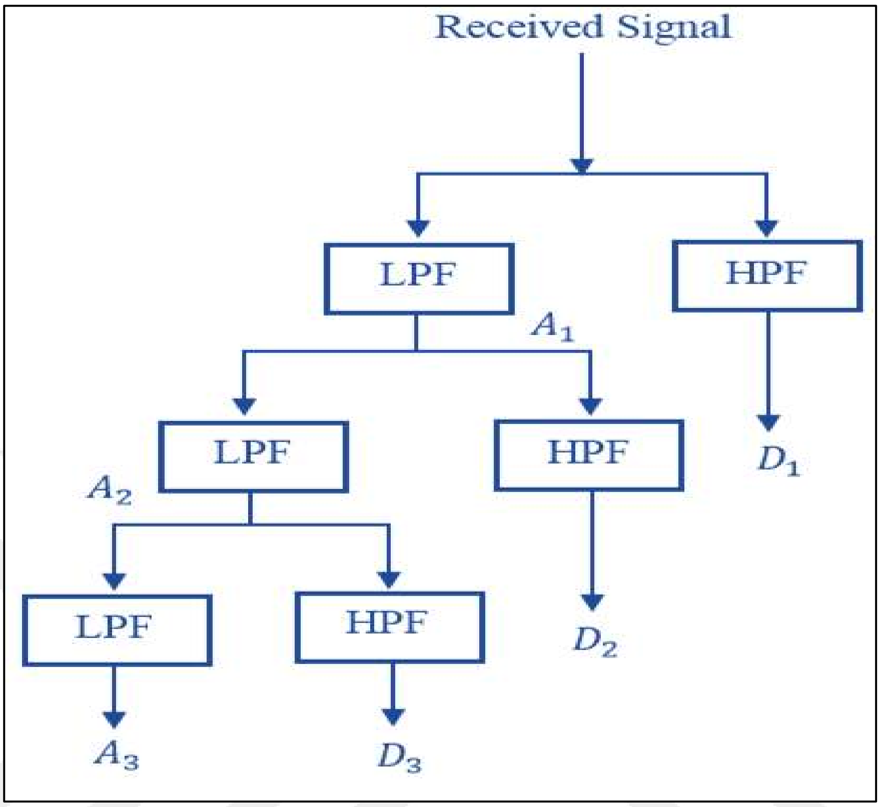

Figure 2.2 Wavelet decomposition.

In [76], the WTs to the amplitudes of the modulation signals, with and without normalisation, were introduced to classify digital signals, including 4QAM, 8QAM, 16QAM, 2PSK, QPSK, 8PSK, 2FSK, QFSK, and 8FSK under corruption by the AWGN channel. The advantages of the proposed system are that it is simulated and has lower calculation complexity. Further, the system performs adequately with noise variations. However, the classification success rates are over 97% when the noise ratio is higher than 5 dB.

In [77], in order to discriminate between QAM, PSK, and FSK signals, the continuous wavelet transform of the modulated signals has been extracted as the main classifier feature. The performance of the recognition-modulation signal was investigated during simulations, as long as the SNR is greater than 5 dB, and the classification rate was approximately 97%. Similarly, in [78], the modulation-recognition method to classify

ASK, PSK, FSK, QAM, and OFDM under channel corruption with AWGN was introduced. A discrete-wavelet transform (DWT) was presented as a signal feature. Further, they considered a fuzzy logic for an adaptive network-based fuzzy inference system (ANFIS) as a pattern-recognition classifier.

The results demonstrated a significant improvement in the overall classification rate; however, there were disadvantages in terms of the number of modulation schemes and range of SNR.

In [79], WT is used as the input feature to the supervised classifier by using SVMs for classifying of the eight modulation schemes (2ASK, 4ASK, 2FSK, 4FSK, 2PSK, 4PSK, MSK, and 16QAM). The four WT- coefficients' key features were extracted for these signals; the presented set of signal attributes has advantages, including high identification accuracy and robustness to noise variations. The results indicated an overall correct classification rate equal to 95% at an SNR of 10 dB. Therefore, it could be concluded that this algorithm required high values of SNR to work well. Further, in [80], a modulation-recognition method for recognising 16 different types of digital-modulation signals has been presented. Here, wavelet-transform coefficients, along with two feature types, were extracted to be used as inputs for the hierarchical structure of the SVM classifier, which represents a high-precision method for pattern recognition. On the other hand, particle-swarm optimisation (PSO) was used to configure kernel parameters. The results demonstrated good performance in the classification of interest signals, but it required high values of SNR to obtain 99% accuracy.

In [81], MEL-frequency cepstral coefficients and DWT with a discrete-cosine transform (DCT) and a discrete-sine transform (DST) were extracted from the digitally modulated signal. These feature vectors were input to an SVM and artificial neural network classifier to distinguish the modulation order and type. The advantages of the presented algorithm include avoiding overfitting and local-minimum problems that occur in the training of ANNs. The results showed that the classifier is capable of recognising the modulation type of signals in different ranges of SNR, with a successful clarification rate of 90% in the presence of AWGN and Rayleigh-fading channels. In [82], a DWT and SVM were used to classify 2PSK and QPSK; the algorithm was implemented using Vivado Design Suite 2015.2.

The results demonstrated good performance of the system, in addition to low power consumption. According to [42], the extracted wavelet transform characteristics can provide distinct attributes that yield simple-pattern identification. Three features for classifying PSK FSK, M PSK, and M FSK were introduced. The results showed good performance, albeit at low SNR values. On the other hand, in [74], to identify QPSK, QAM, GMSK, and MFSK, wavelet transforms and histograms were calculated. It became clear that histogram peaks simplified the recognition procedure. These results demonstrated that the high accuracy is possible at a lower range of SNR–5 dB for GMSK and 12 dB for QPSK. However, at SNRs greater than 5 dB, the correct classification rate of this algorithm is higher than 97.8%. It is worth mentioning that this algorithm was quite sensitive to noise variations and was limited in the number of signals that it could identify.

In [83] and [74], WTs and histograms were used as input-feature vectors; however, [83] had a significantly higher accuracy than [74]. It was claimed that the correct classification accuracy reaches 97.8%, even at an SNR of 5 dB, for two schemes of the studied modulated signals. Similarly, in [84], the histogram of the signal is used as a feature to determine the modulated signal's properties. It was mentioned that the signal studied could be recognised with a high accuracy, which reaches 100% at SNRs higher than 20 dB.

The WT, as a feature vector, was applied as an input to the ANN to create a decision classifier to identify a set of modulated signals [85]. Here, the considered modulation types were FSK, PSK, and QAM; it was mentioned that the classification accuracy reaches 97% at an SNR of 5 dB.

In [83], an algorithm was developed that used the WT and statistical parameters extracted from modulated signals for pattern recognition, as a vector of signal features. These special features were used to identify MPSK, MQAM, GMSK, and MFSK modulations. The results show that successful classification is possible at SNRs below

5 dB, analysed based on the confusion matrix. The probability of correct recognition for SNRs above 5 dB is greater than 96.8%. Similarly, in [86], the continuous wavelet transform was used for modulation recognition, to classify PSK, QAM, FSK, and ASK modulation signals. Here, the Haar wavelet is extracted as the mother wavelet.

In addition to the SNR range, another advantage of this algorithm is that it does not require further information about the modulated signal, such as bandwidth or carrier frequency. The results of the simulation showed that the algorithm had almost 100% accuracy for SNRs greater than 12 dB, and achieved low rates of incorrect classification at SNR=10 dB.

An analogue- and digital-modulation signal-identification algorithm based on HWT has been introduced. The modulation signals that could be recognised include AM, FM, DSB, LSB, USB, 2ASK, 2PSK, 4ASK, QPSK, 8PSK, 16QAM, and [87]. The HWT is an extraction method for the separation of analogue-modulated signals and digitally modulated signals. The higher-order moment of the envelope and the spectrum symmetry are used to recognise the analogue-signal set; on the other hand, to distinguish between the digital-signal set, high-order cumulants are extracted as signal features. The results from simulations show that the recognition method in this paper is potentially applicable to signal recognition. However, it appears that the correct classification rate reduced with noise variations. Further, it requires SNRs above 15 dB to work well.

In [88], a novel algorithm for AMC is presented, which depends on the concept of pattern recognition. The new feature was introduced to facilitate the identification of modulation signals including 2ASK, 2FSK, 2BPSK, 4-ASK, 4-FSK, QPSK, and 16-QAM. These signals are transmuted in the AWGN channel model, and are one of the highest numbers of transmission channels considered by researchers in communication systems.

Three types of features were considered; time, frequency-, and wavelet-domains. Moreover, to overcome the multi-class classification problem, a hierarchical architecture is investigated based on binary SVMs. The simulation shows excellent functionality of the proposed features to accurately distinguish between digital-modulated signals in very noisy environments at very low SNR values. Nevertheless, the authors claimed that the success classification rate is 98.15% at an SNR of –10 dB.

In [89], an algorithm is developed for the classification of modulation signals, such as MASK, MSK, MPSK, and MQAM. The algorithm presented in this paper uses higher-order statistical moments of WTs accurate signal features. Multi-layer network topology, with a resilient backpropagation-learning algorithm, was used for creating the pattern-recognition system. In the pre-processing system block, they suggested feature optimisation by using principal component analysis, which will reduce the network complexity and increase the effectiveness of the recogniser.

2.3.1.3 FB- Statistical signals features high-order moments (HOMs) and high-order cumulants (HOCs)

Random variable moments are interpreted as the expected value of the signal that defines the power associated with the order of each moment.

The mean of the discrete random variable is the first-order moment, whereas the second-order moment usually refers to the power of the signal. For a complex-formed stationary random process, y_n, the p^{th}order moment is defined in Table 2.3, where $y^*$is the complex conjugate of y and q is the power of the conjugate signal y^*. High-order cumulants are another way to compute a signal's statistics.

In order to present discrete signal cumulants, we first describe the first and second characteristic functions of any discrete-time signal x, while the discrete-time signal cumulants are the derivatives of the second characteristic function about the origin, which are defined in Table 2.3. Here, P specifies the order of the cumulant. Usually, HOCs are written as functions of a signal's high-order moments (HOMs), as in [90]. Generally, HOMs are computed for zero-mean signals. Hence, the value of the signal's mean is subtracted from the modulated signal's data symbols, as described in Table 2.3.

Table 2.3 Definitions of cumulants' expressions.

Description	**Characteristics**
The p^{th} order- a complex-valued moment for the stationary random process y_n.	$M_{pq} = \mathrm{E}[y^{p-q}(y^*)^q]$
The first characteristic function of any random variable x	$\Phi(s) = \int_{-\infty}^{\infty} f(x)e^{sx}\,dx$
The second characteristic function of any random variable x	$\varphi(s) = \ln(\Phi(s))$
Signal cumulants	$\lambda_p = \frac{d^p\varphi(s)}{ds_p}$
Zero-mean signals, where M_{y_n} is the mean value of a signal	$\check{y}_n = y_n - M_{y_n}$

Table 2.4 expresses the relationship between HOMs and HOCs that used commonly in the literature.

Table 2.4 High-order cumulants (HOCs).

HOCs	**Expression in HOMS**
Second-order Cumulants	$C_{20} = M_{20}$ $C_{21} = M_{21}$
Fourth-order Cumulants	$C_{40} = M_{40} - 3M^2{}_{20}$ $C_{41} = M_{40} - 3M_{20}M_{21}$ $C_{42} = M_{42} - \lvert M_{20}\rvert^2 - 2M^2{}_{21}$
Sixth-order Cumulants	$C_{60} = M_{60} - 15M_{20}M_{40} + 30M^3{}_{20}$ $C_{61} = M_{61} - 5M_{21}M_{40} - 10M_{20}M_{41} + 30M^2{}_{20}M_{21}$ $C_{62} = M_{62} - 6M_{20}M_{42} - 8M_{21}M_{41} - M_{22}M_{40} + 6M^2{}_{20}M_{22} + 24M^2{}_{21}M_{20}$ $C_{63} = M_{63} - 9M_{21}M_{42} + 12M^3{}_{21} - 3M_{20}M_{43} - 3M_{22}M_{41} + 18M_{20}M_{21}M_{22}$

It can be clearly seen that the magnitude of both the 6th- and 4th- order cumulants are larger than the magnitude of the second-order cumulants.

This results in a contrast in the values of cumulants for different HOC orders. Therefore, feature normalisation is essential for achieving proper functionality of machine-learning algorithms. To facilitate normalisation, HOCs are rescaled as shown in table 2.5, based on [68]. Each cumulant is modified by rescaling to the power of $\frac{2}{b}$, where b is the order of the cumulant.

Table 2.5 Normalization of High Order Cumulants (HOCs).

Normalised (HOCs)	Normalisation
$\breve{C}_{20}$	${C^{1}}_{20}$
$\breve{C}_{21}$	${C^{1}}_{21}$
$\breve{C}_{40}$	${C^{\frac{1}{2}}}_{40}$
$\breve{C}_{41}$	${C^{\frac{1}{2}}}_{41}$
$\breve{C}_{42}$	${C^{\frac{1}{2}}}_{42}$
$\breve{C}_{60}$	${C^{\frac{1}{3}}}_{60}$
$\breve{C}_{61}$	${C^{\frac{1}{3}}}_{61}$
$\breve{C}_{62}$	${C^{\frac{1}{3}}}_{62}$
$\breve{C}_{63}$	${C^{\frac{1}{3}}}_{63}$

For additional simplification, the magnitudes of the cumulants are used instead of their complex values. This operation has significant advantages in reducing the time required for the training process; thus, recogniser weights have real values here, rather than complex ones. In addition to their advantages in reducing training time, they also reduce the vulnerability to shifts in a constellation, as the phase shift does not influence the magnitude of the cumulants, although it could disturb the imaginary component. Through evidence, it has become clear that some HOCs help distinguish between specific groups of modulation types more than others. Determining which HOCs are suitable for use in distinguishing between modulated signals is another issue. The values of the HOCs for MQAM modulation schemes at different noise ratios are briefly discussed in the next chapter.

The fourth-order cumulant standards for pulse amplitude modulated (PAM), PSK, and QAM signals under noise-free conditions are reported in [16]. It is confirmed that HOCs have distinct values for each type of modulated signal. For example, C_{20} is zero for all modulated signals other than 8-PAM. Using this, if $C_{20}$is computed for each modulated signal and is not equal to zero, the signal is recognised as 8-PAM. In the same context, the modulated signal type can be classified by comparing the values of the 4th-order cumulants through prior determination of the thresholds level [44]. The former hierarchical method is usually used in distinguishing many modulated signals, as it is powerful and has low calculation complexity. The combination of multiple order-moments is used to distinguish among several levels of M QAM signals, as reported in [16]. In this work, researchers presented two new parameters, which are listed in table 2.6.

Table 2.6 Mixed of high-order moments.

Description	**Parameters**
V_{20}	$\frac{M_{42}(s)}{M^2{}_{21}(s)}$
V_{30}	$\frac{M_{63}(s)}{M^3{}_{21}(s)}$

These features are extracted from each modulated signal of interest and projected using linear-discriminant projection, based on a Fisher criterion, into one-dimensional space. The modulated signal type is recognised by comparing the projected value to some constant thresholds.

In [91], a novel automatic-modulation classification method based on the radial basis function neural network (RBFNN) and gravitational search algorithm (GSA) is presented, for distinguishing between six signals, including 2PSK, QPSK, 8PSK, 16QAM, 32QAM, and 64QAM. This method combined three HOCs with three low-order statistical features extracted from modulated signals and applied to the classifier; for feature extraction, it was assumed that the signal was travelling in an AWGN-channel model. It is shown that this method yields a significant improvement in the probability of correct classification in low-SNR conditions. However, it can only classify a small number of modulation and signal types.

Following the research in [92], a modulation-recognition method based on high-order cumulants has been presented to study the classification problem for 2ASK 2PSK, 4ASK, 8ASK, 2FSK, 4FSK, 8FSK, 4PSK, and 16QAM modulation signals. Further, a new approach for signals having the same cumulants, such as 8PSK and MFSK, has been developed. Simulation results examine the performance of this algorithm.

In [93], a new modulation-recognition method using fourth-order cumulant statistics in a multipath-fading channel was proposed. In this study, the typical modulation types considered included 2PSK, QPSK, 8-PSK, 16-QAM, and 64-QAM. Further, the influence of multi-path fading on cumulants of the modulated signal is investigated. During simulation analysis, researchers claimed that their algorithms had high confidence in terms of the classification rate, especially for the considered signals.

In [29], a blind modulation-recognition method was developed using a decision-tree twin-SVM classifier. The modulated-signal features comprised a set of HOCs and cyclic spectrum after compressed sensing. The advantages of this method include fast computing speed and a reduction in the performance specifications for sampling schemes in the receiver, even in cases of low optical SNRs. The simulation results presented the correct classification rate for a set of optical modulation types including OOK, DPSK, QPSK, OQPSK, 16QAM, and 64QAM. The accuracy recorded was over 95% when the optical-SNR was –5 dB, and the recognition time is 4.3 faster than typical SVM classifiers.

On the other hand, a stacked sparse auto-encoder (SSAE) based on eight features, comprising two instantaneous features and six HOCs was applied in [94] to build an AMC algorithm for identifying common digital-modulation signals, including 2PSK, QPSK, 8PSK, 16QAM, 64QAM,16APSK, and 32APSK. The simulation results indicate that the total successful classification rate reaches 100% at an SNR of 5 dB. The performance of the proposed method was compared to that of the conventional

SVM-based technique, and it was found that the accuracy of classification using this technique is significantly enhanced.

Similarly, in [95], a modulation-classification method using HOCs and subspace decomposition was proposed. This method involves extracting different orders of cumulant from modulated signals as vectors, and then using linear transformation to convert the vector set to a group of orthogonal bases of the subspace, to facilitate classification of signal type using the different projection signals in the subspace. The suggested method can recognise several modulated signals, including 4ASK, 8ASK, 8QAM, 16QAM, 2-PSK, QPSK, and 8PSK. The proposed classification method has a significant advantage in terms of reducing the correlation of different-order cumulant vectors, overcoming the shortage of a single cumulant.

In [96], an AMC method to classify common modulation signals – including 2ASK, 4ASK, 8ASK, 4PSK, 8PSK, 8QAM, 16QAM, and 32QAM – is proposed. This work used an HOC as the signals' eigenvalues to recognise the set of interest signals. The extracted signal-feature vectors are applied to an SVM classifier. The simulation results show the classification efficiency using this method was good at low SNRs, where researchers claimed that the success rate was 90% at an SNR of –5 dB.

On the other hand, in [97], a system is presented to overcome the difficulty in determining suitable decision-threshold values to recognise modulated signals in the cumulant domain. The algorithm presented in this paper using a binary tree of an SVM to recognise the decision of high-dimensional space, which can then automatically identify the type of modulation. The modulated signals considered in this work include 2ASK, 2PSK, 4ASK, 2FSK, 4FSK, QPSK, 8PSK, and 16QAM. The advantages of this method are that it is simple to implement and can efficiently identify signals, with a success recognition rate of 94% at SNRs above –1 dB.

In [98], 7-HOCs with 18 types of signal features were extracted from a set of modulated signals, including MASK, MFSK, MPSK, and 16QAM. The FB-method presented in this work focuses on developing an algorithm to overcome the issue of retraining the classifier when SNRs change.

In the training phase, the method selects features that are less sensitive to noise variations to ensure that the trained model will be robust to variations in the SNR. Good results were recorded for classification accuracy, and the results remained reasonable when the SNR varied between 5 dB and 20 dB.

In [99], deep learning with three input data points was used, which were extracted from received samples. The high-order cumulants of the modulated signal were used to learn unsupervised-sparse autoencoders, and a supervised soft-max classifier was employed for studying pattern recognition, where the set of modulation signals included 2PSK, 4QAM, 16QAM, and 64QAM. The results indicated that this classification method with a deep learning model achieved better successful classification at a low SNR of 0 dB.

Nevertheless, in [100], fourth- and sixth-order cumulants were extracted from the modulated signals and used as features vectors for the identification set of modulated signals, including {2,4}-ASK, 2PSK, {2,4,8}-FSK, and 16QAM. The SVM classifier was used to distinguish between high-dimensional feature spaces. Experimentation determined that the classifier had high performance and was robust to variations in the noise level. The modulation-recognition algorithm that has been reported in [101] focused on the extraction of three types of HOCs and four instantaneous parameters for use in the recognition of modulated signals, including MASK, MFSK, MPSK, and MQAM. In addition, in this work, three structures of machine learning were presented – a DT-classifier, neural-network classifier, and SVM. Authors in this work claimed that the classification method has low computational complexity and good successful classification rate at low SNRs.

In [102], a modulation-recognition algorithm focusing on HOCs was used to recognise a set of modulated signals, which included 2ASK, 4ASK, 2PSK, QPSK, 2FSK, and 4FSK. The recognition algorithm presented in this work has acceptable performance even with heavily noisy channels, with a recognition success rate of 84 % at an SNR of –2 dB.

In [103], a set of HOC were used to classify MQAM signals' content, for 128 QAM and 256 QAM. The recognition method presented in this work focuses on a multiple decision-tree classifier. The simulation results confirmed that the recognition rate was not affected by noise variation and signal length, and stated that the average successful classification was increased at low SNRs, i.e. 81.66% at an SNR of –5 dB.

In [104], a new modulation-recognition method using SNR estimation and statistical features extracted from the HOCs of modulated signals was developed. The SNR-estimation algorithm was used to reduce the requirements of SNR and provides a significant improvement in reducing misclassification for modulation recognition. In addition, the HOC features were extracted from signals and applied as impute-data vectors to a decision-tree classifier. In this work, the authors investigated QPSK, 16QAM, and 64QAM signals. Simulations confirmed that the presented logarithmic features, with fixed thresholds. could maintain a recognition rate around 80% when the SNR was changed from 11 dB to 6 dB.

2.3.1.4 FB- Other attributes extracted from the signal

The shape of the constellation diagrams of each modulation signal is different from one signal type to another. This description is associated with the number of samples M and their position in the I–Q diagram. Each point in the I–Q diagram has a different distance from the origin, and a special phase. Constellation rotation was adopted in [46]. Similarly, [32] presented a new modulation-recognition method to identify I–Q modulation types, such as MPSK and MQAM. The presented method suggested that the constellation shape is a robust feature for digital-modulation recognition. The geometry of the constellation diagram represents the transmuted samples. Modulated signals at the receiver site, in turn, represent the recovered constellation diagram that is modified by the transmission- and receiver-noise ratio. In addition, fuzzy c-means clustering can be used for further powerful recovery of the unknown constellation. The unknown-constellation diagram is then recognised by an ML rule based on the supervised-learning model. This method is appropriate for digital-modulation signals with arbitrary size and dimensions.

On the other hand, [105] proposed a new recognition technique using the TTSAS algorithm and pattern-recognition method to recognise a set of modulation signals, including 4-QAM,16-QAM, 64-QAM, and 256-QAM. This recognition method considered the constellation diagram of modulated signals to determine which modulation type was transmuted. Results indicate that this method has good classification accuracy for the studied modulation signals.

In [106], the constellation diagram has been used to recognise M-QAM signals, including 16QAM, 32QAM, and 64QAM. The features used for classification are extracted from reconstructions of the constellation shape of the received signals by using a k-means clustering algorithm to calculate the number of signal-constellation samples. The simulation results confirmed that this method is effective for the recognition of MQAM modulation schemes. The correct recognition ratio was recorded as 100% at SNRs higher than 15 dB. Therefore, it not effective at low values of SNR.

Detecting the number of zero-crossing forms of the received signals has been used to identify the modulation signal with further post-processing functions and likelihood trials [107,108]. It is well known that the rate of zero-crossing of an FSK signal varies according to the symbol; however, it is fixed in PSK signals. Therefore, the zero-crossing feature has been used for identifying the order of FSK signals and to distinguish between FSK and PSK modulation types in [109]. The study presented a flexible instrument for use in measuring digital-modulation signals – the algorithm can recognise the modulated signals automatically, including ASK, PSK, FSK, QAM, and OFDM. The simulation results were obtained under conditions of AWGN, colouration noise, and multi-path fading, with good classification rate.

The zero-crossing feature is effective for distinguishing between a few modulation schemes. Further, the spectrogram definition is the spectral density of signal variation with time [110]. This signal framework is computed by FT, dividing the signal into narrow bands. Since this representation reflects variations in the received signal constraints, it has been introduced to recognise a few digital-modulation types. From spectrogram images, two features can be extracted: principal-component analysis

(PCA) and moment-like features for discrimination of PSK or QAM. In the second stage, it distinguishes among frequency modulations 2FSK, 4FSK, ASK, 8-tones/OFDM, and 16 tones/OFDM[20]. It can be concluded that modulation-signal identification using spectrograms is powerful against carrier-frequency offset.

In [111], three methods are presented for modulation classification using spectrograms; the MASK, MPSK, MFSK, MQAM, and FDM modulation types have been considered. The modulation-recognition method selected moment-as a signal's features, while the other two used PCA with various forms of inputs. This allows the method to have higher performance at SNRs as low as 2 dB. The results indicate that this method is effective under unknown phase and frequency offsets, timing errors, and arriving sequence of symbols. The modulation-classification algorithm presented in [48] deals with the representations of modulated signals in both time and frequency domains; it studied a set of modulated signals including PSK, FSK, and QAM.

In [112], the cyclic–correntropy spectrum (CCES) was used to study the AMC algorithm, and a new method was presented to recognise modulation signals (2ASK, 2PSK, 4PSK, and16QAM). The multi-slices are extracted at various cycle-frequencies from CCES and represent the original features for AMC. Further, PCA is used to optimise the original features. Following optimisation, the pattern-recognition classifier, the radial-basis function (RBF) neural network, is employed for modulation classification, as researchers claimed that the results demonstrate outstanding classification rates; however, it did not perform so well at low SNR values.

Finally, [113] presented a modulation-recognition algorithm that used a similarity measure called the chronotropic coefficient. The presented modulation-recognition method considered common modulation signals, including OOK, 2PSK, MSK, 4PSK, and 16-QAM. Further, it provides numerical results demonstrating the robustness of using correntropy in the classification algorithm. It has a good success rate in the classification of interest signals.

2.3.2 Classifier

Following feature determination, the system must guess which modulation signal is received. In FB-algorithms, decisions can be reached through two methods. The first is the DT-method or threshold decisions, which is well-documented in literature [18,58,86,103,114,115]. The second method depends on pattern-recognition theories such as SVM, which have been reported in [75,79,100] Further, ANNs are briefly described in the literature [47,57,116,117] which can also be combined with the continuous wavelet transform [118], or mixed as multiple trees that include more than one artificial-intelligence (AI) method to facilitate more accurate classification [83]. The main purpose of using pattern-recognition methods is improving the accuracy of the classification rate at low SNR values [119]. Nevertheless, some investigations presented classifiers comprising the K-nearest neighbourhood algorithm, along with a conventional algorithm such as genetic programming (GP) [120], where a conventional optimisation method is utilised to choose the best features from a vector set of features. The former technique is used to recognise the modulation signals 2PSK, 4PSK, 16 QAM, and 64 QAM. Next, this subsection presents a comprehensive review on the classifiers that are most-used in modulation-recognition algorithms ANNs, SVMs, and DT.

The essential concept of SVM involves obtaining the maximum discrimination between two classes [41]. In the case of non-linear features, characteristics can be made distinct by using a kernel function that maps the vector features from the input space into the feature space, in case of more than two classification targets. In this case, binary SVM is applied. Here, the classification algorithm uses the first SVM to recognise the first target against all of the others. Subsequently, to identify the second target among the rest of the targets, another SVM is constructed; this approach continues until all classes are identified. Similarly, multi-class SVM is used to solve the classification problems of a multi-class system, and utilises higher feature-vector dimension spaces. In this subsection, an outline of the literature related to the use of SVMs in AMC is presented. There are two main frameworks for SVM that are addressed in most studies – binary SVM [119] and multi-class SVM directed acyclic graphic SVM, which is addressed in [75,79].

The design of SVM classifiers based on different kernels, such as polynomial functions [30,79] and kernel-based on RBF [79,100], have been shown to outperform DT and ANNs in the classification of modulated signals, such as in [100], owing to their robustness against over-fitting. Over-fitting is an issue with ANNs, which require linearity in chosen features, and a problem when using the DT method, which requires careful selection of thresholds DT. Therefore, even features with poor separation characteristics can have excellent performance when employed with an SVM classifier. According to [20], signal features that include only the amplitude and phase have been extracted from signals and used as inputs for training SVMs, in order derive models used for the recognition of 2PSK, ASK, 8FSK, and 16QAM. This technique is capable of providing higher performance than the two likelihood-based methods. The genetic algorithm has been used to optimise the training parameters of SVM, with the kernel and wavelets as input features [121]. The work focused on the identification of modulation types, including MASK, MFSK, and MPSK. This approach helped optimise the classification parameters, but showed no significant effect on the classification rate. In [80], an SVM designed with an optimisation algorithm using particle-swarm optimisation (PSO) was developed to select optimum kernel parameters.

Similarly, in [122], binary SVM was used for the recognition of modulation signals (2ASK, 4ASK, 2FSK, 4FSK, 2PSK, and 4PSK). The presented SVM- classifier used RBF kernels as multi-class pattern-recognition system. The simulation results revealed that the performance of the SVM classifier reached a successful classification rate of 85%.

In [123], four features were used as the inputs of an SVM used for the classification of modulation signals, including 2ASK, 4ASK, 2FSK, 4FSK, 2PSK, and 4PSK. The results demonstrated the good performance of the recognition system. In order to overcome the multi-class pattern-recognition problem, a hierarchical structure of the binary SVM classifier was studied [88]. The presented algorithm can recognise several modulation schemes ({2,4}-ASK, {2,4}-FSK, {2,4}-PSK, and 16-QAM).

This technique has perfect identification at low SNR values. The binary tree of an SVM with multi-classes is also considered in [124].

One of the most typical classifiers used in AMC is an artificial neural network (ANN). This classifier type is effective when applied to pattern-recognition problems. Further, ANNs can solve complex classification problems owing to their advantages in adaptability and learning [125]. ANNs can be categorised according to their learning algorithm – they can be either supervised or unsupervised networks. In a supervised learning technique, the received data is divided into two parts, training and testing. Training is used to adjust network parameters, while testing is used to assess the performance of the model. One the other hand, in the unsupervised technique, the received data is first clustered, and then network parameters are adjusted.

Unlike unsupervised learning algorithms, supervised algorithms provide highly accurate results. However, they required a significant amount of training data, unlike unsupervised training algorithms. Here, almost all of the algorithms that have been presented in the field of AMC use supervised training algorithms and the network structures comprising multi-layer perceptrons (MLP) and RBF. Self-organising map (SOM) network models have been used to implement AMC algorithms; SOM networks depend on unsupervised learning, which implies that no human intervention is necessary during the training, and little needs to be known about the properties of the input samples.

Owing to the advantages of MLP, in terms of low memory requirements and short learning times, they have become very attractive prospects for researchers. The single MLP-ANN is used in several studies [50], whereas others have suggested the use of cascade structures, including three MLP ANNs [18]. In a cascade structure, the output of the primary or secondary AN-network is applied as the input-feature vector to the second or third ANN.

The overall performance of the MLP-network is better than that of DT [126]. Unlike the MLP-ANN structure, the RBFNN structure has the advantage of faster training rates when used in AMC.

There is no significant advantage in terms of classification accuracy when using MLP-network in comparison to RBF-networks, only that the RBF structure is more efficient in the training stage. SOM NNs are qualified to compute network architectures, as they temporarily decide the proper number of neurons in ANNs, and require no prior knowledge on the number of clusters [62,118,127]. A comparison between MLP and SOM in the modulated-signal classification problem is addressed in [62], where an algorithm based on SOM provides an excellent classification rate, but it required a good-quality transmission channel. A study on the use of the discrete-wavelet adaptive network-based fuzzy-inference system (DWANFIS) in modulated-signal recognition is presented in [128]. The work investigated the classification of modulation signals, including CW, 2ASK, 2FSK, 2PSK, and 8QAM. Researchers claimed that DW-ANFIS could provide a better classification rate than the use of DW-NNs. According to [127], the extracted features are processed using the genetic algorithm (GA), in order to select the suitable samples from instantaneous time-domain features, and a group of HOCs are applied to the input layer of the MLP classifier.

The principle of the DT method is choosing suitable thresholds to distinguish between modulation schemes and modulation orders. Several investigations have focused on modulation recognition using DT- classifiers, as noted in [60,114,129]. The advantages of the decision-tree method are that it has a simple structure and easy implementation [109]. Furthermore, DT-algorithms could be extended to classify more modulations by combining new decision branches.

2.4 Summary and Evaluation of a Past Algorithm

This chapter has presented a comprehensive review and the essential principles for AMC methods from relevant literature. Table 2.7 provides a review of papers on FB-methods. Details such as the feature type, classifier structure, modulation type, channel noise, and the simulation tool used are fully considered, particularly the nuances when designing the internal block of the AMC system. Based on the review conducted on various FB-methods, it can be concluded that more research is needed on high-order modulation signals, such as 256 QAM and above. Although the DT algorithm is represented as less complex than SVM and ANN, it gives a reduced classification rate, whereas the performance of SVM is significantly better and provides a recognition rate higher than that of ANNs. As a result, all pattern-recognition methods perform better than DT. Nevertheless, DT is simple to implement and can identify an ample range of modulation types by adding new, extra decision nodes without any requirement to relearn the classifier, as in conventional pattern-recognition methods. In addition, it should be noted that several published papers have considered AWGN for transmission-channel modelling. On the other hand, almost algorithms are tested using computer simulations through native computer simulation program.

Table 2.7 Review of most previously discussed studies.

Reference	Features type	Classifier	Modulation signals	Channel type	Simulation tool
[19]	Instantaneous Group	ANN	(2,4)-ASK, (2,4)-FSK, (2,4)-PSK, AM, FM	band-limited Gaussian noise	Not-specified
[57]	Instantaneous Group	ANN	(2,4)-ASK,2FSK, (2,4)-PSK, (16,64)-QAM, OFDM, AM, FM	AWGN	MATLAB
[62]	Other attributes	ANN	(2, 4) FSK, (2, 8)-PSK, (16, 64) QAM.	AWGN	Not-specified
[118]	Transformation Group, WT	ANN	(2,4,8)-ASK, (2,4,8)-FSK, (2,4,8)-PSK, (16,32,64) QAM, MSK	AWGN	Not-specified
[127]	Instantaneous Group and HOC	ANN	(2,4)-ASK, (2,4) FSK, (2,4)-PSK, (16,64) QAM,32V,V29	AWGN	MATLAB
[128]	Transformation Group, DWT	ANFIS	(2,4,8)-ASK, (2,4,8)-FSK, (2,4,8)-PSK,	AWGN	MATLAB
[20]	HOC	SVM	(2,8)-PSK, 4-PAM, 16-QAM	AWGN	Not-specified
[75]	Transformation Group, WT	SVM	(2, 4) ASK, (2,4)FSK, (2, 4)PSK, 16QAM, TFM, π/4QPSK, OQPSK	Not-specified	Not-specified
[79]	Transformation Group, WT	SVM	(2,4)-ASK,(2,4)-FSK,(2,4) PSK,MSK,16QAM	AWGN	MATLAB
[100]	HOC & HOM	SVM	(2,4) ASK, (2,4) PSK (2,4,8)FSK ,16 QAM	AWGN	Not-specified

Table 2.7 Continued.

[130]	Other attributes	SVM	MQAM	AWGN	Not-specified
[119]	HOC	SVM	(2,4,8)-ASK, (2,4,8)-PSK, 16QAM	AWGN	Monte-Carlo simulation
[120]	HOC	SVM	(2,4)-PSK, (16,64) QAM	AWGN	MATLAB
[121]	Transformation Group, WT	SVM	(2,4,8)-ASK, (2,4,8)-FSK, (2,4,8)-PSK	Not-specified	MATLAB
[131]	Instantaneous Group	SVM	(2,4)-ASK, (2,4)-PSK, AM,FM,CW	AWGN	Not-specified
[132]	Other attributes	SVM	CPM	AWGN	MATLAB
[133]	Instantaneous Group & HOC & HOM	SVM	(2,4) ASK, (2,4)PSK, (2,4,8)FSK ,16 QAM	AWGN	Not-specified
[16]	HOC	DT	(2,4,8)-ASK, (2,4,8)-FSK, (2,4,8)-PSK, (16,64) QAM	AWGN	Not-specified
[47]	Other attributes	DT	MQAM	AWGN	Not-specified
[58]	Instantaneous Group	DT	(2,4,8)-ASK, (2,4,8)-FSK, (2,4,8)-PSK, (16,64)QAM	AWGN	Not-specified

Table 2.7 Continued.

[60]	Instantaneous Group	DT	(2,4)-FSK, (2,4,) PSK, (16,32) QAM	AWGN	MATLAB
[61]	Instantaneous Group	DT	(2,4,8)-ASK, (2, 4, 8) FSK, (2, 4.8)-PSK, (16, 64) QAM.	AWGN	DSP equips the RTSA.
[65]	Other attributes & HOC	DT	(2,4,8) PSK, (16,32,64) QAM	AWGN	Not-specified
[83]	Transformation Group, WT, and HOM	DT	(2,4,8,16)-PSK, (8,16,32) QAM	AWGN	MATLAB
[86]	Transformation Group, WT	DT	(2,4,8)-FSK, (2,4,8) PSK, (16,32,64) QAM	AWGN	Not-specified
[103]	HOC & HOM	DT	(16,32,64,128,256) QAM	AWGN	MATLAB
[109]	Instantaneous Group	DT	(4,8) ASK,(2,4,8)PSK (2,4,8)FSK,(16,64)QAM ,ADSL VDSL PLC Other	AWGN	Not-specified
[110]	Transformation Group, FT	DT	(2,4,8)-PSK	AWGN	Not-specified
[111]	Other attributes	DT	(2,4)-ASK,2FSK, (2,4)-PSK, (16,64)-QAM,8 tone-FDM,16-tons FDM	AWGN	Not-specified

Table 2.7 Continued.

[134]	Other attributes	DT	(2,4,8)-FSK, (2,4,8) PSK, (16,32,64) QAM	Not-specified	Not-specified
[135]	Zero-crossing	DT	(2,4,8)-FSK,(2,4,8) PSK,	Not-specified	Not-specified
[136]	Transformation Group, FT	DT	MFSK	AWGN	Not-specified
[137]	HOC	DT	(4,16,64) QAM, V29	Not-specified	Not-specified

2.5 Place of the Present Work in Literature

Based on the review presented in this chapter, there are already numerous methods for digital-modulation classification; some studies confirmed that using a decision-theoretical method has more reliable performance than methods depending on feature extraction. Nevertheless, when using the decision-theoretical method, most signal specifications must be prior knowledge at the receiver. In the FB-method, the overall performance of the recogniser is entirely dependent on the chosen features. Based on the presented literature review, numerous features can be proposed for the recognition of different modulation schemes. Apart from these features, most previous studies have aimed at exploring new algorithms, characterised by a focus on reducing the sensitivity of features to variations in SNR, as well as improving the recognition ability by focusing on finding robust features and suitable designs for the classifier. However, to the best of our knowledge, there has been no work on the recognition of high-order quadrature-amplitude modulation (QAM) schemes to date. Therefore, in AWGN-channels, this dissertation proposes a classification algorithm for high-order MQAM modulation signals, with an attractive logarithmic classifier. The distribution curves of the new features are becoming less sensitive to the SNR. Here, the logarithmic classifier has the ability to recognise MQAM types from the signals set – from 4QAM to 1024QAM.

The simulation results demonstrate that the recognition algorithm can recognise MQAM signals well in an AWGN-channel environment, and is more robust against pulse deviation and changes in the shaping-filter coefficient. Furthermore, the features based on logarithmic cumulants have appeared to be highly effective in the classification of QAM signals, even in transmission media suffering from harsh noise.

Also, in this thesis, the design of an intelligent scheme to recognise MAPSK signals is proposed. An MLP architecture, with the maximum value of the power-spectral density and a set of high-order spectral densities, could provide further merits and excellent classification accuracy for high-order APSK signals; in addition, an MLP gives a reasonable recognition rate, even at SNR = 0 dB.

CHAPTER THREE

SIGNAL MODEL, SIGNAL FEATURES, AND OVERVIEW OF PATTERN-RECOGNITION METHODS

3.1 Introduction

In this chapter, the transmitter-side and receiver-side components of communication systems are briefly explained. A concise review for common modulation techniques is provided, such as; M-ary phase-shift keying (MPSK), M-ary quadrature-amplitude modulation (MQAM), and amplitude phase-shift keying (APSK). Further, their constellation diagrams are summarised, with a brief mathematical framework for each. Furthermore, diverse types of signal impairments involving noise and channel fading are also addressed. The effects of different Doppler-shift values on the modulation constellation are explained. Finally, some criticisms of traditional AMR algorithms have been presented. Moreover, their proposed features were verified by simulations.

3.2 Signal Model

3.2.1 Communication system model

The main goal of any communication system is transmitting information signals through communication channels without losses. Information signals degrade in quality when travelling through a channel, owing to the effects of noise, distortion, attenuation, and energy losses due to channel impedance [138]. Further, the shape of the signal travelling through the channel is distorted when the receiver is receiving more than one signal at the same frequency simultaneously.

Random noise, which includes unwanted signals, is unpredictable and causes significant deterioration of the transmitted signal.

This noise is a crucial point of investigation for researchers in the field of telecommunication systems owing to the appearance of retrogressions in the transmission signal when it travels through a channel, it becomes difficult for the receiver to recognise the modulation type of the signal. Figure 3.1 shows the model of a primary communication system. It can be seen that the receiver includes an automatic modulation classifier, which comprises two main sub-modules the received signal pre-processing module and classifier module. The function of the pre-processing block is to measure the synchronisation parameters, such as the received signal's frequency offset, timing recovery, signal power, etc. Furthermore, it helps the classifier select a satisfactory classification algorithm for modulation recognition.

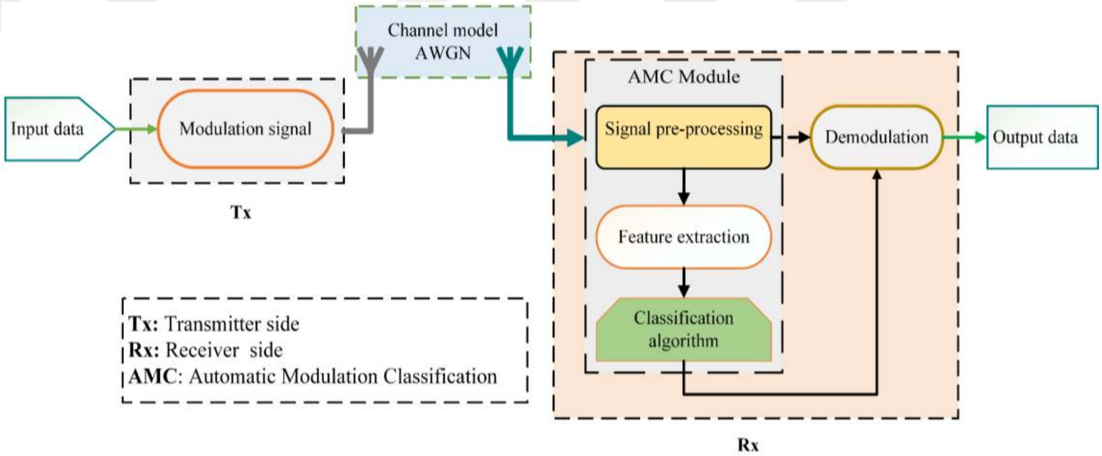

Figure 3.1 Communication scheme model.

3.2.2 Typical signal and channel model

To study the behaviour of any communications system, the transmission channel is commonly assumed to be ideal. In this assumption, the transmitted signals are usually weakened by AWGN, which includes all unwanted random signals that occur naturally. This channel model is exposed to a normal distribution of random variables with a zero mean and a constant power-spectrum density.

This assumption is a good description of the performance of any wireless system, as it reflects their main characteristics. Therefore, in this work, the focus is on transmitted signals that have been corrupted by random noise, which is in commonly known as an AWGN-channel model. The deterioration of the transmission signal while it travels from the transmitter to the receiver-end is studied [139]. According to these assumptions, noise is a proper limitation to the robustness of classification. Figure 3.2 shows the model of the AWGN. The other types of noise are not in the scope of this thesis. Consequently, the received signal can be written as:

$$y(t) = S(t) + N(t) \qquad\qquad 0 \le t \le m \tag{3.1}$$

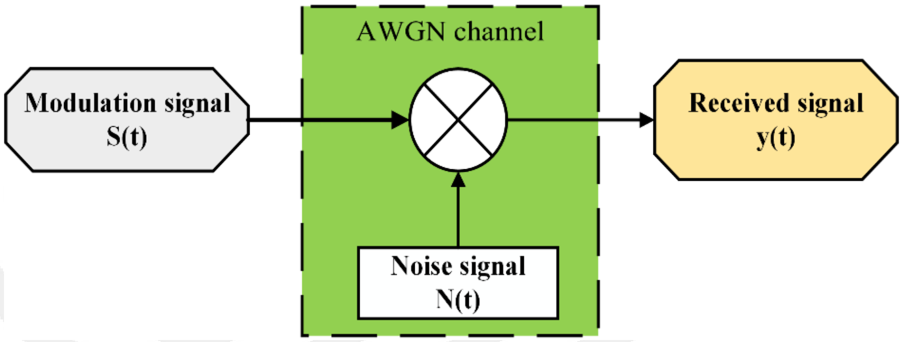

Figure 3.2 The model of channel.

where $y(t)$ is a base-band envelope complex signal after noise corruption, from the point of the received site; $S(t)$ is the modulation-transmitted signal that carries information signal; $N(t)$ is additive white Gaussian noise; $m = nT$; n is the number of symbols transmitted; and T is symbol time. Eq. (3.1) and Eq. (3.2) have been described [129]. The general representation of a discrete-baseband signal with zero mean is

$$r(n) = Ae^{-j(\omega_0 nT + \theta_n)} \sum_{k=-\infty}^{k=\infty} S(\mathcal{L})\, h\big(nT - kT + \varepsilon_{T_s} T\big) \qquad \omega_0 = 2\pi f_0 \tag{3.2}$$

While S(L) is the complex conjugation of the signal, and is expressed as;

$$S(\mathcal{L}) = i + jQ \tag{3.3}$$

where $S(\mathcal{L})$ is the input symbol staring, which can be expressed as an M constellation of familiar symbols. It is not significant that symbols have equal probability. **A** represents magnitude value of a modulated signal; ω_0 is the offset frequency, which is constant; θ_n is the phase offset the distance from symbol to another; $h(\dots,)$ is the channel impact; and $\boldsymbol{\varepsilon}_{\mathbf{T}}$ is timing error.

3.3 Modulation

In communications standards, the most conventional modulation methods used in modern digital communications systems. These comprise of the hybrid modulation standards called quadrature-amplitude modulation (QAM) and standard amplitude phase-shift keying (APSK). The former represents digital modulation that carries a data signal by modulating both the amplitude and phase of the high-frequency signal. It includes both ASK- and PSK-modulation schemes. The latter is similar to the former in the processing of data, and is a variation of the QAM scheme. Nevertheless, in this thesis, we have studied different orders of PSK and QAM-modulation schemes. Furthermore, typical DVB-S2X standard-specific asymmetric MAPSK is also considered.

3.3.1 M-ary phase shift keying

In the PSK modulation technique, the data signal is transmitted using various phase angles of the carrier signal. Both the amplitude and frequency of the reference signal ('carrier wave') remain constant. The binary data signal is encoded in sets of bits to create so-called 'symbols'. A different phase is assigned to each symbol of the data signal ('baseband'). The pattern of the phase angles is based on the total number of the bits per symbol. In the case of binary phase-shift keying (BPSK), the two phases are used as they have one bit per symbol. On the other hand, for 4-PSK, each symbol includes two-bit information; therefore, four phases are employed. For other types of MPSK, the same criteria are considered. The PSK transmitted signal is expressed as [140] :

$$\mathrm{s_i(t)} = \left\{ \sqrt{\frac{2\mathrm{E_s}}{\mathrm{T}_s}} \cos\left(2\pi f_c t + \frac{2\pi}{M_s} i\right) \quad i = 0,1,\dots,\mathrm{M_s}-1 \right. \tag{3.4}$$

$$\mathrm{M_s} = 2^{\mathrm{N_b}}$$

where E_s , M_s, and N_b represent the signal constant energy per symbol, number of discrete signals ('symbols'), and the total number of bits per symbol, respectively. T_s is the duration of the signalling interval and f_c is the frequency reference ('carrier wave'). In the case of M=2, the two diverged phase angles are generated to express logic 0 and 1. Hence, the reference wave will oscillate between sine and cosine, i.e. it will be either in-phase or out-of-phase with respect to the carrier waveform, as follows [140] :

$$s_i(t) = \begin{cases} \sqrt{\frac{2E_s}{T_s}}\cos(2\pi f_c t) & \text{for symbol "0."} \\ \sqrt{\frac{2E_s}{T_s}}\cos(2\pi f_c t + \pi) = -\sqrt{\frac{2E_s}{T_s}}\cos(2\pi f_c t) & \text{for symbol "1."} \end{cases} \quad (3.5)$$

The binary BPSK is more widely used than other binary types, such as 2ASK and 2FSK. This is because PSK depends on phase variation, which is less sensitive to noise than the ASK technique, which depends on varying the amplitude of the carrier signal. Amplitude is more susceptible to noise than the phase. Unlike the FSK technique, the BPSK technique requires one carrier signal, which allows management of the bandwidth [141].

For $M_s = 4$, four difference angles for the conveyed signal are produced, signifying four differences symbols among phase shifts $0, \frac{\pi}{2}, \pi, \text{and} \frac{3\pi}{2}$.Therefore, the signal output will be:

$$
s_i(t) = \begin{cases} \sqrt{\frac{2E_s}{T_s}}\cos(2\pi f_c t) & \text{for symbol "00."} \\ \sqrt{\frac{2E_s}{T_s}}\sin(2\pi f_c t) & \text{for symbol "01."} \\ -\sqrt{\frac{2E_s}{T_s}}\cos(2\pi f_c t) & \text{for symbol "10."} \\ -\sqrt{\frac{2E_s}{T_s}}\sin(2\pi f_c t) & \text{for symbol "11."} \end{cases} \tag{3.6}
$$

It should be noted that, in Eq. (3.6), that the signal comprises both sines and cosines. This indicates that all parts are uncorrelated in time during a symbol period. More precisely, two independent BPSK-modulation schemes are used. The minor real axis points to the in-phase (I), and the major axis points to quadrature (Q). Based on this, this method is called quadrature PSK (QPSK). The two independent BPSK signals could be transmitted from the same antenna and receiver, without any interception.

Even if the signals have the same carrier frequencies, it is clear that the real part 'in-phase component' and the imaginary part quadrature component for different states is a set of points on a two-dimensional plane. This two-dimensional plane is called a constellation diagram, which depicts each symbol as a point based on the type of modulation as shown in Figure 3.3.

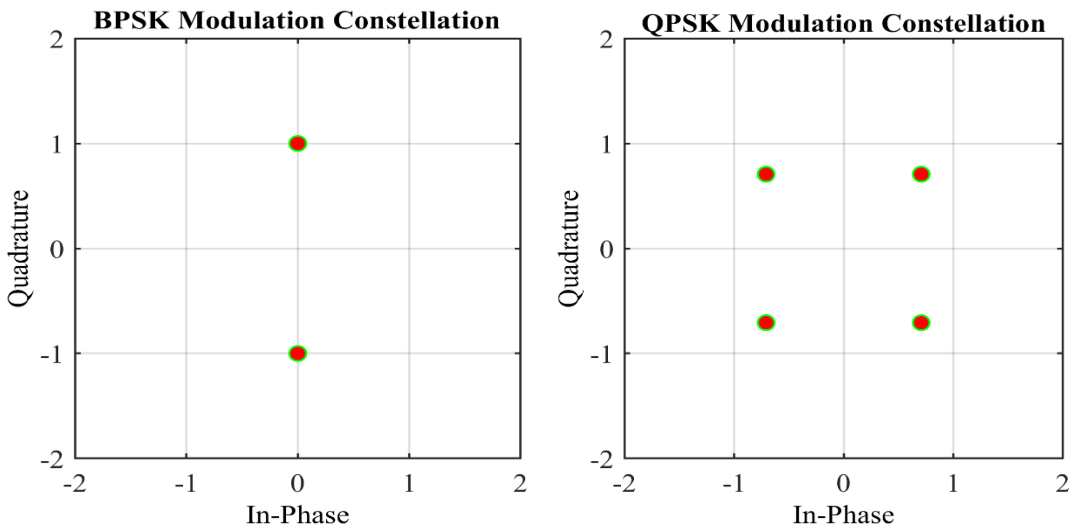

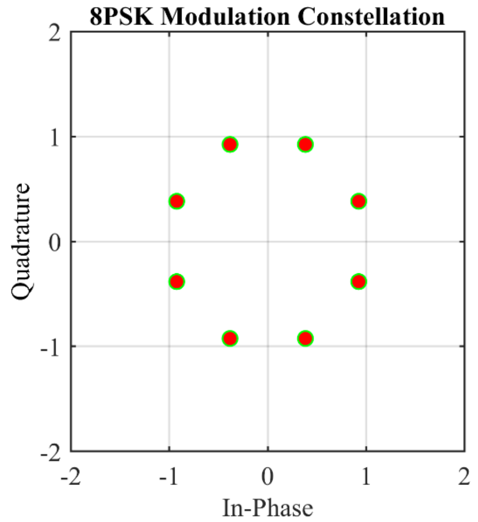

Figure 3.3 MPSK constellation diagram with M=2, 4, and 8, and each symbol represents 1, 2, and 3 transmitted bits, respectively, for each scheme.

Both (I–Q) components for M-ary PSK-transmitted signals are correlated in such a manner that the amplitude of the signal is restrained to a constant value of $\sqrt{E_s}$ for every symbol [47]. This represents a major advantage of M-ary PSK. In some cases, the PSK signals have a supplementary phase offset to restrict the phase shift that occurred during the modulation process [142]. The additional angle revolves the points in the constellation diagram by a uniform angle, depending on the modulation model.

3.3.2 M–ary quadrature amplitude modulation

The receiver precision for distinguishing small differences in the phase angle restricts the possible bit rate in the PSK scheme. This restriction is caused by changing one of the three variables of the reference signal in time [141]. On the other hand, quadrature-amplitude modulation (QAM) is a modulation scheme that transmits the digital signal by varying both the amplitude and phase of the carrier signal. It is similar to the PSK scheme; however, rather than changing in the carrier phase only, it varies both the phase and amplitude of the carrier signal relative to a base-band signal. Unlike MPSK, it is a combination of the PSK and ASK schemes, so each symbol in the constellation diagram has an optimal space. The symbols' waveforms can be represented as follows [140]:

$$s_i(t) = \sqrt{\frac{2E_s}{T_s}}\, a_i \cos(2\pi f_c t) \; - \sqrt{\frac{2E_s}{T_s}}\, b_i \sin(2\pi f_c t) \;\; i = 0,1,\dots,M_s - 1 \tag{3.7}$$

$$M_s = 2^{N_b}$$

where a_i and b_i represented in-phase component and quadrature component, respectively. These components are orthogonal to each other. The constellation diagram represents a graphical distribution of each symbol's state for a complex envelope (I–Q), and the x-axis represents the complex discrete envelope in-phase component. The quadrature component is represented by the y-axis. The probability of bit error is affected by the distance between the adjacent signals in the constellation. The modulated signal with a densely packed constellation has lower energy efficiency than a modulated signal with low-density constellation [140]. Several constellation diagrams describing symbol distributions for 16-QAM and 64-QAM constellations are depicted in Figure 3.4.

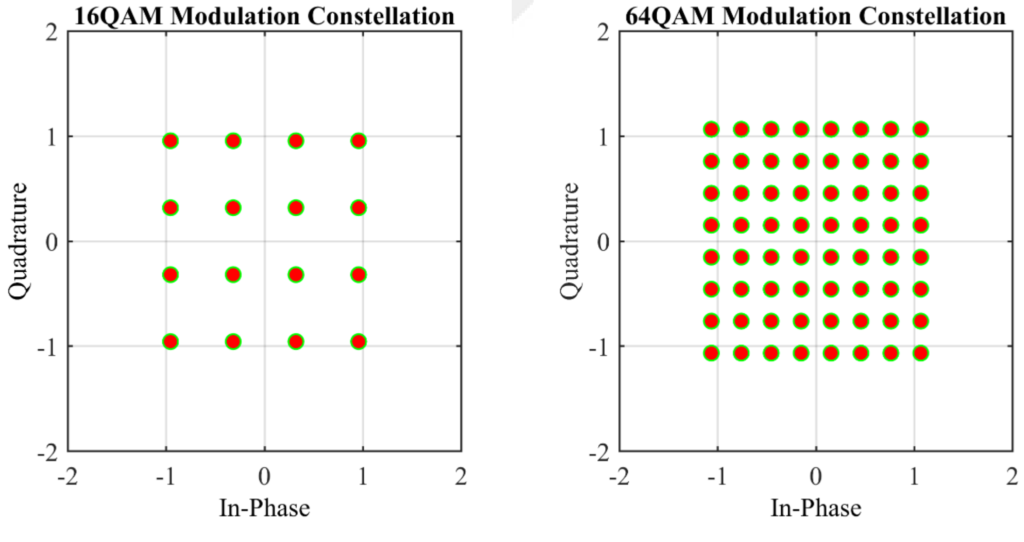

Figure 3.4 16-QAM and 64-QAM constellation.

3.3.3 Amplitude and phase–shift keying

This technique is also called 'asymmetric phase-shift keying'. The M-APSK is a standard digital-modulation method that transmits information by modulating two parameters in the high-frequency signal the amplitude and the phase angle. It merges both ASK and PSK to increase the symbol-set. An M-APSK signal constellation consists of R concentric rings, each with uniformly distanced phase-shift keying points. This is mathematically represented as follows [143].

$$s_i(t) = \begin{cases} r_1 e^{\left(j\left(\frac{2\pi}{n_1}i+\theta_1\right)\right)} & i = 0, \dots, n_1 - 1 \\ r_2 e^{\left(j\left(\frac{2\pi}{n_2}i+\theta_2\right)\right)} & i = 0, \dots, n_2 - 1 \\ \vdots & \\ r_R e^{\left(j\left(\frac{2\pi}{n_R}i+\theta_R\right)\right)} & i = 0, \dots, n_R - 1 \end{cases} \tag{3.8}$$

where n_ℓ is the number of points, r_ℓ is the radius, θ_ℓ is the phase offset of the $\ell -$ th ring, and $\ell = 1, \dots, R$, $\sum_{\ell=1}^{R} n_\ell = M_s$ as in [144]. The radius constellations for 16APSK, 32APSK, and 64 APSK are shown in Figure 3.5

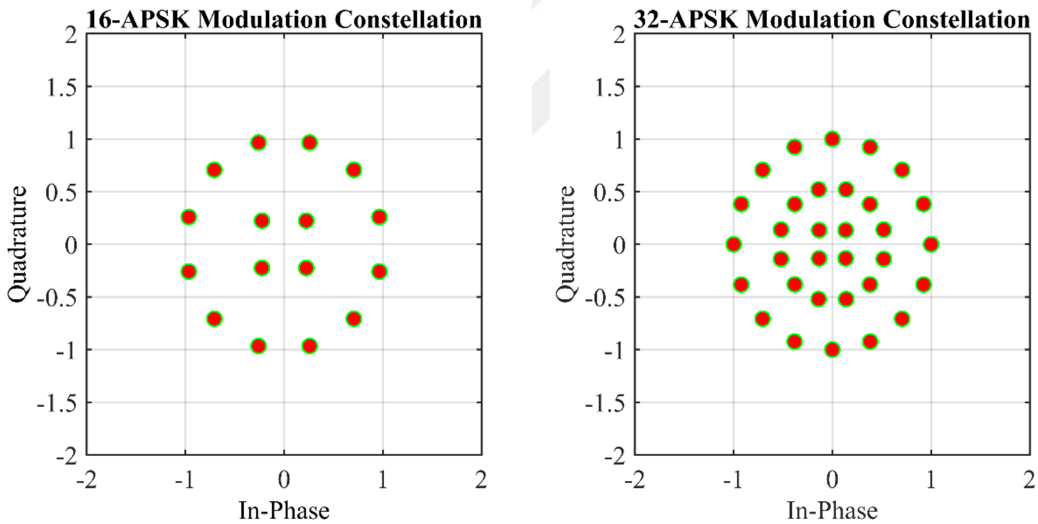

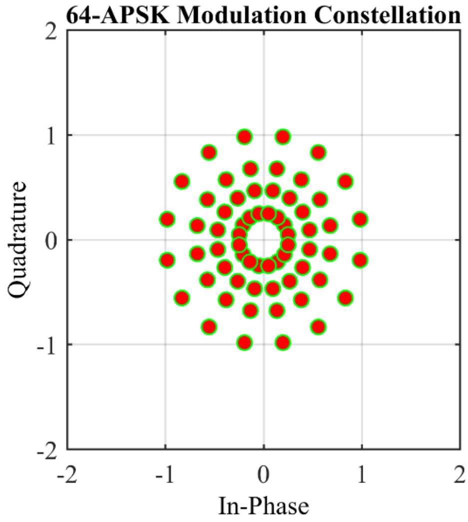

Figure 3.5 Radius-constellations of 16APSK , 32APSK, and 64APSK.

3.4 Transmission Channel Noise Model

Unwanted signals, also called noise, are a major issue in wireless-communication systems. There are many sources of noise, such as thermal noise or non-linear characteristics of some components of the radio. The noise affects modulated radio signals and can damage the information transmitted or lead to glitches. Figure 3.6 shows the power-spectrum density of AWGN-transmission media. The power density has a fixed magnitude value at all frequencies. The influence of noise on the radio signal can be defined by a ratio of the modulated signal power and noise power, which is expressed SNR. Further, in some cases, it can be represented in terms of a ratio of the symbol energy $\mathrm{E_s}$ and noise power spectrum density $\mathrm{N_o}$:

$$\mathrm{SNR} = \frac{\mathrm{E_s}}{\mathrm{N_s}} \tag{3.9}$$

In practical communication systems, noise is not the only factor that deteriorates in the transmitted signal; there are several impairment effects on the power of radio signals that cause losses in information. Severe degradation of the received signal occurs due to the fading phenomenon. In this phenomenon, multiple copies of the same radio signal reach the receiver. However, communication engineers have suggested various models to investigate the performance of wireless-radio devices. The primary transmission channel is free space, which represents a pure-channel model that will be explained in the next sub-section.

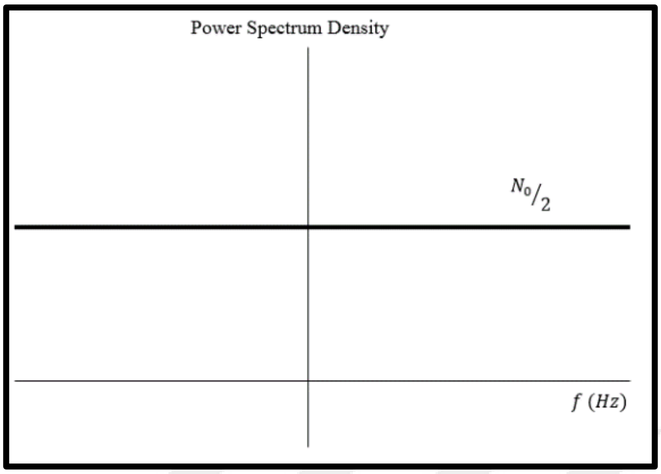

Figure 3.6 PSD for white noise.

3.4.1 Model of propagation in the free space

The model of communication-signal propagation in free space describes the power of the modulated signal without considering signal reflection between the sender and receiver. The modulated-signal power is inversely proportional to the square of the length between the sender and receiver:

$$P_r = \frac{P_t G_t G_r \lambda^2}{(4\pi d)^2} \tag{3.10}$$

where P_r, P_t, and λ denote to the modulated signal power, transmitted signal power, and the wavelength of the transmitted signal, respectively. G_t is the gain ratio of the transmitter antenna, G_r is the gain of the receiver antenna, and d is the distance between the sender and the receiver.

3.4.2 Channels fading

When evaluating the performance of any radio system, communication engineers assume the wireless channel to be ideal, which indicates that the modulated signal is conveyed over a pure-AWGN channel. As a matter of fact, this hypothesis describes the behaviour of communication systems and reflects their main problems. However, this assumption is not sufficient owing to the interference between the transmitted signal and other signals in the spectrum, or among multiple copies of the same signal. These could have a significant impact on the transmitted signal and yield severe degradation in the performance of the radio system [145]. In general, the transmission environment between the sender and listener varies against frequency and time. This variation could be classified into two types, as follows.

a. **Large-scale fading degradation:** When transmitting communication signals, the distance between the sender and receiver weakens the power of the transmitted signal. Additionally, the shadowing phenomenon caused by buildings and mountains also leads to degradation of the power of the transmitted signal. In general, this fading type occurs in long distances, where all transmitted signals with various frequencies facing the same issues are frequency-invariant.

a. **Small-scale fading degradation:** At shorter distances between the sender and receiver, this type of fading occurs. This always occurs for distances that similar to the range of the signal wavelength, primarily owing to multipath problems. The multipath phenomena occur because of reflected duplicates of the same signal arriving at the receiver, leading to two types of degradation. The first is constructive, and the second is destructive, which arriving signal copies are added together [146]. Figure 3.7 illustrates an actual case of multipath fading.

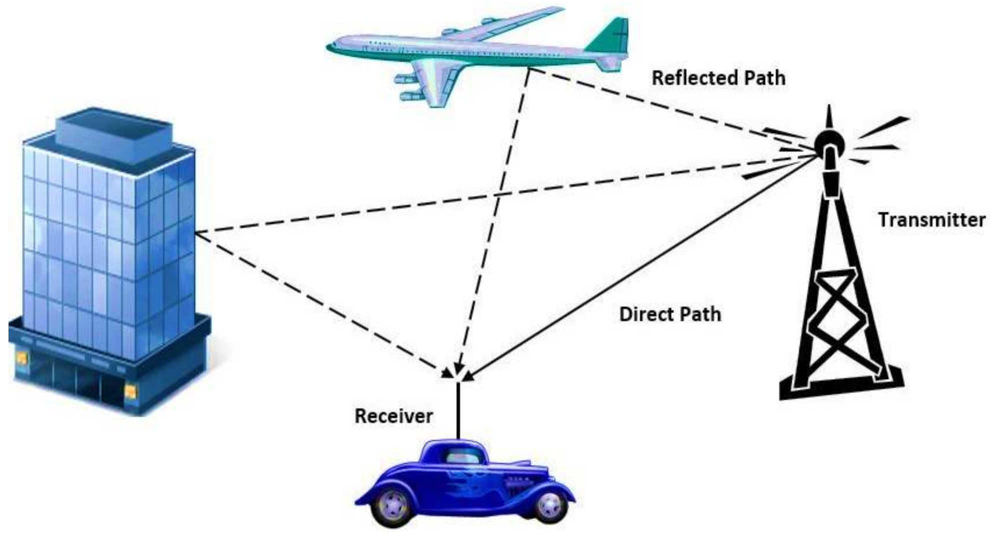

Figure 3.7 Effected of the Multipath fading.

3.4.2.1 Small–scale fading narrow

In the communication-system channel, for multipath time-delay propagation model, narrow or small-scale fading can be split into two classes. The first is flat fading and the second is frequency-selective fading, which are described as follows.

a. **Flat-fading model:** This is a model of the fading effect where the transmitted signal travels over a constant gain and bandwidth. As a result, all the frequency components of the transmitted signal are multiplied by the constant gain and subjected to the same fading degradation. The flat-fading model occurs when: $B_s \ll B_c$ and $T_s \ll \sigma_\tau$, where B_c and B_s indicate the coherence bandwidth of the channel and the bandwidth of the transmitted signal, respectively.

Further, this type of fading can also be represented in terms of the symbol time of the transmitted signal T_s and the channel propagation delay σ_τ. This assumption states that all the reflections of the transmitted information arrive at the receiver with a similar symbol period of the signal, yielding a synchronicity between the sequence of transmitted symbols [145].

b. **Frequency-selective fading:** This fading model has a more crucial impact on the behaviour and performance of radio signals than the flat-fading model. In this type of fading, the coherence bandwidth of the transmission medium is smaller than the signal bandwidth. Simply put, the symbol period of the transmitted signal is shorter than the delay propagation of the transmission medium (communication channel). Hence, the duplicates of the reflected signal arrive at the radio system at the same time of receiving the next symbol or perhaps further symbols following that. Further, the frequency-selective fading model suffers from inter-symbol interference (ISI), which occurs among the sequence of symbols at the receiver. An equaliser is required on the radio side to make up for the variations in results caused by the fading nature of the transmission medium. As a mathematical formulation, the frequency-selective fading model occurs when: $\mathrm{B_s} \gg B_c$ and $\mathrm{T_s} \ll \sigma_\tau$.

Further, the narrow-scale fading model can also be further divided according to the Doppler propagation of the channel, as fast or slow fading:

a. **Fast-fading model**: This type of fading occurs when the relative motion between the sender and receiver is fast. Therefore, the impulse response of the transmission medium quickly varies during the symbol duration. Accordingly, the transmitted symbols have different gains when travelling from the transmitter to the receiver through the transmission medium, distorting the final received signal. The parameter $\mathrm{T_D}$ is described as the tenacity time of a channel, in which the time over the channel includes a constant impulse response. In cases where the channel-tenacity time is shorter than symbol duration, then the transmitted signal is not affected by the fast-fading model [147]. This can be represented mathematically as: $\mathrm{B_s} \gg \mathrm{B_D}$ and $\mathrm{T_s} \gg \mathrm{T_D}$.

b. **Slow-fading model:** This fading model generally has an insignificant impact on wireless-communication systems because the transmission-medium impulse response is constant over the time of sending a symbol. Therefore, the symbol sent is multiplied with the constant gain value without creating any symbol interference among the contiguous conveyed symbols. The slow-fading model occurs when the conveyed signal parameters are: $\mathrm{B_s} \gg \mathrm{B_D}$ and $\mathrm{T_s} \ll \mathrm{T_D}$.

3.4.2.2 Rayleigh fading

Rayleigh fading refers to the effect of a spread medium on a radio signal. In this fading model, the magnitude of the source signal is assumed to varying randomly, or based on the Rayleigh distribution. This assumption provides a good representation of the multi-path reception of the same signal on the receiver side. The complex phasor of the envelope form of the received signal having N copies of the received signal is expressed as:

$$\widetilde{\mathrm{E}} = \sum_{n=1}^{N} \mathrm{E}_n \, e^{j\Phi_n} \tag{3.11}$$

where E_n is the relative magnitude of each medium ('n-path') and $e^{j\Phi_n}$ denotes the phase of each medium. Φ_n is considered to be independent and uniformly distributed; therefore, the phase magnitude is particularly sensitive to small variations in the medium length. Based on the central-limit theorem, the representation in Eq. (3.13) can be described by the Gaussian distribution for a substantial value of the independent reflected medium. Therefore, the probability-density function (PDF) of the radio receiving the signal envelope is written as [148]:

$$\mathrm{P(r)} = \frac{r}{\delta^2} e^{-\frac{r^2}{2\delta^2}} \quad r \geq 0 \tag{3.12}$$

where δ is the signal magnitude ('RMS-value') with no clear path. Rayleigh fading is a reasonable model for signal spread in the troposphere and ionosphere, and can also adequately describe the blocking caused by densely built-up urban environments on spread radio signals.

3.4.2.3 Rician fading

In the preceding fading model (Rayleigh fading), the multi-path reception signal is assumed to carry approximately equal power. Therefore, in this type of fading, the line-of-sight wave (LOS-W) feature between the transmitter and receiver is not considered. For instance, LOS-W is possible in transmitter and receiver in indoor wireless radio systems. Therefore, the statistical-Rayleigh fading channel is insufficient to represent the amplitude distribution of the received signal. The Rician-fading model is a stochastic model for signal spreading anomalies that occur owing to partial cancellation of a transmitted signal by itself. In this fading type, multi-path radio signals are assumed to arrive at the receiver along with a line of sight signal. Accordingly, the envelope of the received signal, as a complex phasor, is expressed as:

$$\widetilde{E} = E_o + \sum_{n=1}^{N} E_n \, e^{j\Phi_n} \tag{3.13}$$

where E_o is the LOS-W component of the transmitted signal. Furthermore, the Rician distribution PDF is represented as:

$$P(r) = \frac{r}{\delta^2} e^{-\frac{r^2+v^2}{2\delta^2}} \; I_0\left(\frac{rv}{\delta^2}\right) \quad r \geq 0 \tag{3.14}$$

where v^2 and I_0 denoted the power of the non-fading segment and the modified-Bessel function of zeroth order, respectively. There is an additional dominant component when determining the Rician fading between the power of the direct path and different paths, which is defined by the K factor as follows:

$$K = \frac{v^2}{\sum_{n=1}^{N} |E_n|^2} \tag{3.15}$$

where $|E_n|^2$is the power of different paths. Typically, the probability of the radio signal undergoing a profound fading reduction increases when the factor k rises.

3.4.2.4 Doppler shift

The Doppler shift defines the shift in the frequency of the received radio signal when the source is mobile, or when both the receiver station and the source have relative motion. According to the direction of motion, the detected frequency on the receiver side differs from the original sender frequency. For example, during the movement of the receiver relative to the source side, the detected frequency in the receiver side is higher than the frequency of the source, and vice versa.

For instance, based on the motion of the receiver relative to the source, the frequency of the receiver is expressed as:

$$f_r = f_0(1 \pm \frac{v}{c}) \tag{3.16}$$

where f_0 , v, and c denote the original source frequency ('transmitted frequency'), the speed of the receiver, and the speed of light, respectively. Therefore, the resultant Doppler shift could be represented as:

$$f_D = f_r - f_0 = \pm\frac{v}{c} \tag{3.17}$$

When considering the angle Φ between the movement of the receiver relative to the direction of propagation, the Doppler shift equation becomes:

$$f_D = \pm f_0 \frac{v}{c} \cos\Phi \tag{3.18}$$

However, when the angle between the sender and the receiver is zero, the maximum Doppler phenomenon occurs:

$$f_D(\max) = \pm f_0 \frac{v}{c} \tag{3.19}$$

3.5 Chosen Statistical Features

In this study, the modulated-signal model comprises complex baseband amplitudes. Therefore, in order to evaluate the $(\mathrm{i}+\mathrm{j})^{\mathrm{th}}$ M-moment of the complex random variable x, which is also reported in [44]:

$$\mathrm{M}_{\mathrm{x}_{\mathrm{i,j}}} = \mathrm{M}\{\mathrm{y}^{i}.(\mathrm{y}^{*})^{j}\} \tag{3.20}$$

The modulated signal $(\mathrm{i}+\mathrm{j})^{\mathrm{th}}$ moment is assessed from the length of the row data N when computing the statistical mean of this row-data after matching each point to the power according to its moment level. However, the $(\mathrm{i}+\mathrm{j})^{\mathrm{th}}$ central moment is defined as:

$$\mathrm{M}_{\mathrm{x}_{\mathrm{i,j}}} = \mathrm{M}\{(\mathrm{y}-\bar{\mathrm{y}})^{i}.(\mathrm{y}^{*}-\bar{\mathrm{y}})^{j}\} \tag{3.21}$$

where M is the first-order moment, and $\bar{\mathrm{y}}$ represents the discrete statistical mean of the y random variable. Casein this case, the cumulants can also be represented as a combination of the order of the central moments. This expression not only makes numerical calculation simpler, but also more effective. The mathematical expressions for the most crucial cumulants are listed as follows [68]:

$$\begin{aligned}
\mathrm{C}_{11} &= \mathrm{M}_{11} \\
\mathrm{C}_{22} &= \mathrm{M}_{22} - \mathrm{M}_{20}{}^{2} - 2\mathrm{M}_{11}{}^{2} \\
\mathrm{C}_{33} &= \mathrm{M}_{33} - 6\mathrm{M}_{20}\mathrm{M}_{31} - 9\mathrm{M}_{22}\mathrm{M}_{11} + 18(\mathrm{M}_{20})^{2}\mathrm{M}_{11} + 12\mathrm{M}_{11}{}^{3} \\
\mathrm{C}_{44} &= \mathrm{M}_{44} - \mathrm{M}_{40}{}^{2} - 18\mathrm{M}_{22}{}^{2} - 54\mathrm{M}_{20}{}^{4} - 144\mathrm{M}_{11}{}^{4} \\
&\quad - 432\mathrm{M}_{20}{}^{2}\mathrm{M}_{11}{}^{2} + 12\mathrm{M}_{40}\mathrm{M}_{20}{}^{2} + 192\mathrm{M}_{31}\mathrm{M}_{11}\mathrm{M}_{20} \\
&\quad + 144\mathrm{M}_{22}\mathrm{M}_{11}{}^{2} + 72\mathrm{M}_{22}\mathrm{M}_{20}{}^{2}
\end{aligned} \tag{3.22}$$

The magnitudes of the cumulants' orders are applied to different types of classifiers to distinguish between a set of QAM and PSK modulated signals; more details regarding this are presented in the next chapter.

3.6 Classifiers Structure

3.6.1 Decision tree classifiers

A decision-tree classifier (DTC), also known as a decision-threshold classifier, is used widely in numerous diverse fields. Their most significant merit is obtaining knowledge and classifying applied data. Therefore, the decision tree could be established by training data sets. The DT-classifier is trained by choosing distinct features that typically express each node of the tree. Essentially, the DTC training methods process one feature variable at a time for all data labels.

The feature-choice rule and tree creation involve the learning content, the node clearness, or Fisher's standard. In general, this technique is simple to design and has low complexity. However, the complexity moderately increases if classifier performance needs to be improved. Binary DTCs are usually used in pattern recognition, where each node represents a signal feature. Therefore, the decision thresholds are lateral to the feature axes. The crucial benefit of DT-classifiers is their speed of achieving results. Moreover, it provides the feasibility to understand the decision rule in terms of singular features. This makes the decision-threshold classifier interactive in the pattern-recognition field [149]. The optimal structure of the tree could be obtained by exhaustively exploring and choosing the best structure. The optimum bounds of each node can be determined by selecting a value that produces minimal misclassification. By using this strategy, each feature can be analysed and proper thresholds determined. Meanwhile, in DT-classifiers, the outcome is based on two categories of comparisons; single boundary and multi-boundary. In single-boundary conditions, decision making is based on the predefined value of a feature called the optimum threshold. Therefore, the result is more trustworthy because it has a single decision line that separates each class. In multi-boundary conditions, on the other hand, more than one separation line is used for classification. Thus, it has a relatively lower accuracy because multiple boundaries are used to distinguish the target class from others. Figure 3.8 shows the decision line between two categories. For example, assume that class 1, in orange, is the target class and the other classes are class 2, in blue. The probability of false classification is small in cases of a single separation line.

The orange stars are symmetric about a single boundary, as shown in Figure 3.8a. A classifier that consists of two decision boundaries has a higher probability of the false classification, because orange stars can overlap about two separation lines, as observed in Figure 3.8b.

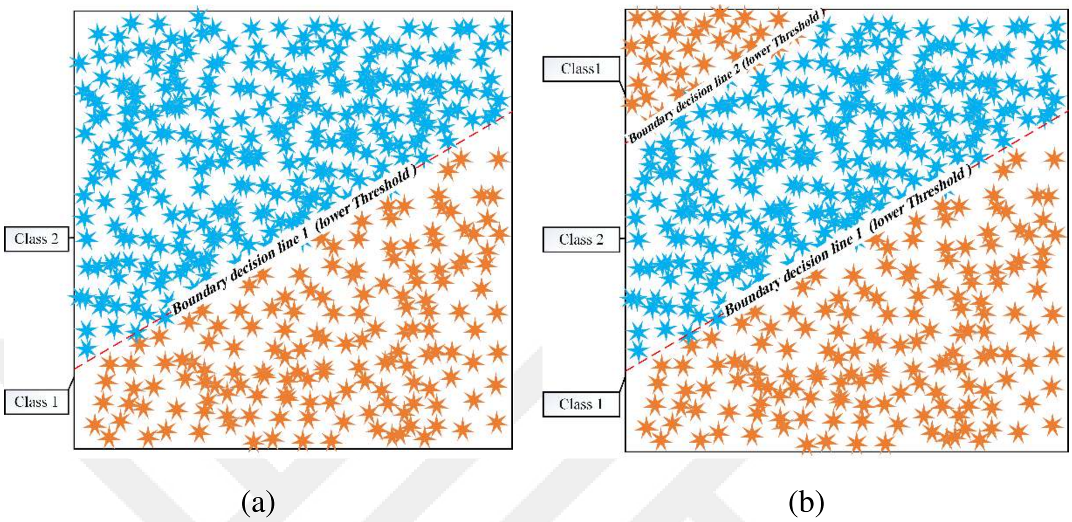

Figure 3.8 Boundary lines among classes.

3.6.2 Neural network classifier multi-layer perceptron (MLP)

The feed-forward neural network with an MLP-architecture is the most conventional standard for modern classifier systems. The MLP structure comprises an input layer, a hidden layer, and an output layer. The number of neurons in the input layer is determined by the number of variables in the input vector – in this case, the number of features. The number of nodes at the output is determined according to the number of target classes [41].

Figure 3.9 illustrates the basic structure of the MLP neural network. In the classification method, the first phase is learning, and the secondary stage is the testing phase. In the learning phase, the network-weight values are updated according to the learning method. The network-weight matrix is adjusted using a sub-standard algorithm called the back-propagation (BP) algorithm, and is based on Eq. (3.25), which is also reported in [150].

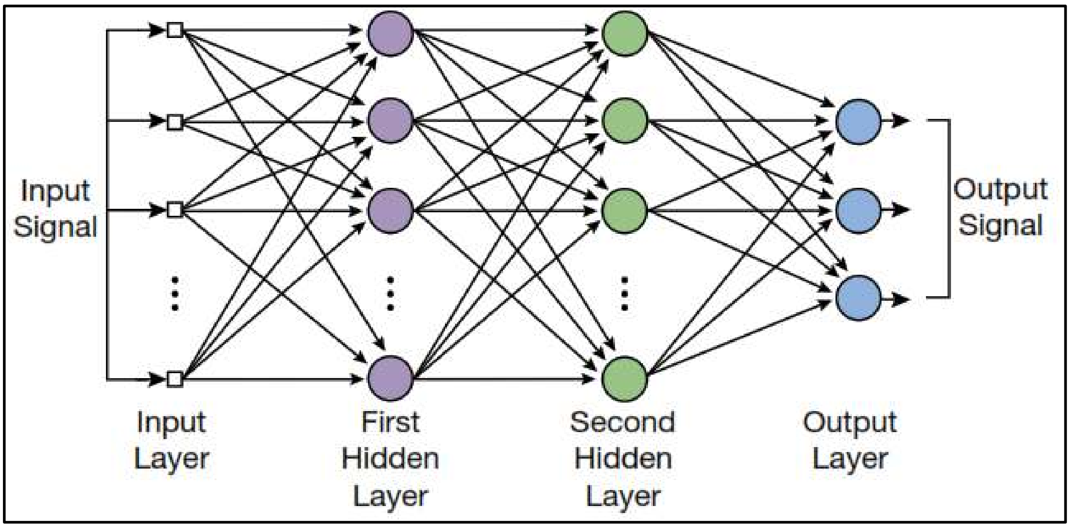

Figure 3.9 MLP neural network structure.

In the training stage, the output of the feed-forward neural network is estimated for every input-learning vector that needs to be classified. The error ratio is computed between the estimated pattern vector and the original pattern vector. The ratio of error is used to adjust the weight matrix of the network according to the back-propagation algorithm criteria [150].

$$W_{ij}(t+1) = w_{ij}(t) - \varepsilon \frac{dE_f}{dw_{ij}}(t) \tag{3.23}$$

where W_{ij}, E_f, and ε represent the weights between neuron i and neuron j, the error function, and learning rate respectively.

3.6.3 Radial basis function neural networks RBFN- classifier

In addition to the benefits of MLP-network structures, radial-basis function neural networks (RBFNs) provide further merits, including a simple design and training efficiency. This makes them an excellent solution for performing nonlinear mapping among the input variables and the output vector spaces. The essential feed-forward network structure of an RBFN comprises three layers an input layer; one or more hidden layers, which comprise nonlinear processing units in which each neuron of this layer includes an activation function called the radial-basis function; and an output layer [12]. A simple configuration of this network is shown in Figure 3.10. The input layer consists of input neurons that have the same dimensions as the input data vector x_n.

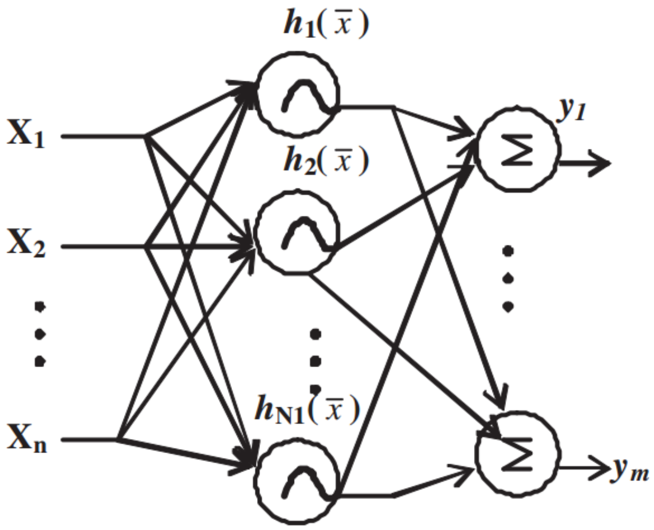

Figure 3.10 Architecture of RBF-neural network.

The output of the j^{th} hidden neuron with a Gaussian-activation function can be expressed as:

$$h_j = e^{\frac{-\|x-c_j\|^2}{\sigma^2}} \tag{3.24}$$

where h_j is the output of the j^{th} node; $x \in \Re^{1xn}$ is the input data; σ is the centre-spread parameter, which controls the width of the j^{th} hidden neuron; $c_j \in \Re^{nx1}$ is the centre of the j^{th} hidden neuron; and the Euclidean norm is represented by $\|.\|^2$.

The output for each node at the output layer of the RBF network is computed as:

$$y_i = \sum_{j=1}^{k} W_{ij} h_j \tag{3.25}$$

where w_{ij} represents the weight links that connect the hidden neuron j and the output neuron number i . k, the number of hidden-layer neurons. It will map the properties of the RBFN by modifying the weights in the output layer that involve the centre of the RBFs and distribution parameters of the Gaussian function.

The techniques of classification that have been explained will be used in the next chapter with the above simulation signals.

3.7 Chapter Summary

This chapter provides an overview of general signal model, along with explanations regarding certain digital-modulation techniques. Feature choice and formation, which represent a crucial component of PR techniques, were also covered. The method of feature selection used in this thesis is explained in detail. Next, the essential principles of different machine-learning classifiers decision tree (threshold algorithm) and ANN are described. In the following chapters, these classifiers will be used to evaluate the selected or generated features.

CHAPTER FOUR

AN M-QAM SIGNAL MODULATION RECOGNITION ALGORITHM

4.1 General

Computing distinct features from input data, before the classification digital signals, is a part of the complexity inherent in AMC and pattern recognition algorithms. The literature includes few studies to date that have performed the classification of high-order M-QAM modulation schemes such as 128-QAM, 256-QAM, 512-QAM and 1,024-QAM. Also, algorithms available in the literature boast many deficiencies in both signals' classification accuracy and computation complexity. Moreover, the previous algorithms are highly sensitive to any change in SNRs. In this chapter, the powerful capability of the natural logarithmic properties in modifying the HOCs features is studied. The algorithm that focuses on multilevel quadrature amplitude modulation (M-QAM) which underneath different channel scenarios is well detailed. The HOCs were obtained under the AWGN-channel with four valid parameters, which were defined to classify the orders of QAM signals from the set 4-QAM to 1,024-QAM. The proposed approach makes classifier more intelligent and improves signals classification success. The results show that the proposed classıfier has superior classification accuracy among that systems proposed in the previous works.

4.2 Background

In the last five years, researchers have widely explored new AMC techniques to reduce the requirements of SNRs and make the classification process more efficient, focusing particularly on finding a robust group of features and optimizing classifier designs. One weak point of previous algorithms (described in Chapter 2) is that the classifier decision requires fixed threshold values; on the other hand, features have been proposed by the authors. As a result, numerous feature groups have been suggested; these features are highly sensitive to SNR, which make threshold values valid for small ranges of SNR. However, in this work, the focus will be on developing new cumulant features and a high-order QAM classification algorithm. The study presented in this chapter will contend that AWGN corrupts the transmission channel during the training phase and feature extraction. The assumption of corruption by AWGN offers a good explanation of system performance and reflects most significant trends. Under the noisy condition, the new relationship among higher-order cumulants and threshold levels is derived.

4.3 Signals Feature and Preparing Datasets

The crucial aspect of the FB-AMC approach is features extraction. As mentioned before in Chapter 2, numerous features are extracted from the received signal. On the other hand, not all features are considered beneficial in the classification process. Therefore, during feature selection, the feature set must be robust against noise, less sensitive to the power of the signal and own a good ability to distinguished among various modulation signals. Moreover, the chosen set of features must be as simple as possible so as to reduce the hardware specifications. To test the performance of the proposed feature set, computer simulation software has been used to prepare signals. The collection of M-QAM modulation schemes included 4-QAM or QPSK, 8-QAM, 16-QAM, 32-QAM, 64-QAM, 128-QAM, 256-QAM, 512-QAM and 1,024-QAM. The realised modulated signals are transmitted through a standard channel type of the AWGN; the length of the signal is 4,096 symbols and a phase offset $\pi/6$ exists during features evaluation. The proposed feature set is plotted against various SNRs to evaluate which one is beneficial in the classification stage.

Figure 4.1 shows a constellation diagram of the M-QAM order modulation of interest. In this figure, the SNR is 10 dB.

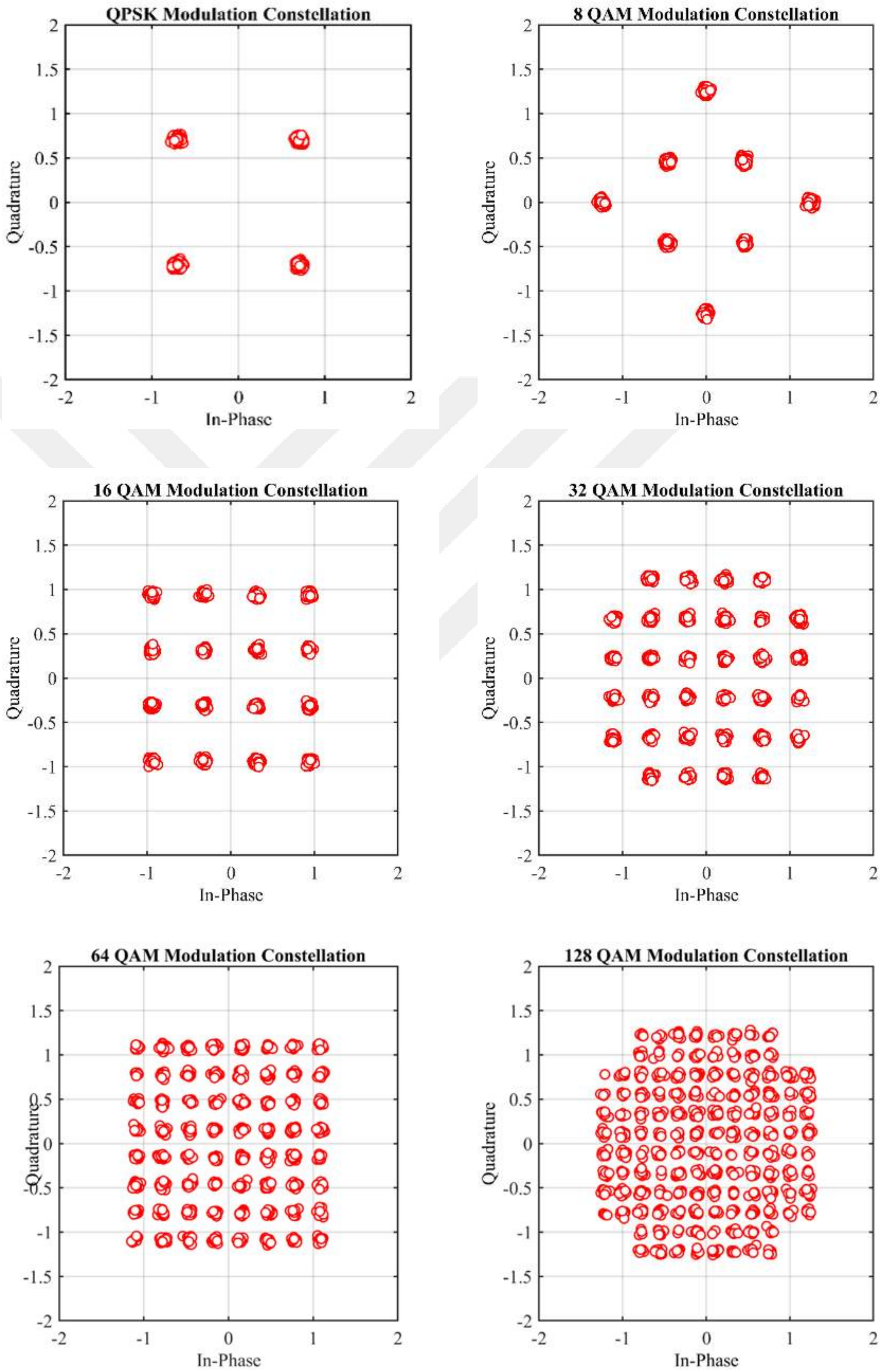

(a) Constellation diagram of 4-, 8-, 16-, 32- and 64-QAM.

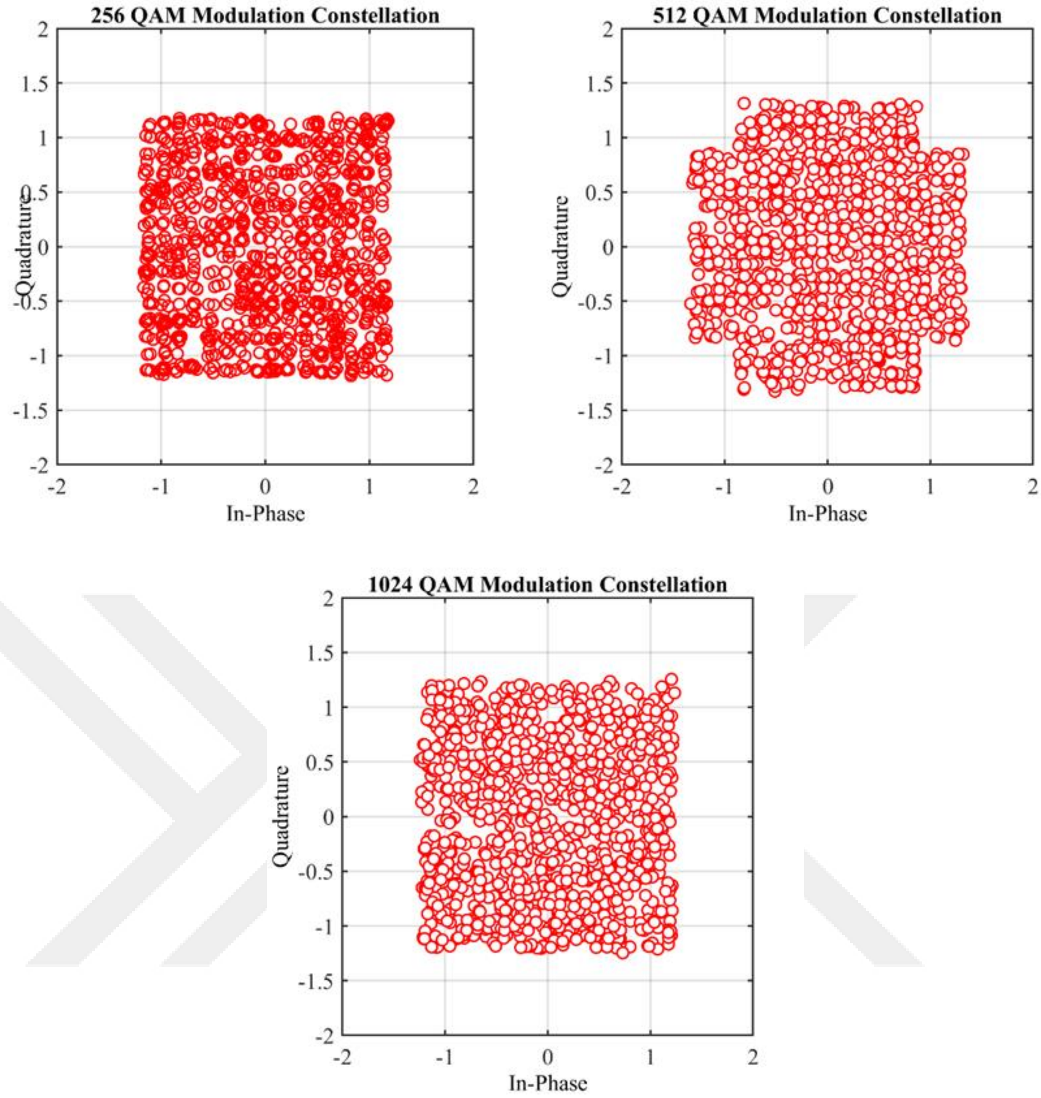

(b) Constellation diagram of 256-, 512- and 1,024-QAM.

Figure 4.1 Constellation points obtained on the receive at SNR 20 dB for {4~1024} QAM modulation schemes.

The dataset is generated as follows:

- **Training phase**

The goal of the training phase for the DT-logarithmic classifier is to elucidate the optimum threshold values in each node by minimising the error between the classifier output and the correct decision. These thresholds were set using the results of direct observations of the feature distributions garnered in a training set of simulated signals with 10,000 signals for each SNR of −5 to 20 dB. In this regard, there exist 260,000 records for each signal.

- **Testing phase**

In the testing phase, the multiple tree classifier requires only the threshold values in each node from the training data. Therefore, testing is performed by taking 10,000 realisations of each value at each SNR (−10 to 20 dB). Here, a total of 310,000 elements is available for each modulated signal.

4.4 Proposed Features Enhancement Approach

Below some theoretical analyses are listed, by assuming that two logarithmic functions denoted $f_1(\mathrm{x}_1)$ and $f_2(\mathrm{x}_2)$ carrying different vector form variable as "x1, x2" but having the same base value "n" which can be written as seen in Equations (4.1):

$$f_1(x_1) = \log_{\mathrm{n}}[\mathrm{x}_1]$$
$$f_1(x_2) = \log_{\mathrm{n}}[\mathrm{x}_2] \tag{4.1}$$

where the range of variables $x_1 \neq x_2$ and the base value are considered to be the same. The ratio between $f_1(\mathrm{x}_1)$ and $f_2(\mathrm{x}_2)$ as seen in Equation 4.2.

$$W(x_1, x_2) = \frac{\log_{\mathrm{n}}[\mathrm{x}_1]}{\log_{\mathrm{n}}[\mathrm{x}_2]} = \frac{\ln[\mathrm{x}_1]/\ln(\mathrm{n})}{\ln[\mathrm{x}_2]/\ln(\mathrm{n})} \tag{4.2}$$

In general, the logarithmic equations can be expressed into another equivalent form, written as seen in Equation 4.3.

$$\log_n[x_1] = \frac{\ln[x_1]}{\ln(n)} \tag{4.3}$$

Since,$\ln[x]$ is a log function, it can also be expressed as $\log_r[x]$, where 'r' represents the base value of the natural logarithm function. At the same time, Equation 4.3 can be rewritten as seen in Equation 4.4.

$$W(x_1, x_2) = \frac{\ln[\mathrm{x}_1] / \ln(\mathrm{n})}{\ln[\mathrm{x}_2] / \ln(\mathrm{n})} \tag{4.4}$$

Due to the equality between the numerator and $\ln(\mathrm{n})$ as the denominator, the base part $\ln(\mathrm{n})$ has been eliminated. This yields the result expressed as seen in Equation 4.5

$$W(x_1, x_2) = \frac{\ln[\mathrm{x}_1]}{\ln[\mathrm{x}_2]} \tag{4.5}$$

where the x_2 is a constant value of '10', making $\mathrm{w}(x_1, x_2)$ a constant as well the logarithmic functions are defined based on High order cumulants. The logarithmic expression formula in Equation 4.6 shows the modified high-order cumulants in terms of logarithmic formulae. The modification not only makes these features insensitive to noise variations but also help the classifiers to classify a number of modulation types with high-order levels.

$$\begin{aligned} f_a &= \log_{10}(|\mathrm{C}_{11}|) \\ f_b &= \log_{10}(|\mathrm{C}_{22}|) \\ f_c &= \log_{10}(|\mathrm{C}_{33}|) \\ f_d &= \log_{10}(|\mathrm{C}_{44}|) \end{aligned} \tag{4.6}$$

4.4.1 Normalisation and the scaling features method

Machine learning can process different types of signals such as audio signals and pixel values of image data, where these signals can involve multiple dimensions. In this case, for the feature normalisation, the value of each modulated signal in the dataset has a zero-mean (achieved by subtracting the mean value of each sample in the dataset) and also shows unit variance. This method is extensively used to normalise input data to numerous machine learning algorithms such as SVM, logistic regression and ANN. The general calculation method aims to determine the distribution mean of a data-row and the minimum and maximum values of data rows. The general formula of the standardisation technique is represented in Equation 4.7 [151].

$$\grave{y} = \frac{y - M_y}{Max(y) - Min\ (y)} \tag{4.7}$$

where y is an original value, $\grave{y}$ is the normalised value.

- **Dataset generation for features extraction**

The signal generation of 4- to 1,024-QAM consists of a signal length N = 4,096 with a phase offset of $\pi/_6$ determined by taking the statistical average value, as shown in Figures 4. 2, 4.3, 4.4 and 4.5, where the distribution curve of each feature has varying values of the SNR. Through verification by using simulation, it is clear that the feature distribution curve is not significantly affected by the variation of noise. However, this modification ensures a greater degree of improvement in achieving classification activity.

4.4.2 Features selection for classifier

The large magnitude of cumulants is represented as a critical problem in M-QAM classification. Therefore, the set of HOCs chosen as a vector of features must be of a reasonable magnitude and offer active discrimination among QAM schemes. Thereby, the modified cumulant designed by a natural logarithmic function provides excellent separation between QAM schemes, considering the parameter f_a: $\log_{10}\|C_{11}\|$ (which is M_{11}) as demonstrated in Figure 4.2. However, under low values of SNR, this parameter is close to the mean of M-QAM schemes of interest. Accordingly, this parameter is proper at an SNR of 0 dB or greater.

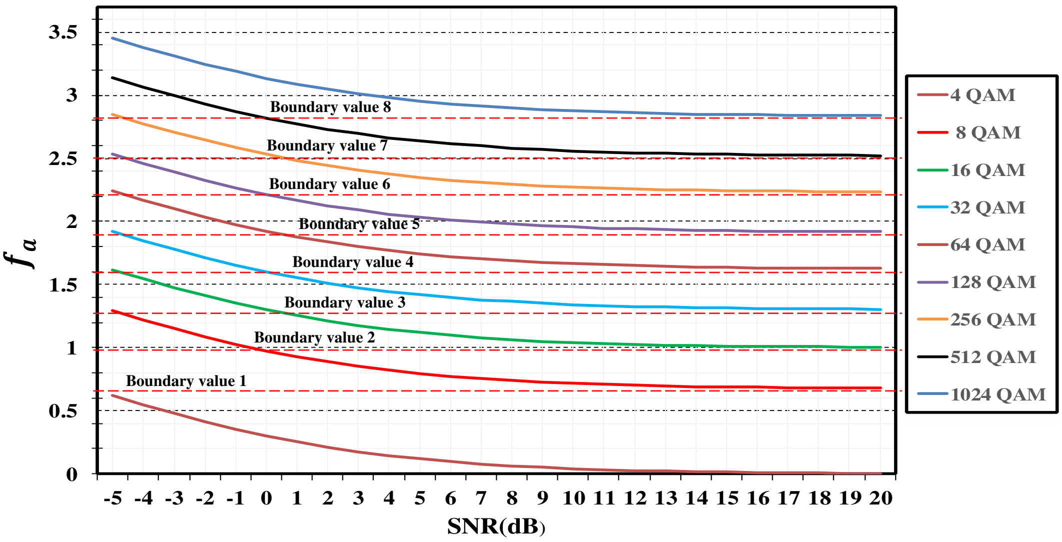

Figure 4.2 Feature 'f_a' distribution curve vs. SNR with the test of 10,000 signal realisations from 4- to 1,024-QAM, where each consists of the signal length N = 4,096 with a phase offset of $^{\pi}/_{6}$.

The most effective modification parameter that can be used for separation among M-QAM schemes is f_b: $\log_{10}\|C_{22}\|$. As can be seen in Figure 4.3, the distributions of this parameter are almost constant for all interest schemes and all SNR ranges. This parameter has the following approximate thresholds for interest signals: 2 for 8-QAM, 2.5 for 16-QAM, 3 for 32-QAM, 3.5 for 64-QAM, 4 for 128-QAM and 4.5 for 256-QAM. The most significant merit of this parameter is less sensitivity against noise variations. Thus, it will be considered as a foremost feature for the classification of considered M-QAM schemes. Furthermore, it provides excellent separation among QPSK or 4-QAM and other QAM schemes, as demonstrated in Figure 4.3.

Accordingly, this parameter is proper to use to discriminate among 4-QAM and other QAMs, as is explained via Equation 4.8.

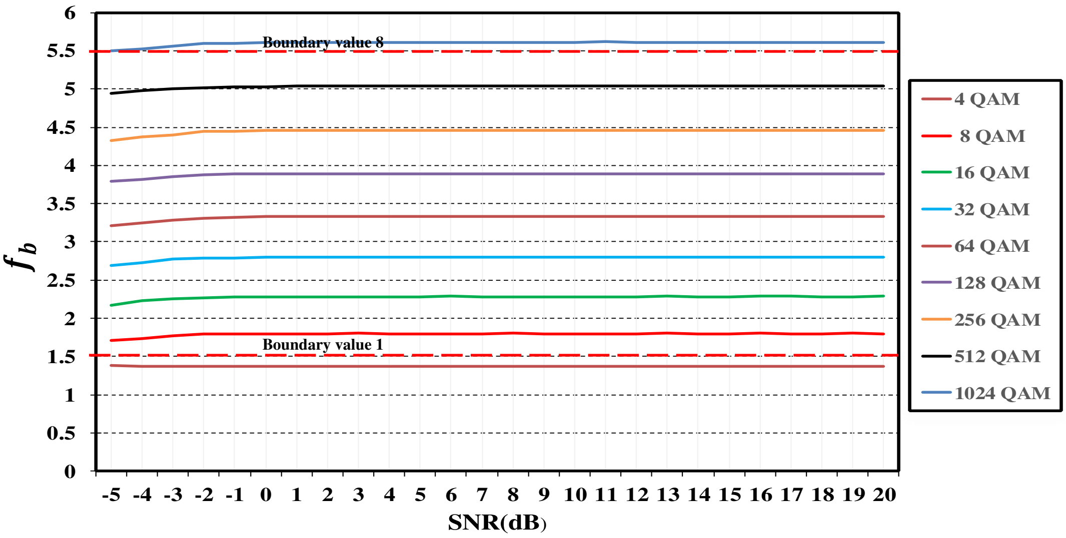

Figure 4.3 Feature 'f_b' distribution curve vs. SNR with the test of 10,000 signal realisations from 4- to 1,024-QAM, where each consists of a signal length N = 4,096 with a phase offset of $^{\pi}/_{6}$.

$$\text{The signal scheme is} \begin{cases} 4-\text{QAM} & \text{if} \log_{10}|\text{C}_{22}| < 1.5 \\ \quad \text{QAM} & \text{if} \log_{10}|\text{C}_{22}| \geq 1.5 \end{cases} \tag{4.8}$$

Another modified parameter useful for separating between QAM schemes is the cumulant C_{33}, which is transformed by logarithmic function to f_c: $\log_{10}\|C_{33}\|$. The distribution of this parameter is shown in Figure 4.4. It appears that the magnitude value of this parameter yields an attractive separation among considered signals. However, it has an approximately large value relative to some consideration schemes such as 512-QAM or 1,024-QAM. Therefore, the advantage of logarithmic transformation applied to the cumulant C_{33} is to make implementation further simplify.

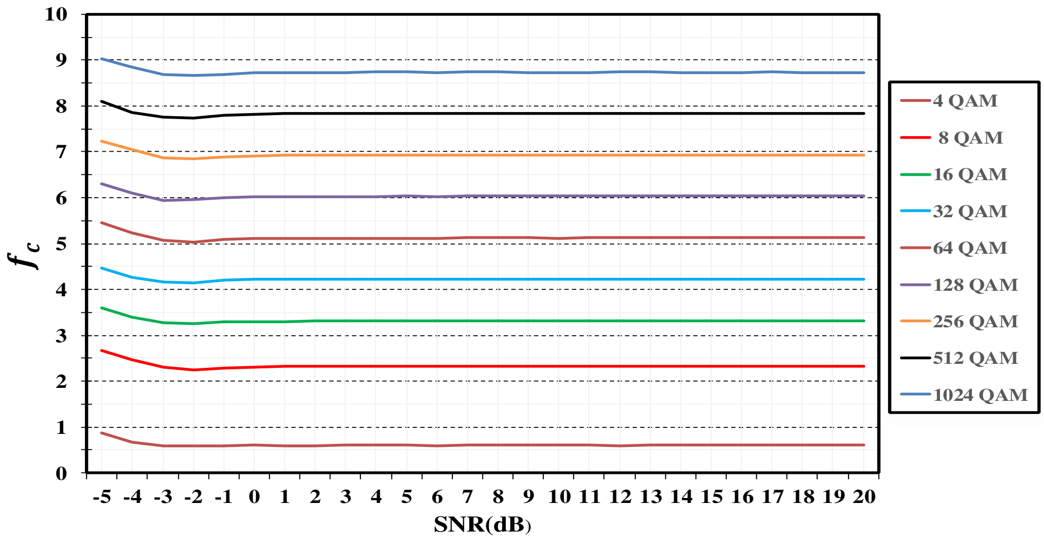

Figure 4.4 Feature 'f_c' distribution curve vs. SNR with the test of 10,000 signal realisations from 4- to 1,024-QAM, where each consists of a signal length N = 4,096 with a phase offset of $^{\pi}/_{6}$.

In some classification cases, to improve the classifier efficiency, an additional feature must be computed and added to the extracted feature vector. Thereby, the cumulant C_{44} is transformed by using logarithmic function to f_d: $\log_{10}\|C_{44}\|$. The logarithmic transformation in this parameter will offer a significant degree of improvement to a separation between considered schemes. Especially, when the SNR is greater than 2 dB, as can be demonstrated in Figure 4.5, the transformed feature has a reasonable discrimination boundary for nine M-QAM signals.

More concisely, the boundary distances of parameters f_a: $\log_{10}\|C_{11}\|$ are shown in Figure 4.2, whereas the transformed parameter f_d: $\log_{10}\|C_{44}\|$ appears in Figure 4.5. As mentioned formerly, the values of parameters f_a and f_d are used for separating between considered schemes at an SNR below 0 dB and SNR of no more than 1 dB, respectively.

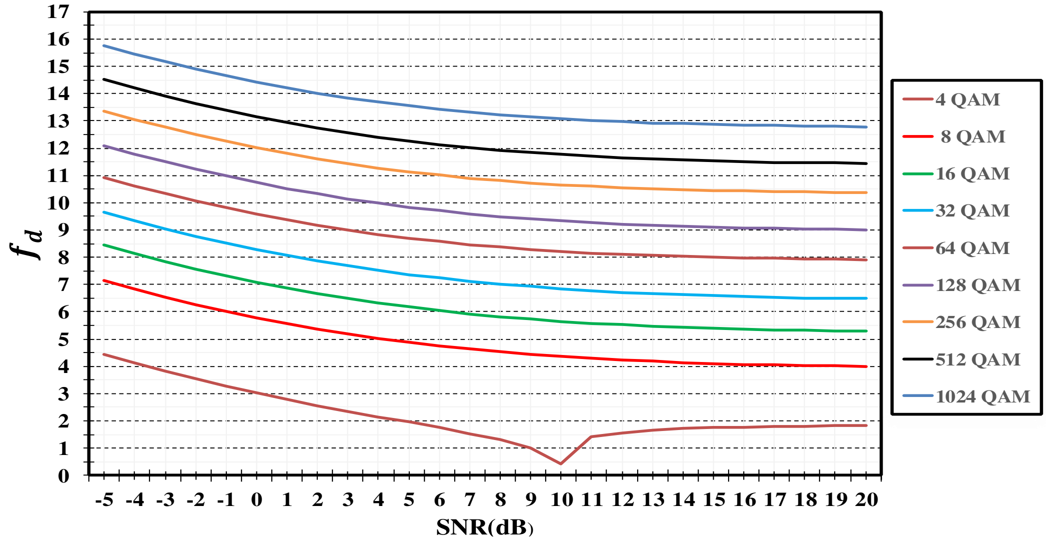

Figure 4.5 Feature 'f_d' distribution curve vs. SNR with the test of 10,000 signal realisations from 4- to 1,024-QAM, where each consists of a signal length N = 4,096 with a phase offset of $^{\pi}/_{6}$.

4.5 Proposed Classifiers

Based on the proposed parameters, three structures of the classifiers are presented to evaluate the preference of proposed parameters: two are conventional types, i.e., the neural network classifiers MLP and RBF, whereas the third classifier is a new classifier suggested by this work. This novel classifier encompasses a hybrid type of multi-threshold decision-making based on the properties of the logarithmic function, which is known as a logarithmic classifier. The logarithmic threshold decision classifier (LTDC) decides the demanded features based on upon the order of M-QAM for enhanced distinguishing of the M-QAM modulations. However, if the magnitude of the $f_b\text{:}\log_{10}\|C_{22}\|$ or $f_c\text{:}\log_{10}\|C_{33}\|$ is less than 1.5, then the received signal is estimated as a 4-QAM scheme. More details about the LTDC are presented in sub-section 4.5.1. The general procedure of the AMC system is shown in Figure 4.6, while the actual decision procedure of the proposed algorithm is demonstrated in Figure 4.7.

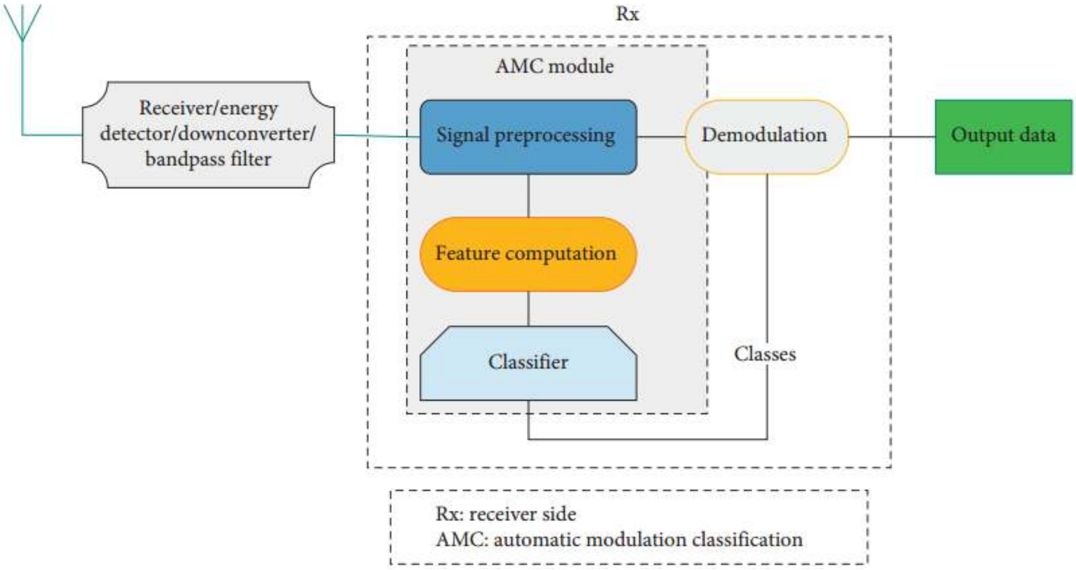

Figure 4.6 The procedure for automatic modulation classification.

4.5.1 The new hybrid multi-threshold M-QAM logarithmic classifier

Four cumulant parameters were derived in section 4.4 by using logarithmic properties to obtain an optimum quality to recognise the M-QAM signals under the AWGN channel. The magnitude value for each parameter was adopted to be the input vector to the proposed M-QAM logarithmic threshold decision classifier. According to the graphical representations of these parameters found in Figures 4.2, 4.3, 4.4 and 4.5, the threshold levels were determined upon the linearity of the features curves according to each parameter; this approach yields a highly effective recognition rate even with a minimum value of SNR.

The LTDC, consisting of four symmetrical structures of decision threshold-classifiers, is the formulation used for four subclassifiers. The identification decision is decided based on a decision tree, as depicted in Figure 4.7. The four sublogarithmic classifiers work simultaneously in this context in a logical manner.

Besides, the structure of each subclassifier is established using the parameter $f_x\colon \log_{10}\|C_{s\,s}\|$, where $ss = 11, 22, 33$ and 44, respectively. Table 4.1 represents feature thresholds that were set empirically. The decisive decision regarding which type of M-QAM signal was received can be expressed using algorithm 1 and algorithm 2. The architecture of subclassifier two was established using the most significant parameter as $f_b: \log_{10}\|C_{22}\|$. So, If the output of this subclassifier is high relative to other subclassifiers' outputs, then this output would be the ultimate choice for the classifier.

The Boolean equation (Equation 4.9) illustrates the logic decision process, while Figure 4.8 demonstrations the block diagram of the M-QAM logarithmic recognition algorithm, which is posterior to implementing an extension of the proposed method in real-time easily.

Algorithm 1 formally describes the procedures for the feature's extraction and the recognition decision. On the other hand, during the features extraction procedure, the input is represented by the data row after being modulated in the M-QAM signal. However, the $s_i = d_x$ signal may pass through a noisy channel $s_i = d'_x$. The first step in selection is fetching $C_{11}, C_{22}, C_{33}, \text{or} C_{44}$, after computing the logarithmic transformation to each element in the cumulant's vector; with this, the process of the logarithmic classification is begun.

To start, one must test whether $\{f_{a_0} < f_x(\varphi_0)\}$; if so, then $\text{index}_1 = 1$ for the 4-QAM signal.

Else, $\text{if}\{f_{x_i} \geq f_x(\varphi_i) \&\& f_{x_i} \leq f_x(\varphi_i)\}\ \text{index}_i = \text{í}$, where $2^{n'}\text{QAM}, n' > 2, i > 1$ and $\text{í} > 1$.

The procedure will keep going for $\{f_{a_i}, f_{b_i}, f_{c_i}, f_{d_i}\}$ and increment the index I, until reaching I = 8.

Algorithm 2 formally describes the procedure of determining the candidate of the goodness classifier; here, the input is the $\{f_{a_i}, f_{b_i}, f_{c_i}, f_{d_i}\}$, i index.

$If\left(indexf_{a_i} == \text{í}\right)||\left(indexf_{b_i} == \text{í}\right)||\left(indexf_{c_i} == \text{í}\right)||\left(indexf_{c_i} == \text{í}\right)$ is true, then an increase in the index $CC_{\text{index SNR}}$ is apparent and the procedure continues until $\{f_{a_i}, f_{b_i}, f_{c_i}, f_{d_i}\}_{i=8}$.

It can be summarised that algorithm 2 is a logical operation that achieves the comparison as a sequential status of $\{f_{a_i}, f_{b_i}, f_{c_i}, f_{d_i}\}_i$.

Algorithm 1: Logarithmic classifier of high-order QAM modulation signals.

Input:	Generate a digital M-QAM modulation signal; $Dx = d_1 d_2\, d_3 .\ldots d_i$ *and* $x \in \{a, b, c, d\}$, $M = \{2^n\}$, $n = 2,3,4,5,6,7,8,9,10$ $s_i = d_x$; s_i *row of data after modulated by M-QAM signal*
Output:	$v \in$ index $\{ f_{a_i}, f_{b_i}, f_{c_i}, f_{d_i}\}$; *output boundary with index* $_i$
Step$_1$	$s_i = d'_x$; *corrupted by Gaussian random noise* Calculate *cumulants* $C_{11}, C_{22}, C_{33}, C_{44}$
Step$_2$	$f_{a_i} = \log_{10}[\lvert C_{11_i}(s_i)\rvert]$; $f_{b_i} = \log_{10}[\lvert C_{22_i}(s_i)\rvert]$; $f_{c_i} = \log_{10}[\lvert C_{33_i}(s_i)\rvert]$; $f_{d_i} = \log_{10}[\lvert C_{44_i}(s_i)\rvert]$;
Step$_3$	If $\{f_{a_0} < f_x(\varphi_0)\}$; 4-QAM index $_i = 1$;
Step$_4$	*Else, if* $\{f_{x_i} \geq f_x(\varphi_i) \&\& f_{x_i} \leq f_x(\varphi_i)\}$; *where* $2^{n'} QAM$; $n' > 2$, $i > 1$, $í > 1$ *index* $_i = í$;
Step$_5$	*Return v.*

Algorithm 2: Choosing a higher and better classifier.

Input:	$v \in$ index$\{ f_{a_i}, f_{b_i}, f_{c_i}, f_{d_i}\}_i$; *input boundary with index*
Output:	P_{CC_i}; probability of correct recognition
Step$_1$	*If* $(indexf_{a_i} == í)$ $\{\|(indexf_{b_i} == í)$ $\|(indexf_{c_i} == í)$ $\|(indexf_{d_i} == í)\}$; $CC_{index\ SNR} = CC_i + 1$; *correct rate counts* End
Step$_2$	*Return* P_{cc}.

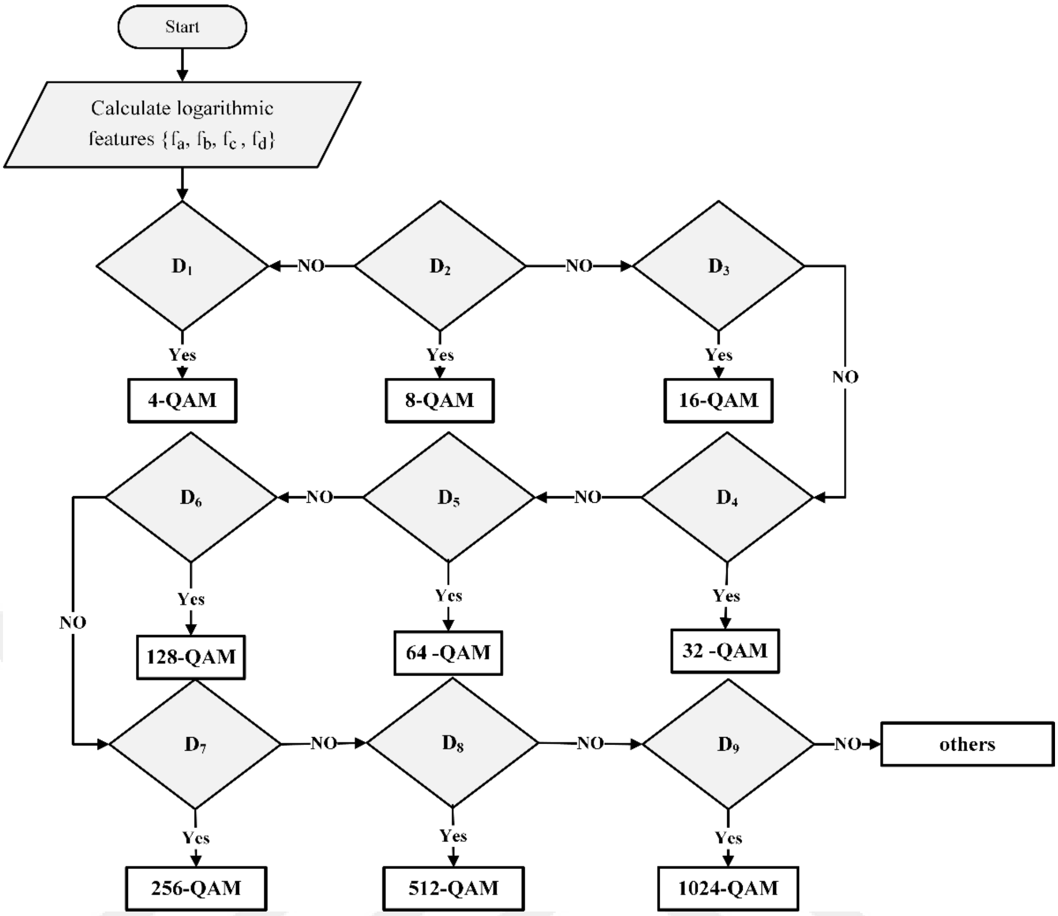

Figure 4.7 Flowchart of M-QAM recognition algorithm.

Table 4.1 Optimum threshold value for each logarithmic feature.

i	f_a	f_b	f_c	f_d
0	0.5	1.5	1.5	3
1	0.95	2.2	3	5
2	1.3	2.7	4	6.4
3	1.52	3.1	5	7.6
4	1.8	3.7	6.3	9
5	2.2	4.3	6.6	10
6	2.5	4.8	7.5	11
7	3	5.7	9	12
8	4.5	7.5	12.5	15.5

The mathematical expression of decision boundaries of the LTDC algorithm of high-order QAM signals are based on the threshold levels in Table 4.1 and decision tree chart in Figure 4.7.

For the input feature $D^{x}_{(1)}$, the threshold levels are taken from Table 4.1 at i = 0 and expressed as a logical status as

$$D^{x}_{(1)} = [f_a \geq f_a(\varphi_0) \& f_a < f_a(\varphi_2)]$$

Notice: í = $(i+1)$ for 4 QAM or QPSK only í $= 1$, likewise the expression of $D^{x}_{(i)>1}$ at $i > 0$ as

$$\begin{aligned}
D^{a}_{(i+1)} &= [f_a \geq f_a(\varphi_{i-1}) \& f_a < f_a(\varphi_{i+1})] \\
D^{b}_{(i+1)} &= [f_b \geq f_b(\varphi_{i-1}) \& f_b < f_b(\varphi_{i+1})] \\
D^{c}_{(i+1)} &= [f_c \geq f_c(\varphi_{i-1}) \& f_c < f_c(\varphi_{i+1})] \\
D^{d}_{(i+1)} &= [f_d \geq f_d(\varphi_{i-1}) \& f_d < f_d(\varphi_{i+1})] \\
D_i &= D^{a}_{(i+1)} || D^{b}_{(i+1)} || D^{c}_{(i+1)} || D^{d}_{(i+1)}
\end{aligned} \tag{4.9}$$

where $\boldsymbol{f_x(\varphi_i)}$ represents the threshold value for each one of the logarithmic features; $\boldsymbol{x} \in \{\mathbf{a}, \mathbf{b}, \mathbf{c}, \mathbf{d}\}$; and $i = 0, 2, 3, 4\ldots.8$ is the threshold count. Also, í = 1, 2, 3, 4….9 is a class pattern number of QAM signals that is recognised.

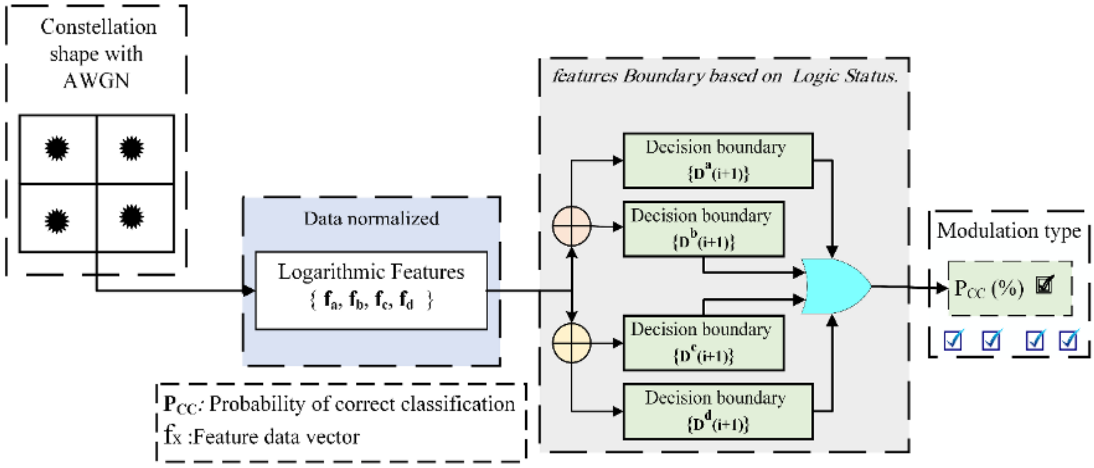

Figure 4.8 The block diagram of our logarithmic classification system.

Based on the flowchart, in Figure 4.7 and Equation 4.9 the SNR reneges from −10 to 20 dB.

- **Dataset generation for testing LTDC**

A total of 10,000 times the realisation of each signal of nine M-QAMs and SNRs then was used for testing the proposed logarithmic classifier. The phase offset was chosen $1/6\,\pi$ as bassline point during simulation analysed, while also using three different degrees to evaluate classifier accuracy.

The modulation classification method proposed in this study yielded some promising results; the simulation results are arranged in Figures 4.9, 4.10, 4.11, 4.12, 4.13, 4.14, 4.15 and 4.16, respectively. The classifier accuracy was estimated by using the probability of correct classification rate (P_{CC}) versus SNR, formulated as follows:

The classifier accuracy is estimated by using the “Probability of Correct Classification rate P_{CC}” versus SNR, which can be formulated as:

$$P_{CC} = \sum_{k=1}^{j} p(\omega_k|\omega_k)P(\omega_k) \tag{4.10}$$

Probability of Correct Classification rate % = P_{cc}.%100

In the same direction, the 'J' is the modulation signal candidate's classification ($\boldsymbol{\omega_1}, \boldsymbol{\omega_2}, \boldsymbol{\omega_3}, \boldsymbol{\omega_j}$), where P($\boldsymbol{\omega_k}$) represents the probability of the modulation scheme $\boldsymbol{\omega_k}$ and P($\boldsymbol{\omega_k}|\boldsymbol{\omega_k}$) is the probability of correct classification when a ($\boldsymbol{\omega_k}$) constellation is transmitted [152].

Promising results appear in Figures 4.9, 4.10, 4.11 and 4.12, suggesting that, when the SNR is 5 or greater, the correct recognition can top 99% albeit with variation in both sample length and phase offset.

In Figure 4.9, the P_{cc}% of the proposed LTDC at different SNRs and signal lengths was 4096 symbols. It can be observed from Figure 4.9 that the P_{cc} is better while the SNR is increased, due to enhancements of the quality of the transmission channel. In other words, the effect of white noise is lessened when the SNR is increased. It can be concluded from when the SNR increases that the P_{cc}% becomes even better; this fact comes from that the transmission quality is good when the SNR is high. Moreover, the probability of error symbols has decreased over the transmission channel.

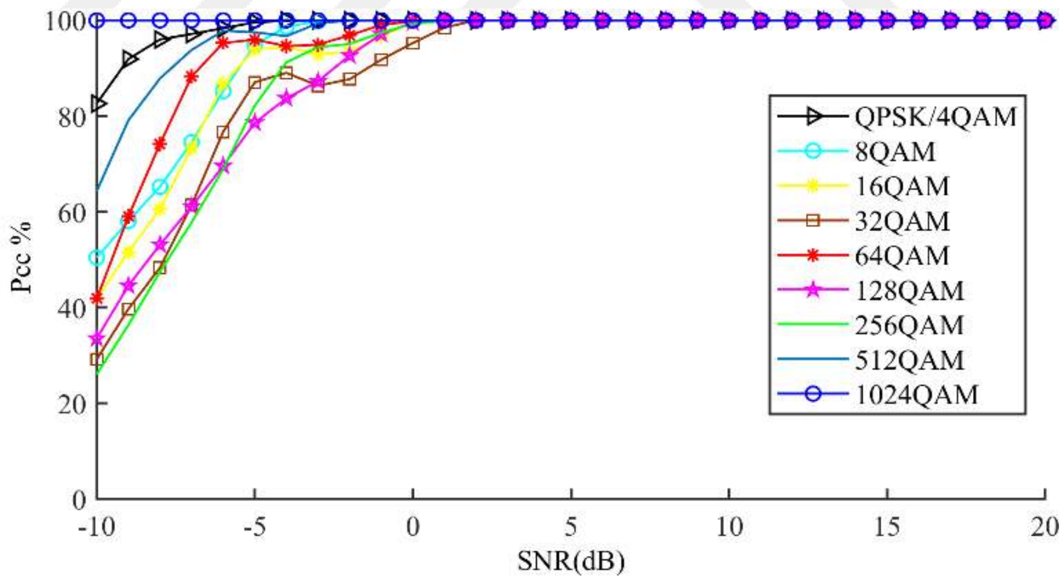

Figure 4.9 The P_{cc} vs. SNR with 10,000 signal realisations from 4- to 1,024-QAM each consists of a signal length N = 4,096 and phase offset of $\pi/6$.

Precisely evaluating the classifier accuracy is also necessary to observe the effect of the carrier phase offset. Figures 4.10 and 4.11 show the effect of phase offset on the proposed LTDC.

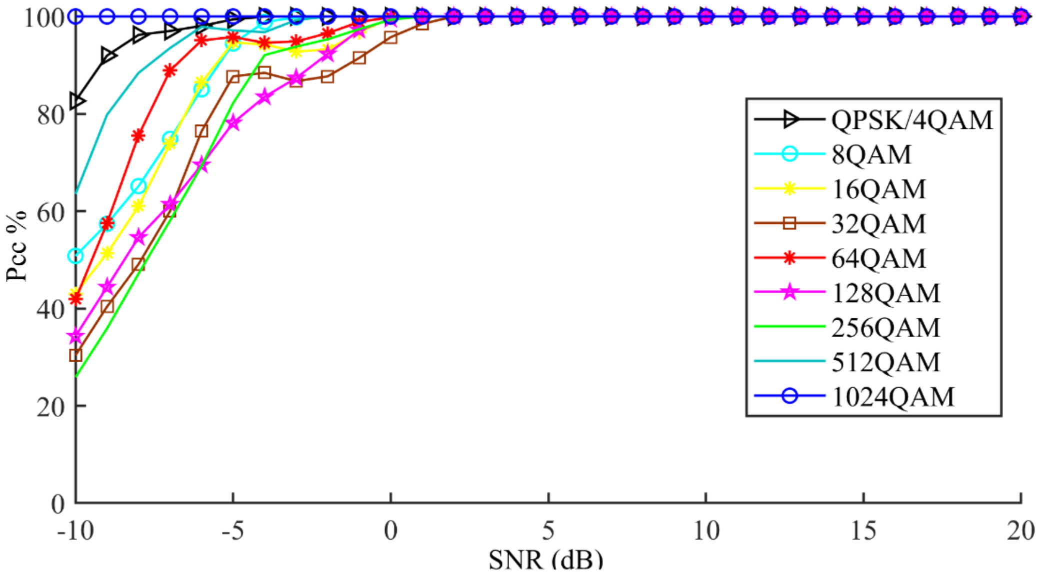

Figure 4.10 The P_{cc} vs. SNR with 10,000 signal realisations from 4- to 1,024-QAM each consists of a signal length N = 4,096 and phase offset of $^{\pi}/_{4}$.

It is worth noting that the LTDC is less impacted when changing the carrier phase offset as can be observed in Figure 4.10 at a phase offset of $^{\pi}/_{4}$and also in Figure 4.11 at a phase offset of $^{\pi}/_{3}$, while the signal length is fixed at 4,096 symbols.

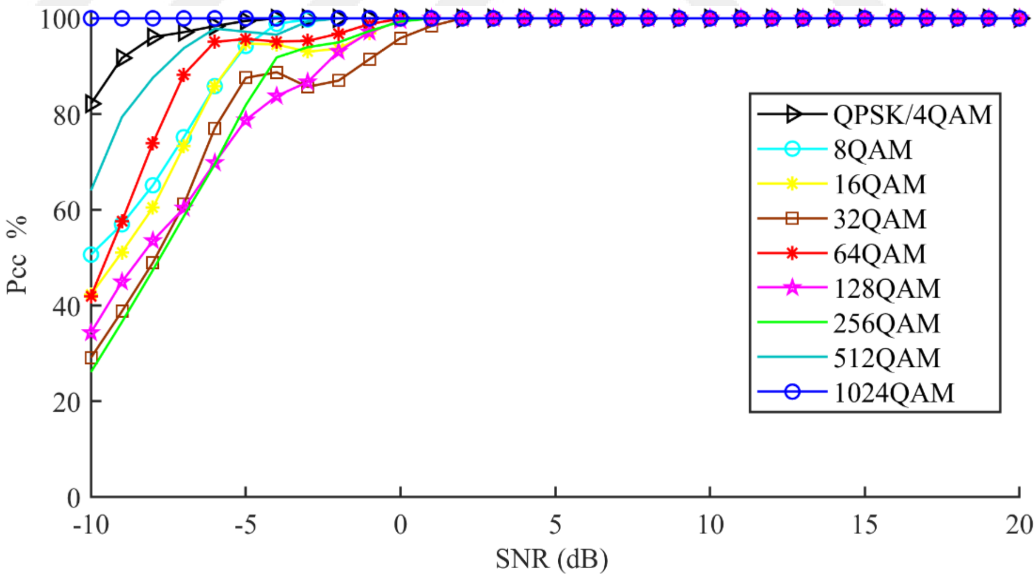

Figure 4.11 The P_{cc} vs. SNR with 10,000 signal realisations from 4- to 1,024-QAM consists of a signal length N = 4,096 and phase offset of $^{\pi}/_{3}$.

Figure 4.12 shows the performances of the proposed LTDC at varying signal lengths from 64 to 4,096, which changes randomly based on the signal's realisation to each

QAM. Meanwhile, the total signal realisation is 10,000 per QAM signal, the SNR is ranging from −10 to 20 dB and the phase offset is $\pi/_6$.

Figures 4.13 through 4.16, on the other hand, reveal the effects of different signal lengths on the correct recognition as 256, 512, 1,024 and 2,048, respectively and the impact of the phase offset of $\pi/_6$ is considered.

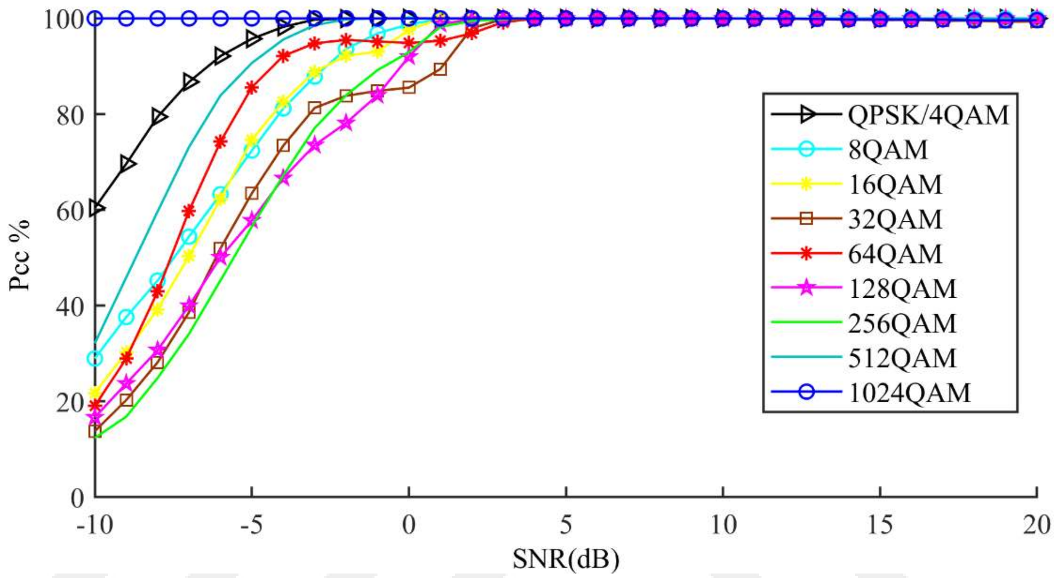

Figure 4.12 The P_{cc} vs. SNR with 10,000 signal realisations from 4- to 1,024-QAM each consists of a variable signal length (N = 64, 128, 265, 512, 1,024, 2,048, 4,096) and a phase offset of $\pi/_6$.

It is evident that the correct recognition level is less influenced when the signal samples randomly vary, as shown in Figure 4.12. It also can be underlined that the best accuracy can be achieved for all QAM signals with an SNR not less than 5 dB.

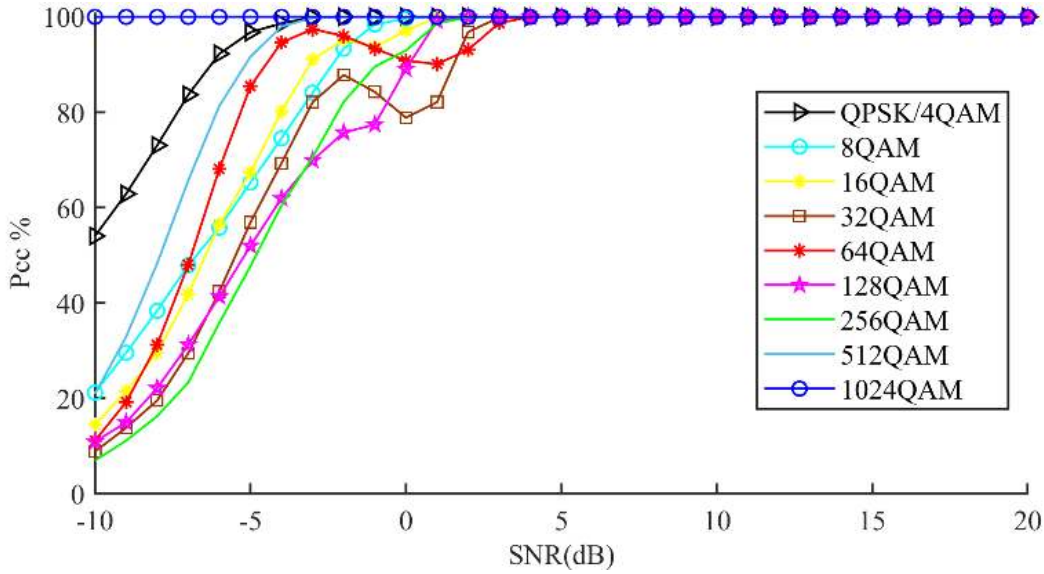

Figure 4.13 The P_{cc} vs. SNR with 10,000 signal realisations 4- to 1,024-QAM each consists of a signal length N = 256 and phase offset of $\pi/6$.

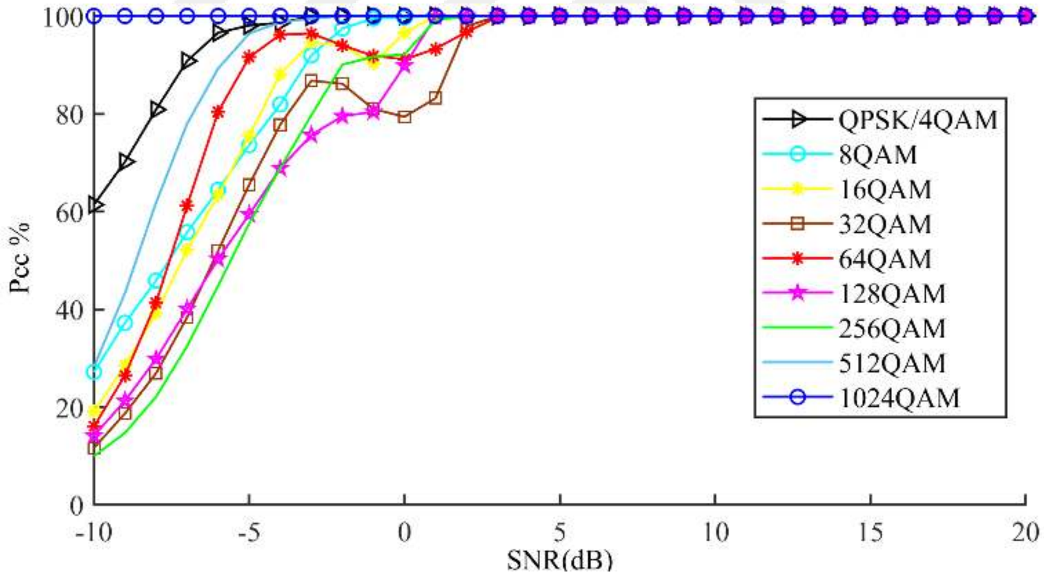

Figure 4.14 The P_{cc} vs. SNR with 10,000 signal realisations from 4- to 1,024-QAM each consists of a signal length N = 512 and phase offset of $\pi/6$.

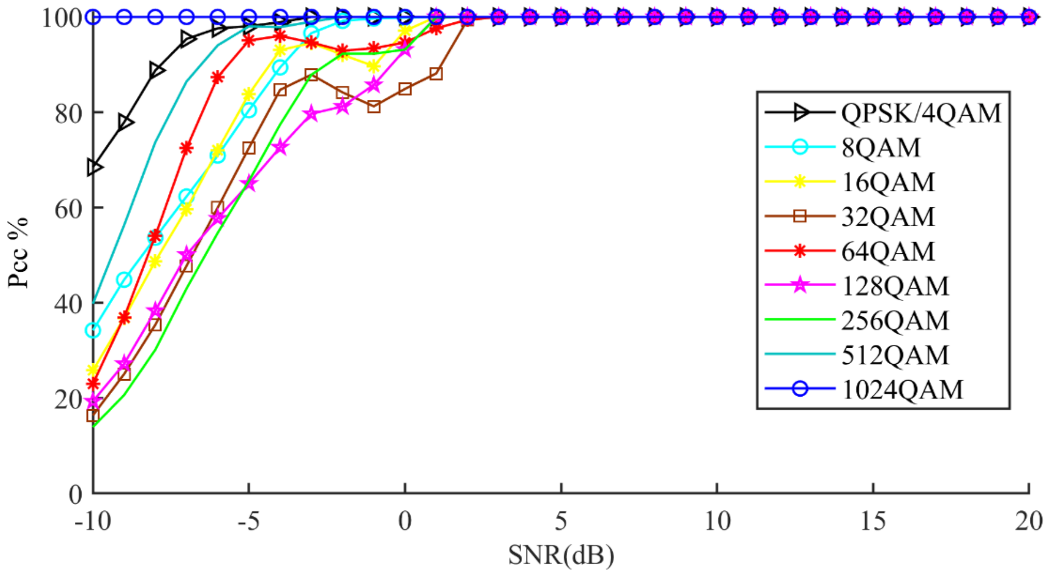

Figure 4.15 The P_{cc} vs. SNR with 10,000 signal realisations from 4- to 1,024-QAM each consists of a signal length N = 1,024 and phase offset of $\pi/6$.

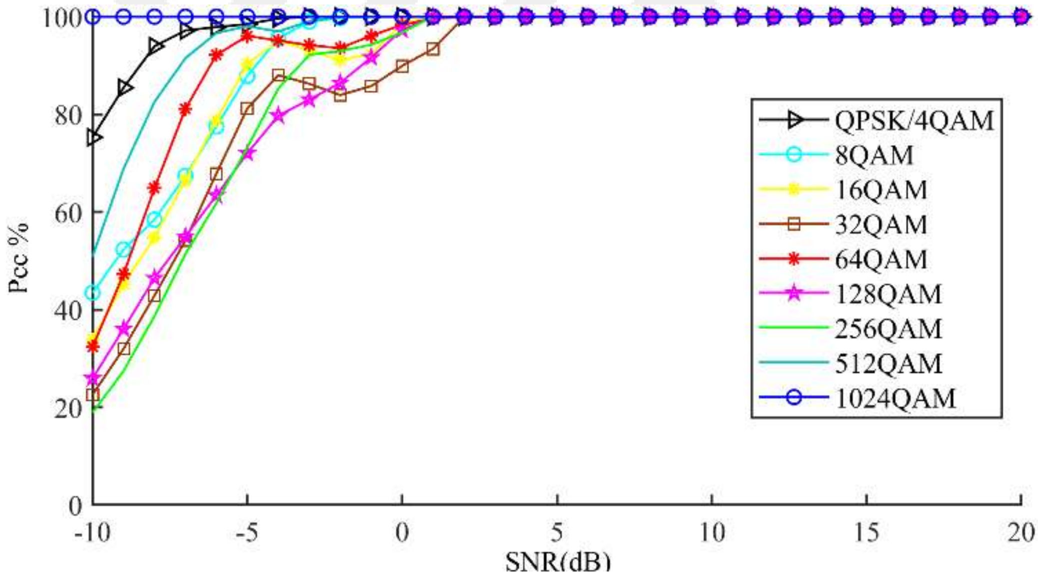

Figure 4.16 The P_{cc} vs. SNR with 10,000 signal realisations from 4- to 1,024-QAM each consists of a signal length N = 2,048 and phase offset of $\pi/6$.

4.5.2 Recording notes of the threshold M-QAM logarithmic classifier

The experiments were carried out in three stages in the presence of AWGN: first, the HOC features were extracted, then passed through the feature's modifier; the latter is a logarithmic classifier based on HOC. Second, a decision is made based on the thresholds algorithm, while the third stage sought to achieve the evaluation of P_{cc}%

for each modulation scheme. It appears from simulation results that the best performance curve is achieved when using a length of the sample of 4,096. However, this correct classification advantage is highest at SNR from −3 dB to 20 dB as had been shown in Figure 4.9.

On the other hand, the curve performance for the variable sample length (64, 128, 256, 512, 1,024, 2,048 and 4,096) indicates a converged accuracy in the same test range of the SNR, which could be observed in Figure 4.12. However, the $P_{cc}\%$ becomes lower when the number of samples transmitted is reduced. It was worth noting that the sample length was reduced as follows: 2,048, 1,024, 512 and 256.

The$P_{cc}\%$ is no less than 80% to 100% at SNR 0 to 20 dB, as shown in Figures 4.13, 4.14, 4.15 and 4.16, respectively. The high level of classification accuracy recorded at different signal lengths and phase offsets could be the reason for this when considering the logarithmic cumulants.

However, when the SNR ≥ -5 classifier accuracy deteriorates but does not collapse, the correct classification rate reaches below 75% and the phase offset will be considered as shown in Figure 4.10. which were the phase offset of $^{\pi}/_{4}$ and signal length of 4,096.

Figure 4.11, on the other hand, includes a phase offset of $^{\pi}/_{3}$. The LTDC gives a consistent correct recognition rate of about 99.7%, in the range of the noise variation of SNR from 2 to 20 dB. It was well-observed that, when the phase offset is changed, the $P_{cc}\%$ is almost equal, due to the high robustness of the internal structure of the logarithmic classifier. Meanwhile, the superior classification accuracy of the LTDC that was gained even despite changing the transmitted signal length and phase offset could be attributed to the efficiency of the logarithmic cumulants.

4.5.2.1 Evaluating the accuracy and complexity using other methods

For assessing the complexity of the classification algorithm, this research suggests adopting a different modulation classification method among the conventional options [16,103].

The proposed classification method required different logarithm operations. Nevertheless, it is still crucial given the high P_{cc}% and reduced process requirements to calculate cumulant orders. At the same time, other studies have not highlighted these promising lines of thought [17,21,137,153,154]. Although cumulant-based classifier methods were convenient to cope with the M-QAM modulation recognition, such does not provide a sufficient classification rate under a fading channel and it also can produce missing classification in some conditions. In contrast, the LTDC of M-QAM signals show better PCC% values at different SNRs.

The performance of the proposed LTDC of M-QAM is superior among previously introduced systems given its ability to distinguish between high-order and very-high-order QAM signals. Thus, due to the unprecedented demand for wireless communication technology expected to reach an estimated 7.6 billion users in 2020, it can be considered that the proposed logarithmic classifier is one of the essential pillars for future classification techniques [155].

According to Table 4.2, the fourth-order cumulant classifier shows the lowest complexity. In contrast, the combination among the fourth-, sixth- and eighth-order cumulant classifiers displayed the highest level of complications due to the involvement of exponential operations. However, it is worth it to clarify that the logarithmic classifier proposed in this thesis depends on an attractive combination among the lowest and highest orders of HOC; these combinations create a classifier that has advantages of less complexity and higher accuracy. The complexity of several methods proposed that have been used in previous works were compared in detail, as shown in Table 4.2. It appears very clearly that the logarithmic classifier has a higher level of classification accuracy of modulation schemes 4- to 1,024-QAM, which similarly achieved a high percentage when the SNR was 5 or greater.

Table 4.2 Comparisons between proposed classifiers according to other systems in the literature.

Reference	Classifier structure			Modulation Type		System performance		Simulation tool
	Cumulants	Complexity		M-QAM	MPSK	SNR (dB)	Accuracy (%)	
[17]	C_{40}, C_{41}, C_{42}, C_{60}, C_{61}, C_{62}, C_{63},	{(3)4^{th}, (4)6^{th}}	High	16, 64	4	−3	#	MATLAB functions are invoked to implement and evaluate performance
						0	#	
						≥ +5	78.4%–100%	
[154]	C_{40}, C_{41}, C_{42}, C_{60}, C_{61}, C_{62}, C_{63},	{(3)4^{th}, (4)6^{th}}	High	16, 32, 64	2,4	−3	#	
						0	#	
						≥ +5	89.8%–100%	
[103]	C_{11}, C_{22}, C_{33}, C_{44},	{(1)1^{th}, (1)2^{th} (1)3^{th}, (1)4^{th}}	Medium	16, 32, 64, 128, 256	#	−3	98.33%	
						0	100%	
						≥ +5	100%	
[21]	C_{20}, C_{21}, C_{40}, C_{41}, C_{42}, C_{60}, C_{61}, C_{62}, C_{63}	{(2)2^{th}, (3)4^{th}, (4)6^{th}}	High	16, 64, 256	2,4,8	−3	#	
						0	#	
						≥ +5	89.8%–100%	

Table 4.2 Continued.

[153]	C_{20}, $C_{21,}$, $C_{40,}$, $C_{41,}$ C_{42}, $C_{60,}$$C_{61,}$$C_{62,}$ C_{63},C_{80}, $C_{81,}$$C_{82,}$ C_{83}, C_{84}	{(2)2th, (3)4th (4)6th, (5)8th}	High	16, 64, 256	2,4,8 and others	−3	#
						0	#
						≥ +5	Unknown
[137]	C_{20}, $C_{21,}$, $C_{41,}$, $C_{42,}$ C_{63}	{(2)2th, (2)4th, (1)6th}	Medium	16, 64, V.29	4	−3	60%
						0	81%
						≥ +5	90%
[16]	C_{20}, $C_{21,}$, $C_{40,}$, $C_{41,}$ C_{42}	{(2)2th, (2)4th, (1)6th}	Medium	8, 16, 32, 64	4, 8, 16, 32 64	−3	26%
						0	45%
						≥ +5	95%
Proposed	Logarithmic cumulant	{(1)1th, (1)2th (1)3th, (1)4th}	Medium	(8–1,024)	4	−3	75%–95%
						0	80%–98%
						≥ +5	100%

Abbreviations:* ‘~ ‘refers from M-QAM to M-QAM,* **‘,’** *M-QAM and M-QAM, note that the signal length N = 4,096.* #not covered

For other scenarios, the results are shown in Figure 4.17, while Figure 4.18 presents the performance degradation of the classification of QAM signals versus their performance in the AWGN channel. It is not difficult to sense the reason for why performance degradation occurs from the multipath channel fading and Doppler fading effects model. The weakness performance of cumulant-based classifiers with fading channels has been previously documented [134]. However, for the logarithmic classifier, the classification accuracy maintains the same level typically at an SNR of greater than 5dB, despite that the different fading channel model has been used.

4.5.3 Robustness evaluation cases

a. Under different channels model

Research in the modulation classification of digital signals approximately started 40 years ago and the robustness of conventional AMC methods under AWGN channels has been well-established in the literature [79,156,157]. Similarly, some investigations confirmed that communication researchers typically use the AWGN channel model in the development of telemetry communication systems [80,158].

Although the channel corruption by AWGN alone could be a proper model for the degradation of signals in free space, the existence of physical obstructions such as buildings and towers can cause multipath propagation losses in transmitted signals.

The effectiveness of the LDT classifier has also been investigated in AWGN with precise, fast frequency-selective fading together with the effect of Rayleigh and Rician magnitude channel fading. In contrast, the phase was randomly distributed and was assumed to be constant through the symbol period, which indicates no loss in signals occurred.

The specifications used were based on research by Molisch et al. [159]. a symbol rate of 3.84×10^6 symbols per second; average path gains of 0, -0.9, -4.9, -8, -7.8 and -23.9 dB; path delays of zero, two, eight, 12, 23 and 37×10^{-7} seconds; and a maximum Doppler shift of 5 kHz. Figures 4.17 and 4.18 depict the probability of the correct recognition rate at a signal length of 4,096 in AWGN plus fast frequency selection at a max ambit of 50 kHz of maximum Doppler shifts in both channels of the Rician and Rayleigh fading model, respectively.

In addition to that, Figures 4.19 and 4.20 show the probability of a correct recognition rate with a variable signal length in AWGN plus fast frequency selection at a max ambit of 50 kHz of maximum Doppler shifts in both channels of the Rician and Rayleigh fading model, respectively.

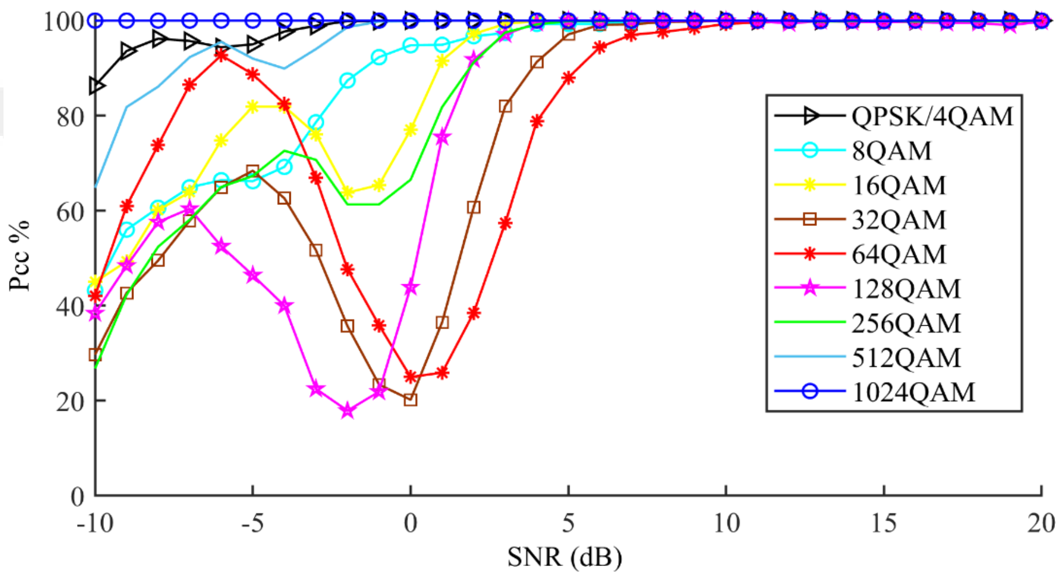

Figure 4.17 The P_{cc} vs. SNR with 10,000 signal realisations from 4- to 1,024-QAM each consists of a signal length N = 4,096 and phase offset of $\pi/6$ under effect in AWGN, plus a fast, frequency-selective Ricean fading channel with $f_D = 5$ kHz.

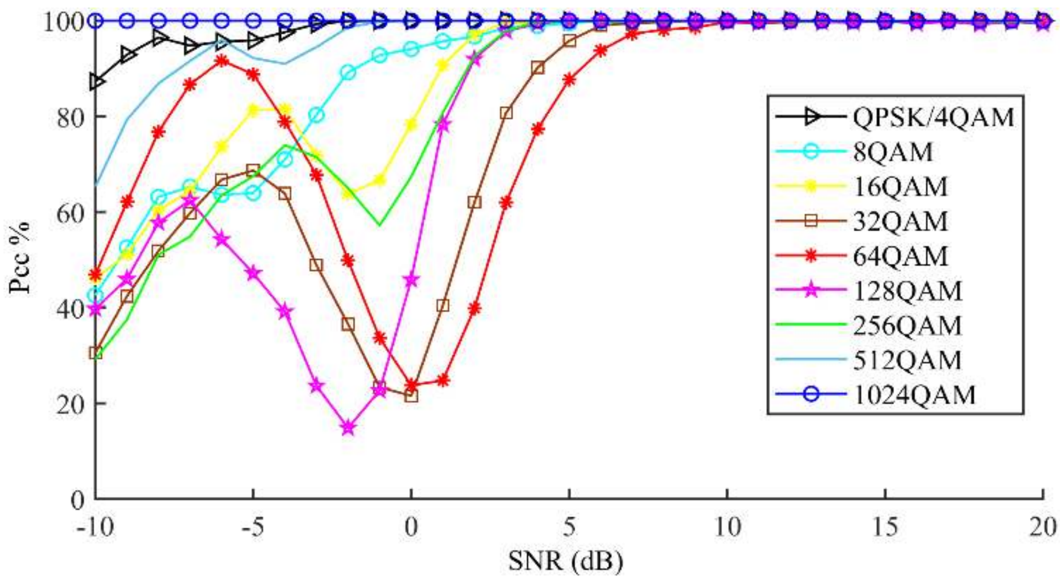

Figure 4.18 The P_{cc} vs. SNR with 10,000 signal realisations from 4- to 1,024-QAM each consists of a signal length N = 4,096 and phase offset of $\pi/6$ under effect in AWGN, plus a fast, frequency-selective Rayleigh fading channel with $f_D = 5$ kHz.

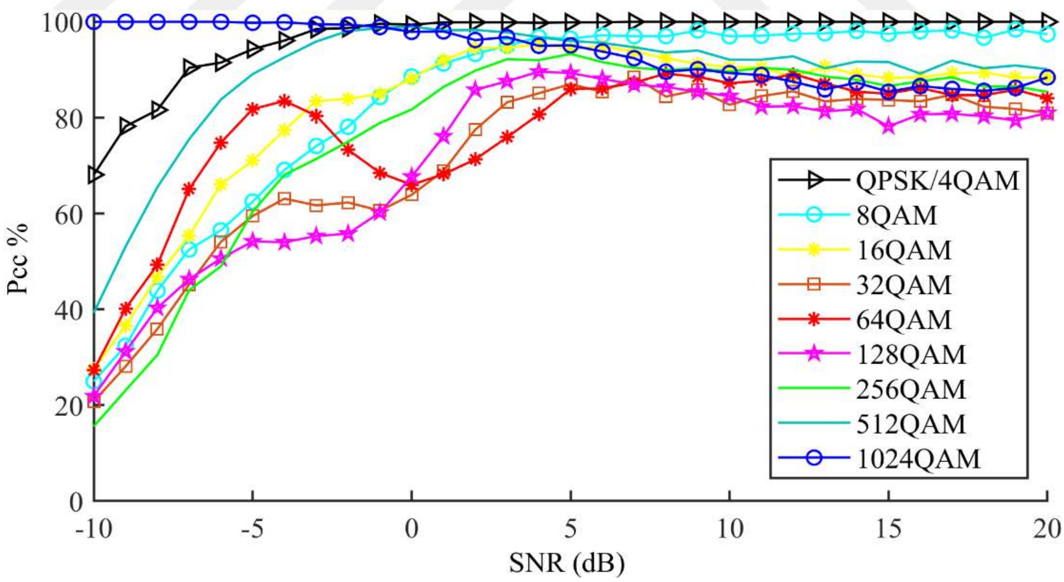

Figure 4.19 The P_{cc} vs. SNR with 10,000 signal realisations from 4- to 1,024-QAM; each consists of variable signal lengths (N = 64, 128, 265, 512, 1,024, 2,048 and 4,096) and a phase offset of $\pi/6$ under effect in AWGN, plus fast, frequency-selective Ricean fading channel with $f_D = 5$ kHz.

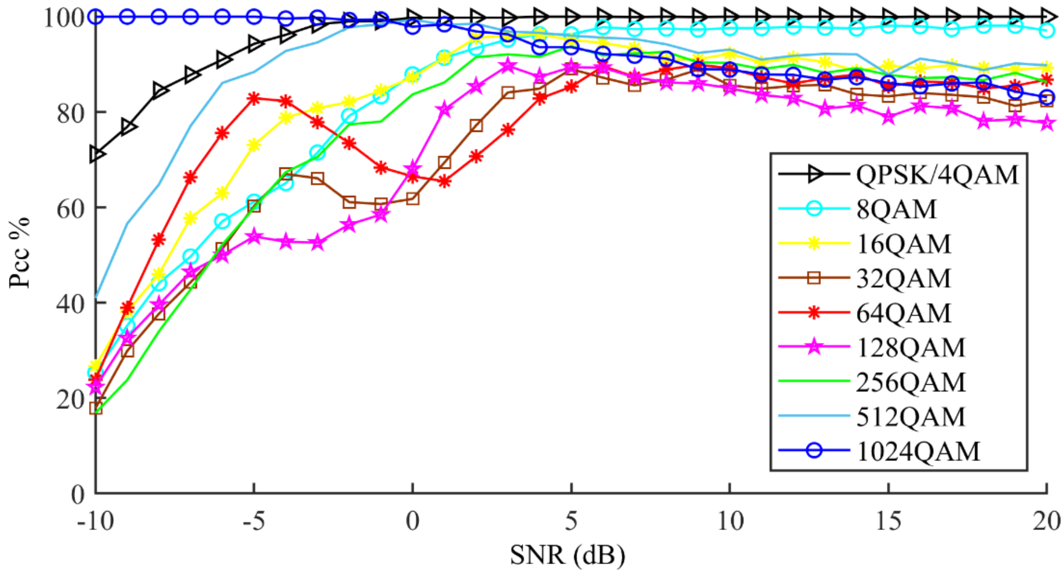

Figure 4.20 The P_{cc} vs. SNR with 10,000 signal realisations from 4- to 1,024-QAM; each consists of variable signal lengths (N = 64, 128, 265, 512, 1,024, 2,048 and 4,096) and phase offset of $\pi/6$ under effect in AWGN, plus fast, frequency-selective Rayleigh fading channel with $f_D = 5$ kHz.

As could be observed in Figures 4.17 and 4.18, respectively, signal propagation via multipath transmission yields an accepted correct classification rate at an SNR that is not lower than 4 dB, although with the presence of an effect of Doppler shift.

Also, it could be observed from Figures 4.17 and 4.18 that the correct classification rate at an SNR of more than 4 dB is approximately higher for Rician fading channels than Rayleigh fading channels; this variation in performance is due to the signal-strength difference given the existence of line-of-sight propagation. It is strongly noted that higher Doppler-shift effects produce a lower possibility of the correct classification [159]. As a contrast to conventional classifiers, the current logarithmic classifier provides unanticipated performance even with the existence of the Doppler shift and the signal is transmitted with a randomly variable length of between 64 to 4,096 symbols. It is also important to underline that the proposed classifier yields safe satisfactory results under both the Rician and Rayleigh fading channels environments.

As could also be observed in Figures 4.16 and 4.17, mainly, at an SNR of lower than −2 dB, the correct classification rate has fallen to less than 80%, especially for 32-, 64-, 128- and 256-QAM signals, which could be observed when the SNR is lower than 0 dB. The intra-class classification by using the logarithmic classifier provides different results based on the M-QAM schemes. For example, the simulations in this study illustrated that this identification would be reasonable for 1,024-QAM and 512-QAM schemes than for other modulation schemes. Whereas, when the SNR is not lower than 0 dB, the results explain that the Pcc% offers the lowest percentage for 32-QAM and 64-QAM signals, which can be observed in Figures 4.17, 4.18, 4.19 and 4.20.

It is also important to mention that overlapping in the correct recognition rate of high-order QAM signals can happen and is due to the internal structures of the logarithmic classifier.

It seems that the effect of variation in frequency offset of the transmitted signals is almost an insignificant influence on the logarithmic classifier, albeit under SNR = −2 and random signal lengths. Figure 4.21a and Figure 4.21b depict the probability of a correct classification rate vs. frequency offset and signal length N = 4,096. Likewise, as could be noted in the same Figure 4.21b, the probability of correct classification rate vs. frequency offset with a variable signal length and signals is corrupted by AWGN.

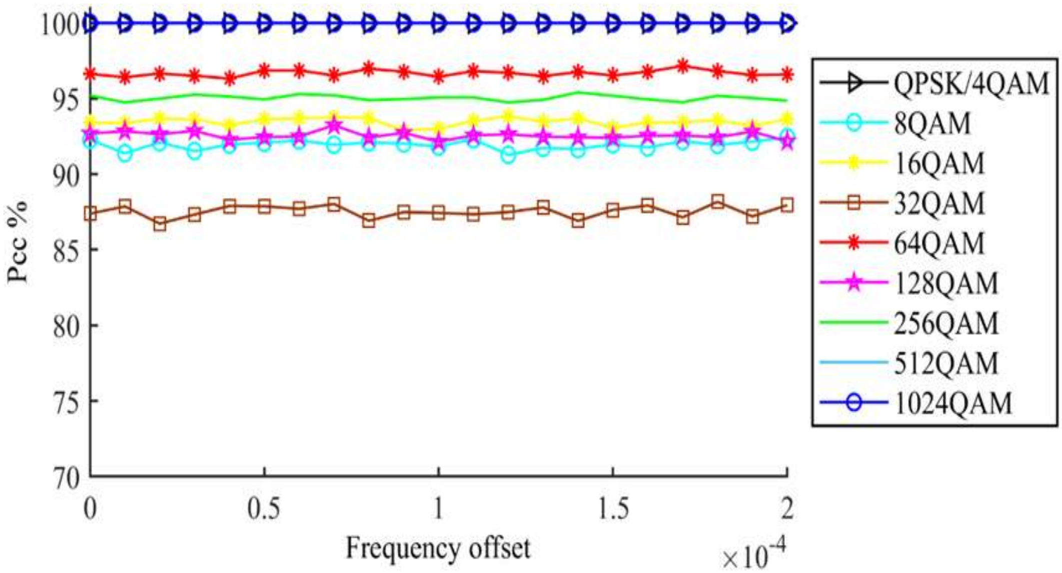

(a) The P_{cc} vs. frequency offset and signal length N = 4,096.

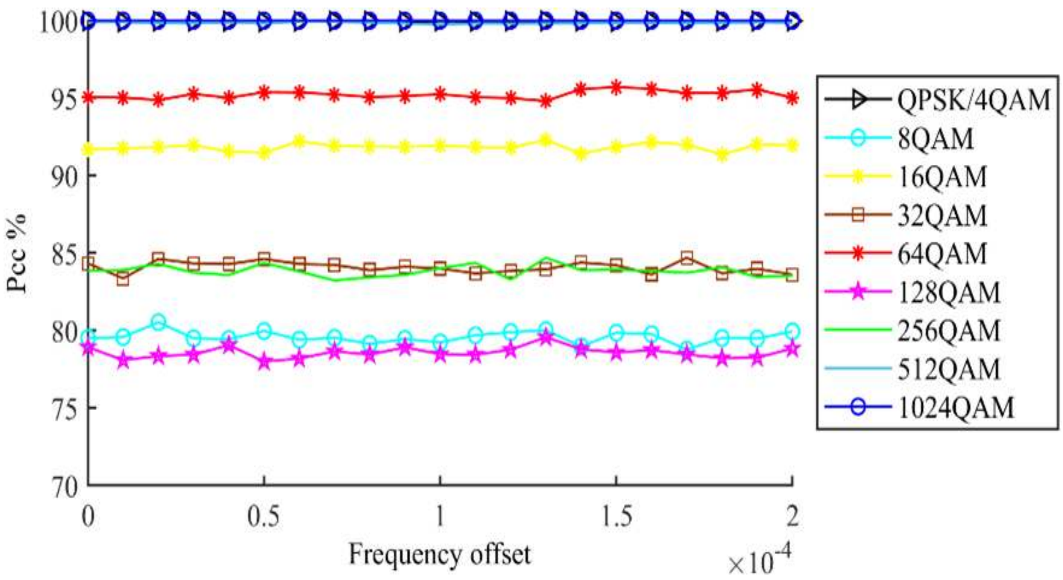

(b) The P_{cc} vs. frequency offset with variable signal length (N = 64, 128, 265, 512, 1,024, 2,048 and 4,096 phase offset of $\pi/6$.

Figure 4.21. The effect of frequency offset to logarithmic classifier for 4- to 1,024-QAM with 10,000 signals under the effect of AWGN-only SNR = −2 dB.

This end could be an important point during consideration of the proposed classifier among AMC methods that have tested the influence of the offset frequency to the transmitted signal. In the same direction, Figure 4.22 shows a change in the number of transmitting symbols vs. the probability of the correct classification rate. It is also well-observed that the proposed method has a better classification rate than the proposed algorithm in [153], even with noise circumstances at SNR = −2 dB in the AWGN channel. Eventually, the logarithmic classification algorithm may not be the best option, but it has facilitated the process of classification of high-order QAM signals. Nevertheless, degradation points of the logarithmic classifier are that it is a channel-dependent model. Any differences in the type of noise (coloured vs. AWGN), the number of transmitting signals present in the channel and the type of possible modulated signals require an overhaul of all four tree threshold levels.

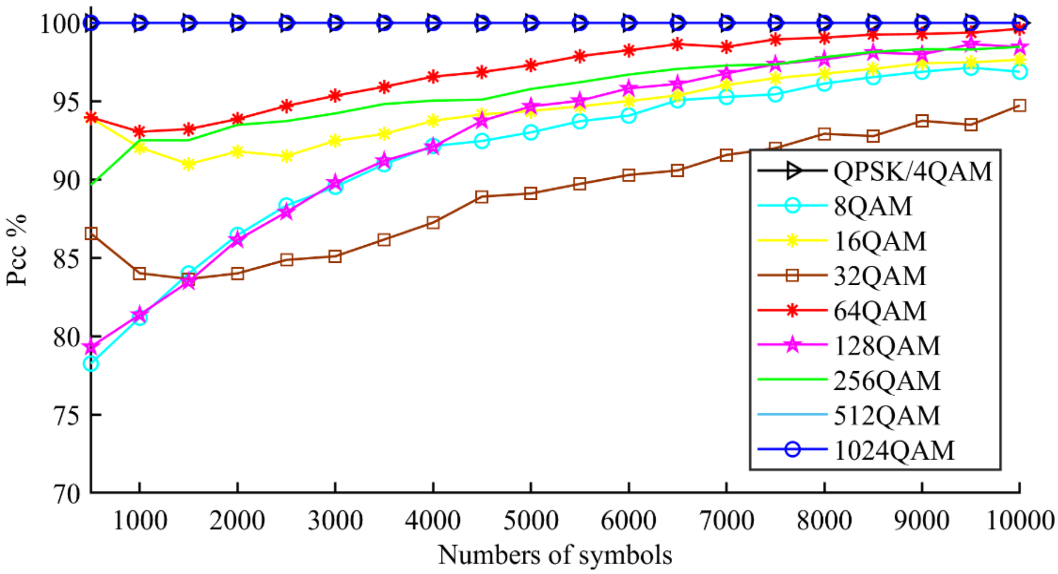

Figure 4.22 The P_{cc} vs. number of symbols of SNR with 10,000 signal realisations from 4- to 1,024-QAM, phase offset of $\pi/6$ and signal degradation under the effect of AWGN-only SNR = −2 dB.

4.5.4 General Trends on Threshold M-QAM Logarithmic Classifier

Unlike traditional AMC algorithms, the logarithmic classifier has functional features, which make them preferable classifiers for the medium- and high-order M-QAM modulation schemes. Likewise, the logarithmic classifier is handy for channels that only receive corruption by AWGN. The prominent results related to the AWGN channel without a fading effect have shown very good performance. The classification of higher-order modulation signals is more challenging than low-order signals due to the distance between the constellation points being small. However, on the other hand, the probability of correct classification is hampered by disparity, especially for low-order modulation schemes at the expense of schemes that have a smaller constellation point's distance. Therefore, to this end, it might be concluded that more research is needed on the LTDC, particularly when the SNR is not less than 0.

Although cumulant-based classifier schemes with many variations constitute a convenient way to cope with M-QAM modulation classification, the cumulant's feature of signal or uncoordinated combinations among cumulants and moments does not provide sufficient classification under multipath fading channels and produces contrast in the classification rate. It is also notable that this classifier technique is not integrated in terms of being utilised with a fixed threshold and there exist various ways to determine threshold levels automatically that will boost the classification process and classifier sensitivity to desired modulation schemes. However, a comprehensive review reveals that the logarithmic classifier with a fixed threshold has overcome all weaknesses, even in a severely noisy environment and under multipath propagation channels. In the same direction, the work presented in this chapter gives references that will help researchers to make progress in the direction of a new generation of AMC systems, so-introduced with the logarithmic classifier.

4.5.5 Conclusion about the results of the threshold M-QAM logarithmic classifier

This section of chapter four presents a method that transacts with high-order M-QAM modulation recognition under the effect of the AWGN channel and usage cumulant-based natural logarithmic characteristics with a fixed-threshold classification algorithm.

The combination between high-order cumulants and properties of the logarithmic functions has created a new generation of cumulant-based classifier that provides superior performance to classify high-order M-QAM signals even with a low range of SNR.

Simulation results indicated that the correct classification rate can top 92% when the SNR is −4 dB under the AWGN channel, even as it seems moderate over different fading effects. Based on the comparison with recently proposed algorithms in the literature, the performance of the logarithmic classifier proposed in this thesis is efficient and also shows less complexity.

4.6 Training Sets of Nonlinear Classifiers MLP and RBF

A total of 260,000 samples was generated for each QAM scheme to train the presented neural network structures. Each signal scheme includes 4,096 symbols. It is worth mentioning that all modulated signals by M-QAM were transmitted through AWGN. This channel is represented as a typical noisy channel model that reflects all weak points in the design of any communication system. In the training phase, the SNR changes from −10 to 20 dB with a padding of 1 dB.

At the same time, the feature vector composes four logarithmic cumulants. Accordingly, the size of the training dataset as a block to each SNR is equal to features vector multiplied by the number of realisations for the n-class of the M-QAM scheme.

It is worth noting there are some gains when utilising the characteristic of the logarithmic function with cumulants features which helps to normalised results among high-, medium- and low-magnitude cumulants. That will be making the magnitude of cumulants takes approximately level. For example, it provides normalised values between large-magnitude cumulants such as $C_{11}$and C_{44}.

In the case of MLP classifiers, a feed-forward MLP structure is developed in this part of the present work to classify the high-order modulated signals of M-QAM schemes. The network structure is learned by applying back-propagation supervised criteria.

The selected features are applied to the network as the input vector. Typically, in the binary PR method, the number of nodes in the output layer refers to the interest classes. Similarly, as seen in the MLP neural network structure, the RBF structure includes the same number of input and output neurons, except that the first and second hidden layers involve the radial basis function (RBF).

4.6.1 Evaluation of the logarithmic features with MLP classifier to recognise M-QAM

The structure of the network includes two hidden layers; the first hidden layer consists of eight neurons, while the second includes 12 neurons. This network model is used to construct the 4- to 1,024-QAM classifiers. According to the logarithmic cumulants that are extracted as signal parameters for the M-QAM recogniser, these features are (f_a: $\log_{10}\|C_{11}\|$, f_b: $\log_{10}\|C_{22}\|$, f_c: $\log_{10}\|C_{33}\|$ and f_a: $\log_{10}\|C_{44}\|$. Thus, the input layer composes four source nodes. On the other side, nine neurons in the output layer are determined to identify one of the nine M-QAM signals.

The nonlinear activation function of the first and second hidden layers is hyperbolic tangent sigmoid (tan-sigmoid) and log-sigmoid, respectively. At the same time, the SoftMax transfer function is used for the output layer. Resilient backpropagation is implemented to learn this network.

The curve of the best performance of this network is shown in Figure 4.23. The classification performance reaches 100% when the same training datasets are used.

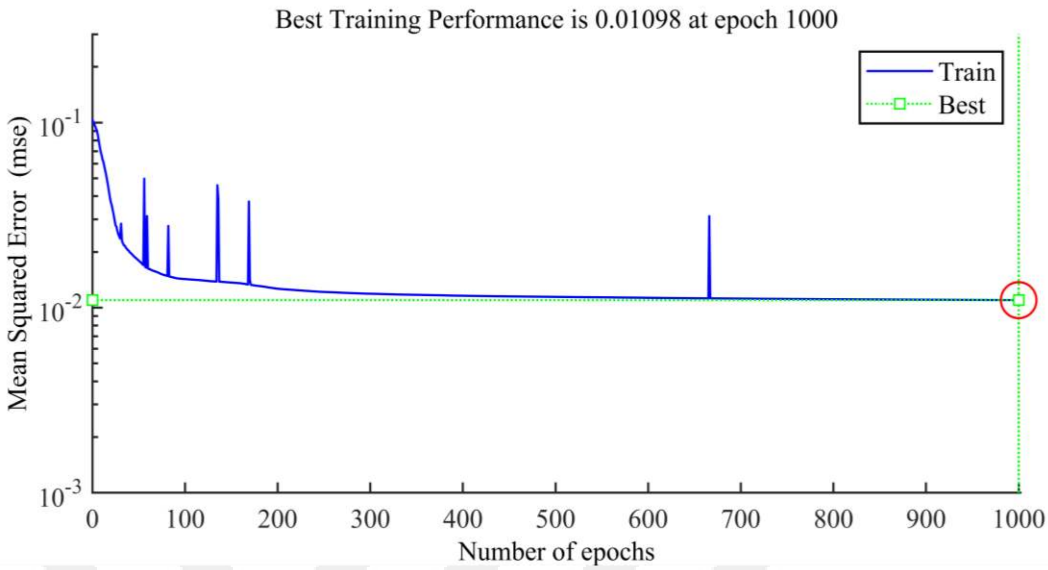

Figure 4.23 Training characteristics of logarithmic features combined with the MLP classifier to recognise the M-QAM scheme.

Nine schemes of M-QAM modulated signals with the order of 4-, 8-, 16-, 32-, 64-, 128-, 256-, 512- and 1,024-QAM were used to measure the success rate and to evaluate the logarithmic cumulants with a nonlinear classifier. In this case, the MLP network was used as a decision-maker. The combination of logarithmic cumulants and MLP network can provide reasonable performance, as shown in Figure 4.24.

The probability of the success classification rate has appeared good in some SNR cases but not so well with others, especially in the case of very low SNRs—for example, in the case of an SNR of −10 dB, the success classification rate becomes zero for the QAM signals 16-QAM, 32-QAM, 64-QAM, 128-QAM, 256-QAM and 512-QAM.

The classification accuracy of the MLP classifier in classifying the considered M-QAM signals are seemingly below the classification accuracy of the LTDC classifier. However, in order to get a guarantee for low misclassification rates, this classifier can be appropriate for the practical design in case of noise of more than −5 dB.

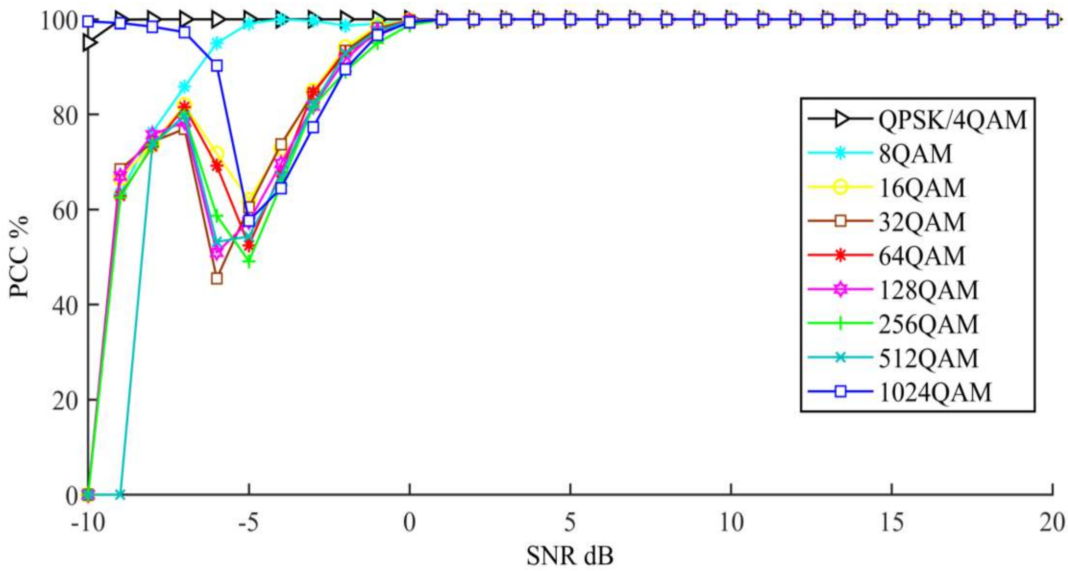

Figure 4.24 The P_{cc} vs. SNR of logarithmic features combined with MLP classifier for identification of the 4- to 1,024-QAM scheme; each consists of a signal length N = 4,096 and phase offset of $^{\pi}/_{6}$.

4.6.2 Evaluation of the logarithmic features with RBF classifier to recognise M-QAM

The M-QAM classifier is constructed depending on four modified cumulants as signals attributed to the RBF neural network. The RBF classifier is used for recognising nine QAM schemes by using logarithmic cumulants as vectors consisting of four elements, which have been described before (f_a: $\log_{10}\|C_{11}\|$, f_b: $\log_{10}\|C_{22}\|$, f_c: $\log_{10}\|C_{33}\|$ and f_a: $\log_{10}\|C_{44}\|$). After feature optimisation, the multi-layer RBF network was used as the classifier, which achieved superior performance in AMC techniques as previously reported [160]. The extracted features arranged as vectors in the dataset $\widehat{\Psi}$ are employed as the input and the output $\varphi(\widehat{\Psi})$ can be written as follows:

$$\varphi(\widehat{\Psi}) = \sum_{j=1}^{q} W_j\, \rho(\widehat{\Psi}, C_j), \qquad (4.11)$$

where q is the number of hidden layer neurons and C_j and W_j are the centre and weight of the j^{th} hidden-layer neurons, respectively. Here, $\rho(\widehat{\Psi}, C_j)$ indicates the RBF, which is the Euclidean distance with respect to $\widehat{\Psi}$ and C_j and is determined by

$$\rho(\widehat{\Psi},C_j)=e^{-\mu_j\|\widehat{\Psi}-C_j\|^2}. \tag{4.12}$$

The RBF neural network is trained in two stages. First, the random sampling method was used to compute C_j. Subsequently, the back-propagation algorithm is used to evaluate W_j and μi. Figure 4.25 shows the training performance of the logarithmic magnitude of the cumulants' features combined with the RBF classifier. In the learning phase, the dataset had a similar size to the dataset that has been used for training the MLP classifier. The performance of the RBF classifier does not provide significant improvement as compared with that of the MLP classifier.

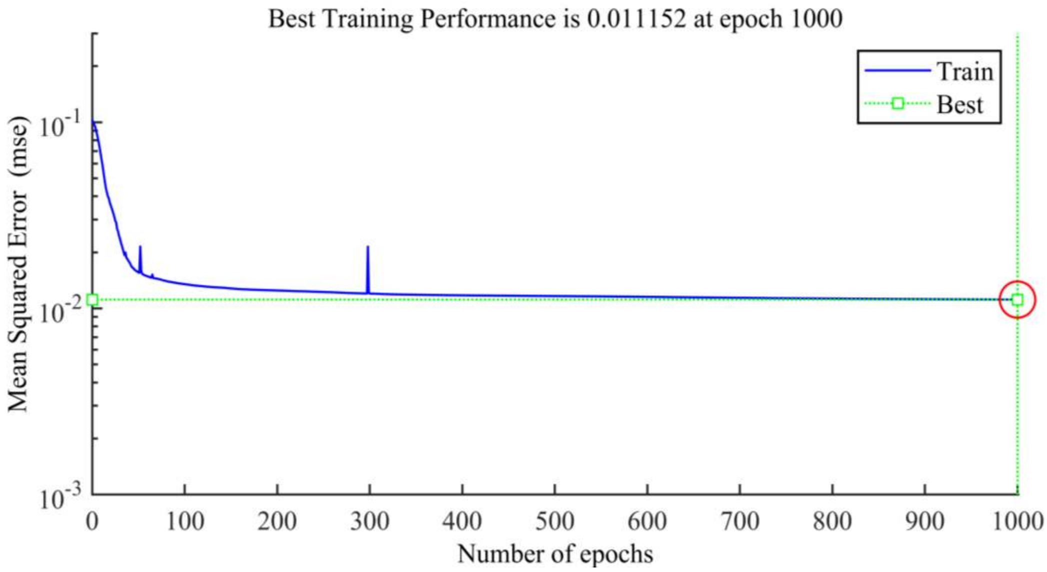

Figure 4.25 Training characteristics of the logarithmic magnitude of the cumulants' features combined with the RBF classifier.

The performance of the RBF classifier is demonstrated in Figure 4.26 and it can be observed that that most dependable performance in this figure for all considered schemes at of SNR is above −5 dB.

Furthermore, the probability of the correct classification rate for interesting signals is evident at no less than 99% for all levels of SNR higher than 0 dB. More carefully, the recognition accuracy of the schemes QPSK/4-QAM has remained 100% for all examined ranges of SNR. On the other hand, it is evident that some decline in performance happened at an SNR of −5 dB. Moreover, the misclassification becomes high in the context of some QAM schemes such as 256-QAM and 512-QAM. To this end, the RBF classifier structure shows a more reliable performance compared relative to the MLP classifier when the SNR is higher than −5 dB. However, the LTD classifier is outperformed in recognising the M-QAM schemes in comparison with the other classifier structures proposed in this chapter.

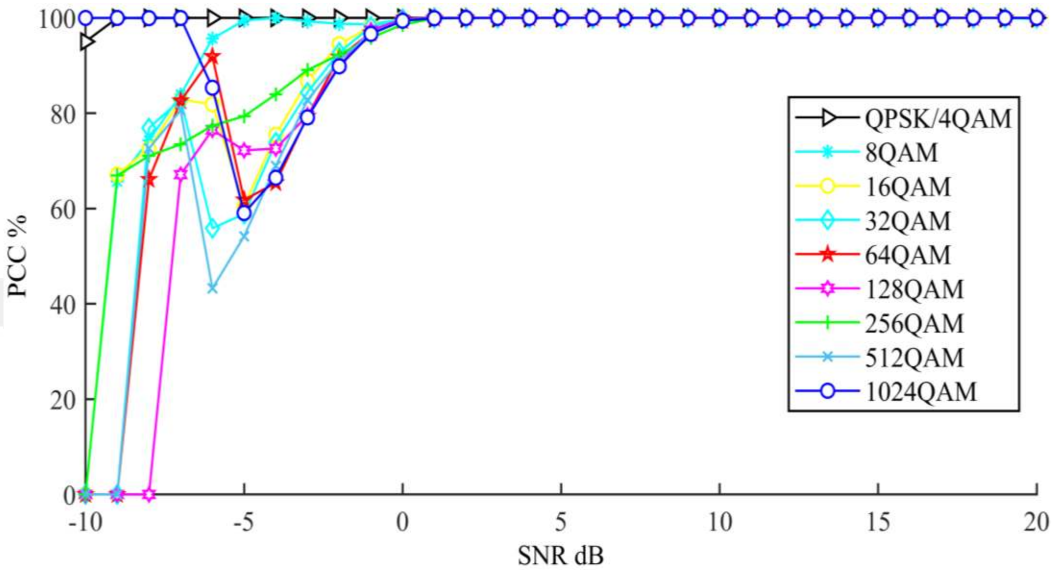

Figure 4.26 The P_{cc} vs. SNR of logarithmic features combined with the RBF classifier for the identification of the 4- to 1,024-QAM scheme; each consists of a signal length N = 4,096 and phase offset of $\pi/6$.

4.7 Performance Comparison of LDT, MLP, and RBF Classifiers

The results that have been obtained demonstrate the possibility of the correct classification of LTD, MLP, and RBF recognisers, which has been considered for the classification set of M-QAM schemes. In other words, the classification accuracy of all considered modulations is more reasonable in both MLP and RBF recognisers. In contrast, the most reliable identification preform for interest schemes has been well-observed in the LDT classifier. However, to compute the performance of the three classifiers, the overall classification accuracy of each classifier must be measured. As shown in Figure 4.27, the proposed logarithmic threshold decision has shown the most reliable performance for considering ranges of SNR, followed by the radial basis function classifier. The disfigurement in performance against various noise is apparent for the classifier's RBF and MLP recognisers, especially at an SNR equal to −1 dB.

On the other hand, the classification accuracy rate of the LDT classifier is deteriorated more than the performance of the RBF and MLP classifiers. Nevertheless, at lower ranges of SNR, the LDT classifier is more reasonable relative to the other RBF and MLP recognisers.

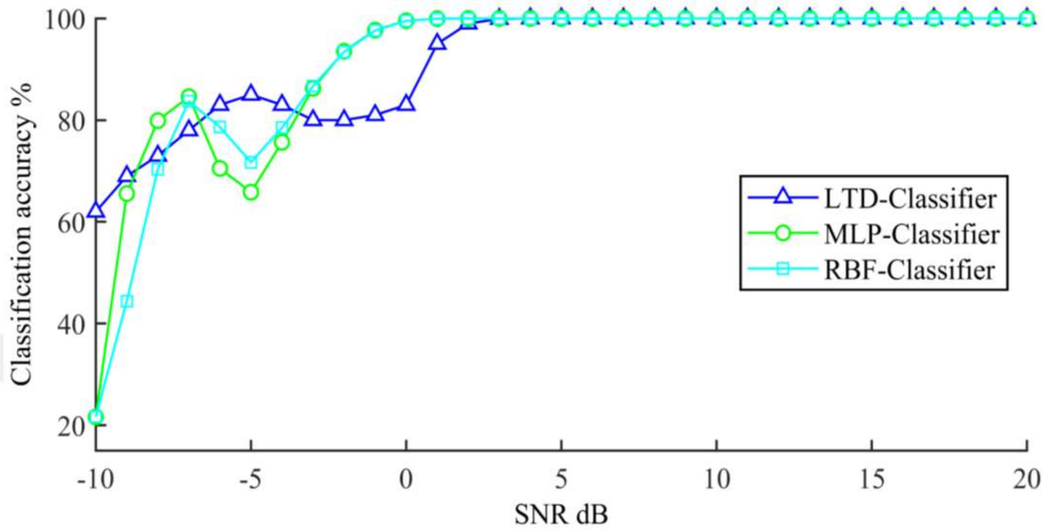

Figure 4.27 Aggregate classification accuracy of the three classifiers.

4.8 Comparison of LDT, RBF, and MLP Classifier Performance with Previous Work

To evaluate the accuracy of the three proposed classifiers, one must assess the accuracy of each classifier in comparison with other systems suggested in the literature. Therefore, to conduct a fair comparison, the same conditions that are used in previous works must be applied to the herein proposed classifiers. The most critical parameters of any classifier are single length, level of the SNR, and the transmission channel type. However, comparing with all classifier aspects is not an efficient solution, due to the fact that each classifier considered different numbers of modulation schemes.

Furthermore, numerous types of modulation schemes are assessed. Thereby, in this comparison, specific modulations are considered, which are the M-QAM signals that were examined in this study the proposed classifiers LDT, RBF, and MLP, where applying the modified feature vector by using logarithmic properties delivered reasonable classification accuracy. In a word, that well appears during comparisons conducted with available classifiers in the literature.

The results of comparison with other systems in the literature are presented in Tables 4.3, 4.4, 4.5, 4.6, and 4.7. Table 4.5 shows a comparison of 64-QAM. Meanwhile, Table 4.6 shows a comparison for 128-QAM and Table 4.7 shows the same for 256-QAM. There are no works until now considered to include the classification of 512-QAM and 1,024-QAM.

Table 4.3 Probability of correct classification rate comparison for 16-QAM

SNR (dB)	P_{cc} %				
	Reference No.	Classifier presented in the literature	Proposed work		
			LDT classifier	MLP classifier	RBF classifier
20	[74]	99	100	100	100
10	[161]	99.95	100	100	100
10	[74]	99.5	100	100	100
10	[17]	98.5	100	100	100
10	[162]	96	100	100	100
5	[163]	94	100	100	100
5	[17]	68.2	100	100	100

Table 4.4 Probability of correct classification rate comparison for 32-QAM.

SNR (dB)	P_{cc} %				
	Reference No.	Classifier presented in the literature	Proposed work		
			LDT classifier	MLP classifier	RBF classifier
17	[163]	95	100	100	100
10	[161]	99.9	100	100	100
10	[162]	98.6	100	100	100

Table 4.5 Probability of correct classification rate comparison for 64-QAM.

SNR (dB)	P_{cc} %				
	Reference No.	Classifier presented in the literature	Proposed work		
			LDT classifier	MLP classifier	RBF classifier
17	[163]	99	100	100	100
10	[161]	99.86	100	100	100
10	[17]	98.1	100	100	100
10	[162]	95	100	100	100
5	[164]	96	100	100	100
5	[17]	65.9	100	100	100
3	[164]	94	99.9	100	99.8

Table 4.6 Probability of correct classification rate comparison for 128-QAM.

SNR (dB)	P_{cc} %				
	Reference No.	Classifier presented in the literature	Proposed work		
			LDT classifier	MLP classifier	RBF classifier
10	[162]	98	100	100	100

Table 4.7 Probability of correct classification rate comparison for 256-QAM.

SNR (dB)	P_{cc} %				
	Reference No.	Classifier presented in the literature	Proposed work		
			LDT classifier	MLP classifier	RBF classifier
10	[162]	96.4	100	100	100
5	[164]	94	100	100	100
3	[164]	90	100	100	100

4.9 Summary of Chapter

In this chapter, a new approach for M-QAM modulation classification has been presented. Furthermore, a novel method to improve the magnitude values of cumulants by using properties of the logarithmic function is suggested. This improvement offers meaningful insight into the behaviour of the distribution curve for each signal class.

- A new recogniser assigned to recognise M-QAM modulated signals problems is introduced. The LDT classifier entirely depends on the logarithmic value of the magnitude of the cumulants. In addition to sharing the advantages of LTDC in identifying the M-QAM schemes, the logarithmic features could provide further merits when combined with nonlinear classifier types. To this end, better performance has been achieved by combining logarithmic cumulants with MLP and RBF classifiers. In a nutshell, the simulation in this chapter shows the outperformance of LDT classifier relative to the other proposed classifiers, albeit with a weak transmission channel and with precise channel fading effects.
- Finally, through a comparison conducted involving numerous previous works, it is observed that researchers have only considered the 16-QAM, 32-QAM, 64-QAM, 128-QAM, and 256-QAM as there is no literature to date that reports the influence of the high order for 512- and 1,024-QAM signals.

CHAPTER FIVE

AUTOMATIC MODULATION RECOGNITION OF DVB-S2X STANDARD-SPECIFIC WITH AN APSK-BASED NEURAL NETWORK CLASSIFIER

5.1 General

Modulation recognition of transmitted signals remains a significant concern in smart, modern communication systems such software-defined radios. Applying machine learning algorithms to interesting features extracted from the input signals are widely used for classification of such signals. Here, we propose leveraging novel higher order spectra features (HOSF) to a classification algorithm based on neural network properties to deal with modulation recognition problems specified for M-APSKDVB-S2X modulation signals standard. The HOSF characteristics are extracted under AWGN-channel, and four individual parameters are defined for distinguishing modulation signals from the set, {16, 32, 64} -APSK. This approach makes the recogniser more intelligent and improves its success rate of classification. The results illustrate excellent classification accuracy obtained at a low SNR of 0 dB, which demonstrates the potential of combining these proposed features with a neural network classifier for the application of M-APSK modulation classification.

5.2 Background

In FB-AMCs, the machine learning algorithms perform merely as a mapping function between the extracted signal features and a binary pattern of the multi-classes. Most of the researches that have been described in chapter 2 focused on modulation recognition algorithms that corrupted by AWGN, which is a typical noisy channel model widely used in studies related to information theory.

Also, this assumption provides a good understanding of the behaviour of systems and reflects major trends. Therefore, in this work, we consider the transmission channel corrupted by the AWGN and derive a new instantaneous relationship between the maximum amplitude and the parameters of (a) the Power Spectral Density (PSD) in terms of the maximum amplitude with a normalized-cantered instantaneous amplitude, and (b) the maximum value of the magnitude of the discrete Fourier transform (DFT) of the transmitted signal embedded with k powers $2, 3, 4, 5, 7,$ and 9, to the signal amplitude. To overcome the problem that occurs at APSK nonlinear amplifier caused by its constellation shape, and improving the performance of the APSK classifier, two new instantaneous features are derived. The first feature is based on the maximum value of the PSD and the second on dividing the *k* power order as {$4^{th}/2^{th}$, $7^{th}/3^{th}$, and $9^{th}/5^{th}$} to create three new distinct instantaneous parameters. These features set are attractive because they have a value less with influence from channel noise and remain nearly constant even with a low SNR. Another significant advantage with these features set is its low computational complexity, as it only requires the computation of the PSD and DFT to the received signal. All proposed features are less sensitive to symbol synchronisation as well as being insensitive to the carrier frequency and phase offsets. As a result, the proposed APSK classifier is comprised of four features extracted from the received signals, including $\{\gamma_{Max}, {}^{\Gamma_4}/_{\Gamma_2}, {}^{\Gamma_7}/_{\Gamma_3}, {}^{\Gamma_9}/_{\Gamma_5}\}$.

The remainder of this chapter is arranged as follows. Section 5.3 introduces a typical representation of the APSK modulation scheme. The details of the APSK-classifier block diagram, the proposed higher-order spectral features (HOSF), and the distribution of signals with the new extracted features are presented in Section 5.4. In Section 4, we propose out AMC-based MLP method with its computational complexity detailed. A detailed description of the classification method follows with a comprehensive analysis in Section 5.5 Simulation results are introduced and discussed in Section 5.6 with a discussion followed by the conclusions of the research presented in Sections 5.7 and 5. 8, respectively.

5.3 Signal Model and APSK Constellation

The typical frame of a sampled signal after passing the matched filter is expressed as [1].

$$r(n) = \alpha e^{-j(2\pi f_o nT + \theta_o)} \sum_{l=-\infty}^{\infty} \Psi(l) h(nT - lT + \varepsilon_T T) + g(n) \tag{5.1}$$

where α is the attenuation factor, f_o is the frequency offset, and θ_o and $g(\mathrm{n})$ are the phase offset and additive noise, respectively. The transmitted signal $\Psi(l)$ is assumed to have unity energy with complex envelope constellation points on the I -Q plane and h is the residual channel effect caused by timing errors ε_T with the symbol timing of T. The parameter of T, f_o, and ε_T have known assumptions. These hypotheses simplify the signal model of the matched filter so that it can be written as

$$r(n) = \alpha \Psi(n) e^{-j(2\pi f_o nT + \theta_o)} + g(n) \tag{5.2}$$

$$\Psi(n) = \sum_{i=1}^{N} \mho_i \, \rho(N - i) \tag{5.3}$$

where *r(n)* is the complex envelope of the received samples. The real and imaginary parts of $\Psi(n)$ are the I and Q components of the transmitted signal, which could be constructed in a two-dimensional scatter plot to obtain the constellation diagram of the transmitted signal as each M-APSK type has a constellation diagram. Also, the $\mho_i$ constellation points at N include symbols inside each data block and the signal power function $\rho(\ell)$ is usually a root-raised cosine with a constant roll-off factor. The constellation points of the APSK modulation of {16, 32, and 64} orders are considered in this work and given in Table 5.1, and the constellation diagrams for the APSK modulation types are presented in Figure 5.1.

Table 5.1 The constellation points of the {16, 32, and 64} APSK modulation type.

Constellation points of 16, 32, and 64 APSK
$\mho_i \in re^{-j2\pi\frac{m}{M_s}}, \text{ where } \left\{\begin{array}{c} r \in [1,2], M_s \in [4,12], m \in [0, \ldots ,11], \text{if } M = 16 \\ r \in [1,2,3], M_s \in [4,12,16], m \in [0, \ldots ,15], \text{if } M = 32 \\ r \in [1,2,3,4], M_s \in [4,12,16,32], m \in [0, \ldots ,31], \text{if } M = 64 \end{array}\right\}$

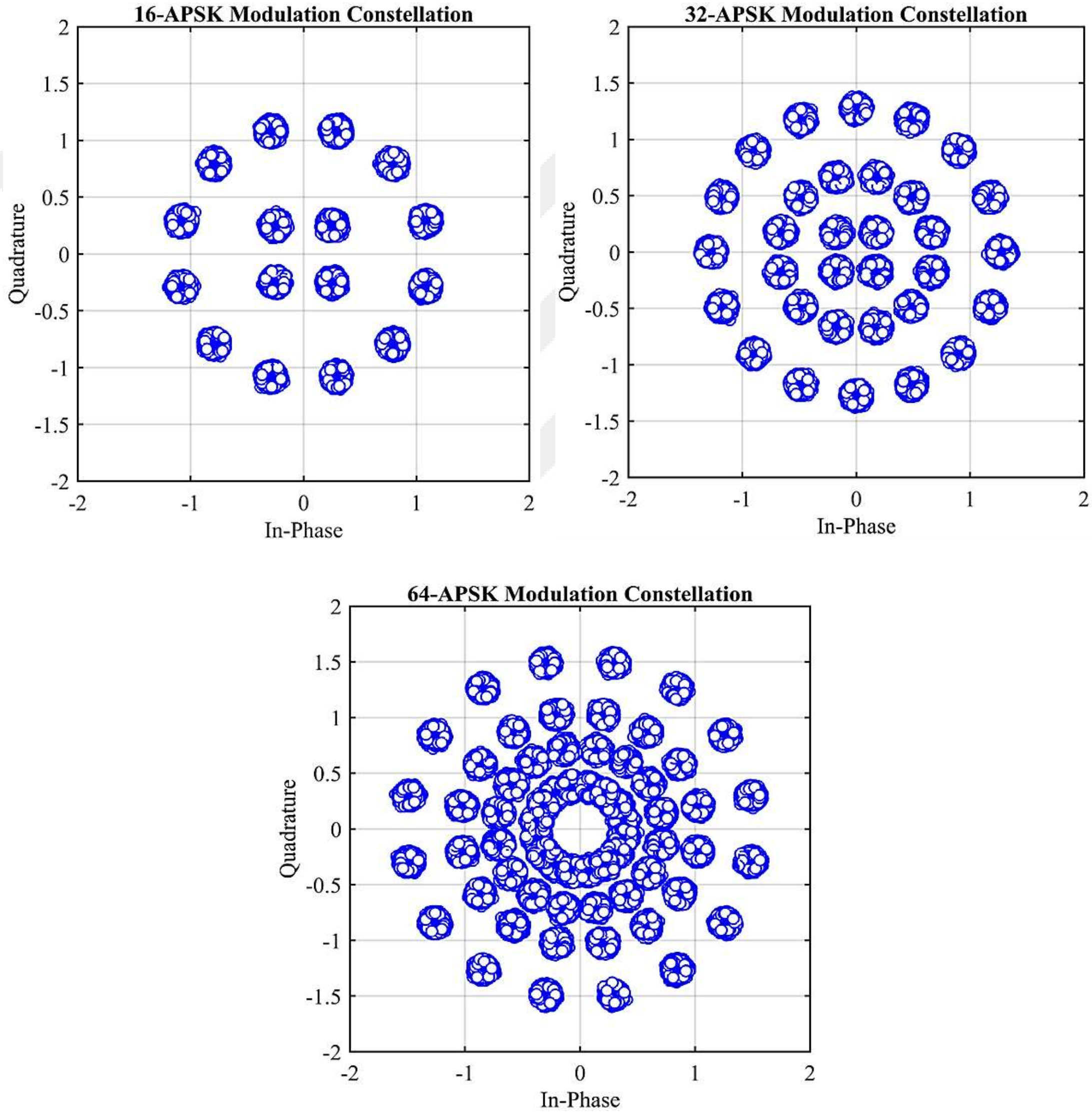

Figure 5.1 The {16, 32, and 64} APSK constellation shapes under the effect of AWGN (where SNR = 30 dB).

5.4 APSK Modulation Recognition Method

We propose a new concept for the APSK classification algorithm using an MLP-classifier and instantaneous time domain-based features, as outlined in Figure 5. 2 and detailed in the following.

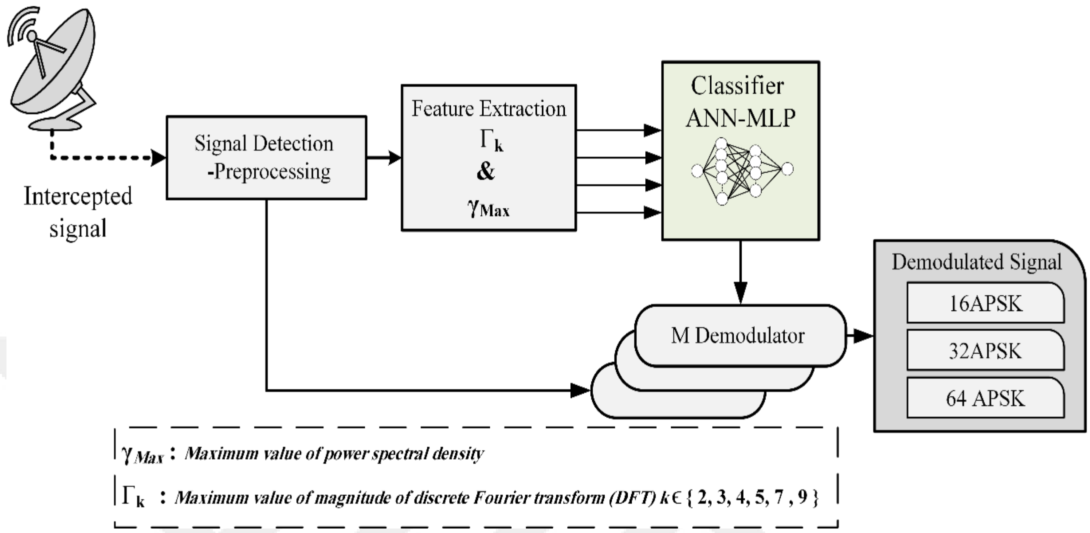

Figure 5.2 The proposed APSK -classifier system.

All aspects of our proposed features and classification mechanism are verified through simulated signal characteristics, as listed in Table 5.2. These generated signals are comprised from 1080 independent signal realisations.

Table 5.2 Simulation signal parameters.

Signal Parameters	Value
Carrier frequency f_c	384kHz
Symbol rate f_d	38.4 kHz
Sampling rate f_s	307.2kHz
Number of symbols N	512*8
Total number of samples N_s	32768

5.4.1 Feature extraction

Different types of digital signals have various properties, so identifying the suitable features for their recognition, especially those at higher-order or that include a close constellation diagram, is a critical challenge. However, time-domain features are hidden in the instantaneous values of digital signals. In this research that is presented in this chapter, we compute and experiment with four novel instantaneous features based on the normalised-centred instantaneous amplitude of a digital signal, and are described in the following.

5.4.1.1 The maximum value of the PSD

The maximum value of the PSD of a normalized-centered instantaneous amplitude is written as [18].

$$\gamma_{Max} = \frac{\mathrm{Max}|\mathrm{DFT}(\mathrm{a_{cn}}(\mathrm{n}))|^2}{N_s} \tag{5.4}$$

$$f_1 = \gamma_{Max}$$

where N_s is the total number of samples in the signal, $\mathrm{a_{cn}}(\mathrm{n}) = \frac{\mathrm{a(n)}}{\mathrm{m_a}} - 1$, $\mathrm{m}_a = 1/N_s \sum_{n=1}^{N_s} a(n)$, a(n) is the absolute value of the analytic form of the transmitted signal, and m_a is the sample mean. Previous research confirmed that this feature has a good separation of PSK in one group [39]. However, for our purposes, we find that it is useful for classifying between {16, 32, and 64} APSK signals. Figure 5.3(a) presents the mean value of the feature against the SNR (in dB) for {16, 32, and 64} APSK signals showing it can separate APSK modulation signals at an SNR as low as -3 dB.

5.4.1.2 The maximum value of the DFT magnitude with the kth power of the analytic expression of the transmuted signal

The maximum DFT instantaneous feature is documented in [110,165] and is represented as

$$\Gamma_k = \frac{\mathrm{Max}|\mathrm{DFT}(a(i)^k)|^2}{N_s} \tag{5.5}$$

Many magnitudes of the $\mathrm{k^{th}}$ power of the maximum value of the DFT used in the literature exploit different aspects of this feature, such as those utilised for the classification of FSK, PSK, and QAM schemes [154,166–168]. Dividing the values of the k^{th} order provides additional benefits along with the Γ_k magnitude feature from the received signal, including good classification near varying amplitude modulations and recognising the order of varying amplitude modulations. In this work, six values of the parameter k are used, where k = 2, 3, 4, 5, 7, and 9. Three new features based on the magnitudes ($^{\Gamma_4}/_{\Gamma_2}$, $^{\Gamma_7}/_{\Gamma_3}$, $^{\Gamma_9}/_{\Gamma_5}$) of the received signal are derived and assigned with the parameters and written as

$$f_2 = \frac{\Gamma_4}{\Gamma_2} \tag{5.6}$$

$$f_3 = \frac{\Gamma_7}{\Gamma_3} \tag{5.7}$$

$$f_4 = \frac{\Gamma_9}{\Gamma_5} \tag{5 8}$$

Figures 5.3 (b), (c), and (d) show the mean value of the variation of f_2, f_3, and f_4 against the SNR. These features enhance the classification accuracy and distinguish the 16-APSK, 32-APSK, and 64-APSK modulations at SNR = 0 dB.

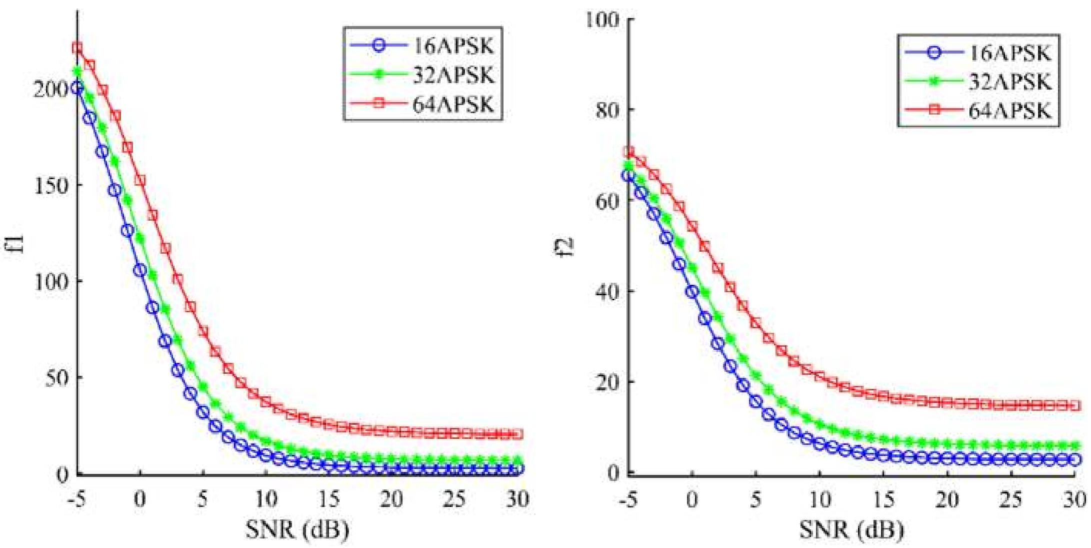

(a) (b)

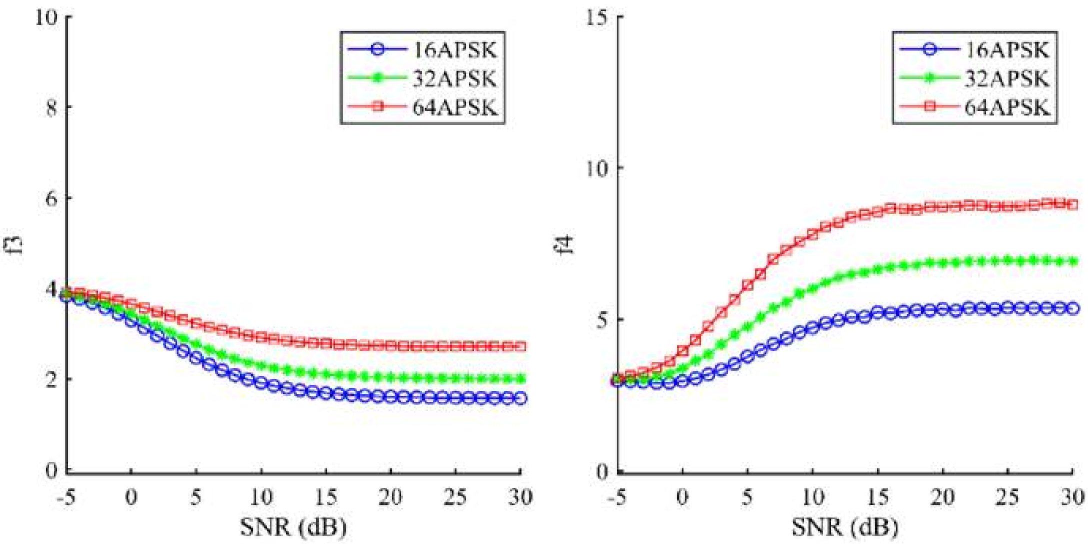

(c) (d)

Figure 5.3 Graphs of the SNR versus the mean value of (a) f_1, (b) f_2, (c) f_3, and (d) f_4.

5.5 The Distribution and Vector Orientation of the Proposed Features

A fixed threshold algorithm to make classification decisions on the modulation is not an optimal solution. Instead, the distribution of the features extracted from the received signal samples over the original two-dimensional space can identify the intersection between the classes. Figures 5.4 (a) and (b) show the features in the original dimensional space at SNR = 5 dB for 1080 singles realisations. Based on Figure 5.4 (a), the 16-APSK is separable from the 32-APSK and 64-APSK according to the features f_1 and f_2. On the other hand, Figure 5.4 also suggests there is no optimal threshold value for f_3 or f_4 that can exactly distinguish the three modulation schemes.

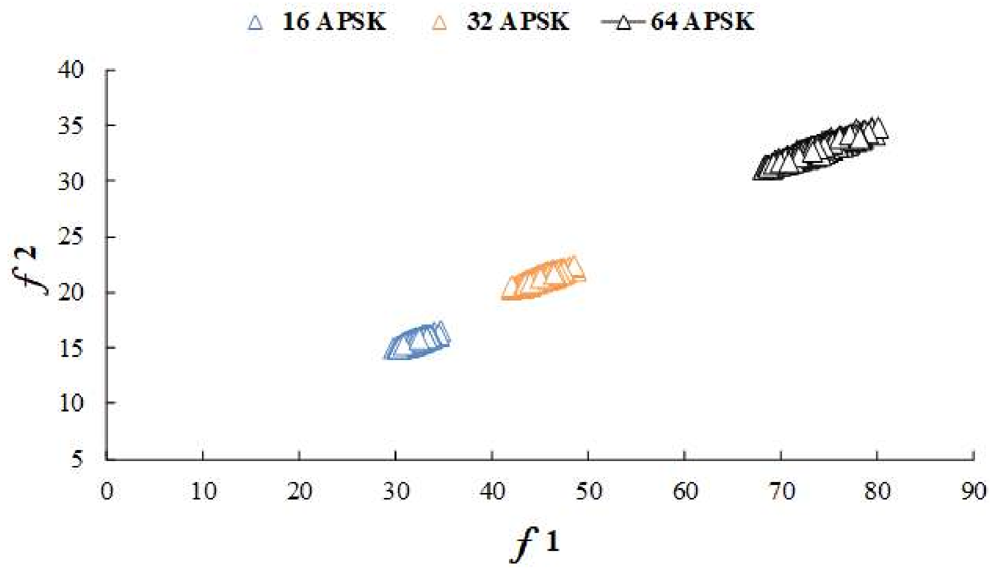

(a)

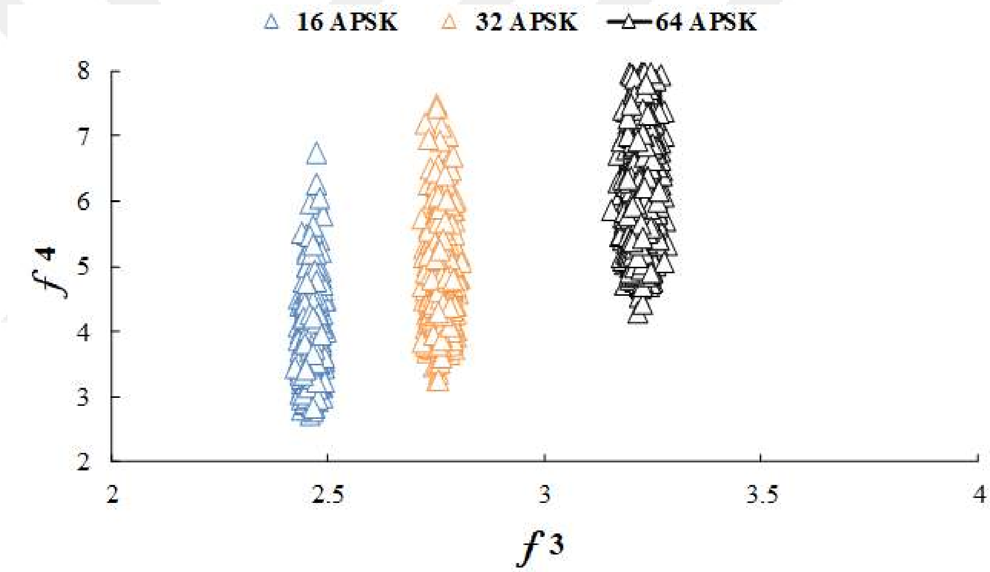

(b)

Figure 5.4 The distribution of the features (a) f_1 vs f_2 and (b) f_3 vs f_4 in the original dimensional space at a signal-to-noise ratio of 5dB.

5.6 APSK Classifier-Based MLP

In this work, an MLP neural network architecture has been used as a classifier for pattern recognition. Conventional MLPs are comprised of an input layer of source nodes, i.e., the dimension of feature vectors, one or more hidden layers that function as computation nodes, and an output layer [169]. In this outer layer, the number of nodes depends on the number of variables representing classes or signals. A feed-forward artificial neural network featured in our proposed pattern recognition system mimics the MLP structure, and consists of a double hidden layer, as illustrated in Figure 5.5.

Pattern recognition methods typically include two stages of training and testing. The weights are calculated at each node during training, and the selected learning algorithm plays a crucial role in the calculation of optimum weight values. The learning algorithm and its convergence speed are critical to an ANN, and numerous training algorithms have been proposed. The back-propagation (BP) algorithm is a family of learning methods used for achieving efficient training in the feed-forward ANN. Under some circumstances, the BP-classifier algorithm can produce non-robust results and take a long time to converge of the global minimum. On the other hand, other learning algorithms, such as the cascade correlation and the Levenberg–Marquardt, require extensive computing memory to accomplish the best training.

For our proposed pattern recognition system, the resilient backpropagation (RPROP) algorithm ha been exploited as a heuristic function, which includes a first-order optimisation [125]. According to the Manhattan weights update rule [170], RPROP enacts only the sign of the partial derivatives as the indication of the direction of the weight update while acting on each weight independently. For performing this computation, the size of the partial derivative does not impact the weight step. The following expression clarifies the adaptation of the update values of Δ_{ij} (the weight tuning) for the RPROP algorithm.

$$\Delta_{ij}(t) = \begin{cases} \eta^{+} \times \Delta_{ij}(t-1); if\, \frac{\delta E}{\delta W_{ij}}(t-1)\frac{\delta E}{\delta W_{ij}} > 0 \\ \eta^{-} \times \Delta_{ij}(t-1); if\, \frac{\delta E}{\delta W_{ij}}(t-1)\frac{\delta E}{\delta W_{ij}} < 0 \\ \eta^{0} \times \Delta_{ij}(t-1); \text{otherwise} \end{cases} \tag{5.9}$$

where $\eta^0 = 1, 0 < \eta^- < 1 < \eta^+, \eta^{-,0.+}$ denotes the weight multiplied by the update factors, W_{ij} indicates the weight value between the neuron j of the current layer and neuron i of the previous layer, and E is the error function for the network output. The partial derivative corresponding to the error function for each weight changing its sign indicates that the previous update value for that weight is excessive and has diverged over the minimum. Therefore, the updated value is modified by multiplying by the factor η^- as expressed in Equation (5.9). If the partial derivative yields the same sign as the previous iteration, then the updated value is increased by multiplying by the factor η^+. This process accelerates the convergence in shallow areas. To avoid over acceleration, each epoch following a multiplication with the factor η^+, the new update value is neither increased nor decreased (η^0) from the previous values, and the results of Δ_{ij} remain non-negative at each epoch. The neurons' weight update values are then followed by an adaptation process to update the actual weight determined by

$$\Delta_{W_{ij}}(t) = \begin{cases} -\Delta_{ij}(t);\ if\ \dfrac{\delta E}{\delta W_{ij}}(t) > 0 \\ +\Delta_{ij}(t);\ if\ \dfrac{\delta E}{\delta W_{ij}}(t) < 0 \\ 0;\ \text{otherwise} \end{cases} \tag{5.10}$$

$$W_{ij}(t+1) = W_{ij}(t) + \Delta_{W_{ij}}(t) \tag{5.11}$$

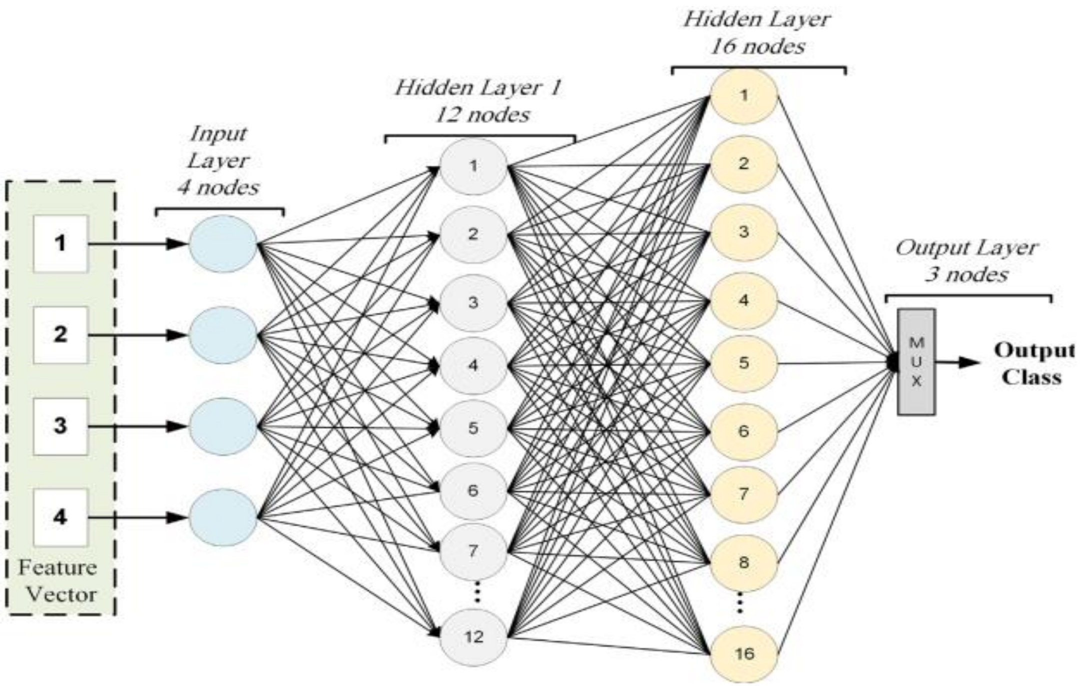

Figure 5.5 The MLP network architecture.

5.6.1 The proposed classifier

The goal of this study is to develop an intelligent AMC system to enable a receiver to recognise the length of the possible modulation scheme used by the transmitter for modulating the datasets. We consider the modulation classifier as a pattern recognition problem, as described above. The distinct group of interest features are extracted from the transmitted signal creating a feature vector used by the classifier to decide the modulation types used by the transmitter. Any pattern recognition scheme applied to the selected features also applies to the classifier and its characteristics. We evaluate classifier performances according to accurate recognition rate probabilities and calculation speed, and we present results for the {16, 32, 64} APSK classifier combinations of an MLP. The architecture of the {16, 32, 64} APSK classifier is shown in Figure 5.6, which depicts the ANN block combined classifier. An advantage of this structure is that it achieves higher classification accuracy compared to conventional pattern recognition systems.

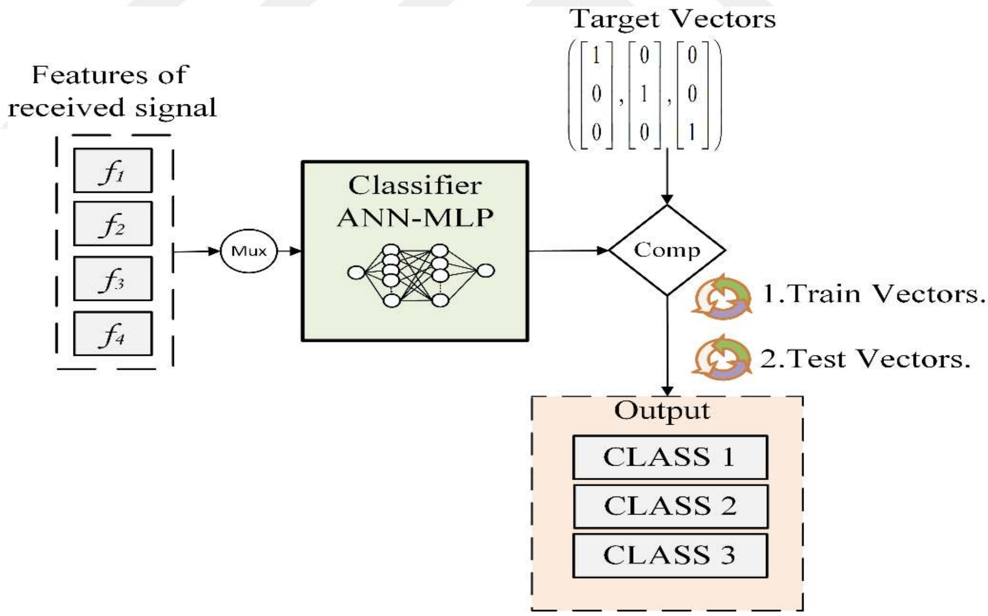

Figure 5.6 The architecture of the proposed {16, 32, 64} APSK classifier algorithm.

All neurons are fully connected, as shown in Figure 5.5, where those in the input layer do not function as part of any calculation. Instead, these four neurons correspond to the number of input features and distribute these to the calculating neurons included in the hidden layer.

The neurons in the hidden layer, comprised of 12 in the first layer and 16 in the second, perform computations on their inputs and pass the results to the three neurons in the output layer. Then, these output neurons correspond to the number of targets of the three-signal scheme, 16-APSK, 32-APSK, and 64-APSK. Each signal is labelled as a 3-bit binary pattern vector.

5.6.2 The classifier entity

With the complexity of emerging developments in digital systems and the trend towards digital telecommunications beyond analogue telecommunication, most modern communication systems use digital signals. Considering the changes in message parameters, three digital signal schemes exist for the DVB-S2 standard, including 16-APSK, 32-APSK, and 64-APSK signals [4]. To evaluate the performance of our proposed classifier under noisy channel or variable data length scenarios, we evaluate our AMC method under AWGN using the invoked signal tools available in conventional computer simulations. We created 1080 samples of each signal type, which included AWGN added to the symbols at various SNRs (0 ~ 20 dB). Each signal type has 512*8 symbols with which the digital information (the message) was created randomly for each 1080 simulated sample to confirm independent results. Classification accuracy assessments of the classes were provided by the classification matrix result with two parameters defined. First, the classification accuracy, $\mathrm{A_{CC}}$, shows the analysis of different classes in percentages, and, second, the probability of correct classification, $\mathrm{P_{cc}}$, is formulated as

$$\mathrm{P_{CC}} = \sum_{k=1}^{j} \mathrm{p}(\omega_\mathrm{k}|\omega_\mathrm{k})\mathrm{P}(\omega_\mathrm{k}). \tag{5.12}$$

For example, a "j" refers to the modulation signal candidates to be classified $(\omega_1, \omega_2, \omega_3, \omega_\mathrm{j})$, where $\mathrm{P}(\omega_k)$ is the probability that the modulation scheme ω_k occurs, and $\mathrm{P}(\omega_k|\omega_k)$ is the probability of a correct classification when a ω_k signal is sent [16].

5.6.3 Network training

As seen in the architecture of the proposed classifier in Figure 5.6, a four-key feature provides the input, and the neural network-based classifier is a feed-forward network referred to as an MLP. Table 5.3 lists the neural network architectural specifications adopted for (training and classification) scenario. In a computer simulation to train the classifier, a training database comprises of 1080x4 data samples with four features set inputs and three target outputs are used in this study with the following training phase steps.

1. The created data consists of an input matrix and a target matrix.

2. The generated data is divided into training, validation, and testing datasets with 70% of the dataset used for training to update the weights of the network.

This training process continues until the performance metric of the mean squire error (MSE) converges to $\leq 1e^{-6}$ of the total training data. Another 15% of the dataset is used to validate the network's efficiency to generalise and halt the training before overfitting occurs. The remaining 15% offers independent testing data to assess the network's generalisation ability.

Table 5.3 Specification of the ANN-based classifier structure.

Network structure	Numbers of Neurons in Each Layer			
	Input	Hidden 1	Hidden 2	Output
MLP	4	12	16	3
	Activation function			
	~	Tanh	Logsig	~
Performance Function	MSE			

5.6.4 Classifier training and test criteria

For the APSK classifier test stage, the only data required from the trained network are the synaptic weights and biases that must be available to on the trained network. Our training stage has been performed using 1080 samples from the realisations for each

APSK signal type with varying SNRs from 0 ~ 20. The performance is evaluated on 720 samples of the new realisation set of interest from an APSK signal scheme ranged with SNRs from 0 ~ 20. The classifier test and performance evaluations are processed through the following steps.

Steps of the proposed classification system.
a. *The vector of the extracted features set is shown in Equation (5.13), where the n_r is a total of the realisation elements. This vector is used in the test stage of the trained classifier.* $$f_0 = \begin{bmatrix} f_1 \\ f_2 \\ f_3 \\ f_4 \end{bmatrix}_{\mathrm{n_r}} \quad (5.13)$$ ***b.*** *The target matrix, T_r, is defined for each class of the modulation signal, as explained in Figure 5.6. For each realisation of the test class, the corresponding output vector, based on the number of hidden layers used, is calculated as follows:*   ***i.*** *The location equivalent to each signal pattern in the output vector is set as* $$\mathrm{T_r} = \begin{bmatrix} \text{16APSK: } \{[001]^{\mathrm{T}}\}_{\mathrm{LSB}} \\ \text{32APSK: } \{[010]^{\mathrm{T}}\}_{\mathrm{LSB}} \\ \text{64APSK: } \{[100]^{\mathrm{T}}\}_{\mathrm{LSB}} \end{bmatrix}_{\mathrm{n_r}} \quad (5.14)$$ ***ii.*** *The adapted output vector should agree to one of the columns of the target matrix Tr, and this agreement referred to as the {16, 32, 64} APSK modulation scheme.*   ***iii.*** *Repeat the complete criteria for each realisation in the test category.*   ***c.*** *The probability of correct recognition is calculated as the percentage of realisations from the testing samples that have the correct modified output vector.*

5.7 Experimental Results

The results of the degradation under the simulation scenarios applied to the APSK classifier are presented in this section, where we assume that the carrier frequency is constant, as mentioned in Table 5.3. Therefore, we only consider complex base-band signals that randomly generate data over each scheme and expose them to a noisy channel of pure AWGN, according to testing ratios of the signal-to-power noise ranged from 0 to 20 dB. All signal samples in the training and testing are labelled with the corresponding modulation type and SNR. Samples in the training dataset are uniformly distributed through SNR range and padded by 1 dB.

5.7.1 Accuracy evaluation

The most striking results from the data are summarised in Table 5.4 which depicts that the best performance is achieved with correct classifications of the $\{16, 32, 64\}$-APSK signal classes at SNR $0, 5, 15,$ and ≥ 20 dB. The confusion matrix in Table 5.4 is for N = 512*8 and an SNR of 0 dB, and the number of overlapping signals, in this case, is higher compared to the SNR of 5 dB, which is expected because channel SNR is lower. Furthermore, most of the modulation misclassification occurs between 16-APSK and 32-APSK because they have similar constellation diagrams, particularly at low SNR. The efficiency of the classifier increases at an SNR >5dB. However, this superior performance could be attributed to the robustness of the internal structure of the APSK classifier and the merits of the proposed features.

Table 5.4 The confusion matrix of the {16, 32, 64} APSK classifier at SNR = 0, 5, 15, and ≥20 dB.

	E_s/N_s = 0 dB			E_s/N_s = 5 dB		
Simulated signal type	Predicted signal type					
	16-APSK	32-APSK	64-APSK	16-APSK	32-APSK	64-APSK
16-APSK	86.0	0.1	0.0	99.9	0.4	0.0
32-APSK	14.0	93.9	1.3	0.1	99.6	0.0
64-APSK	0.0	6.0	98.8	0.0	0.0	100.0
	E_s/N_s = 15 dB			E_s/N_s = ≥20 dB		
Simulated signal type	Predicted signal type					
	16-APSK	32-APSK	64-APSK	16-APSK	32-APSK	64-APSK
16-APKS	100	0	0	100	0	0
32-APSK	0	100	0	0	100	0
64-APSK	0	0	100	0	0	100

Predicted signal type: PCC %

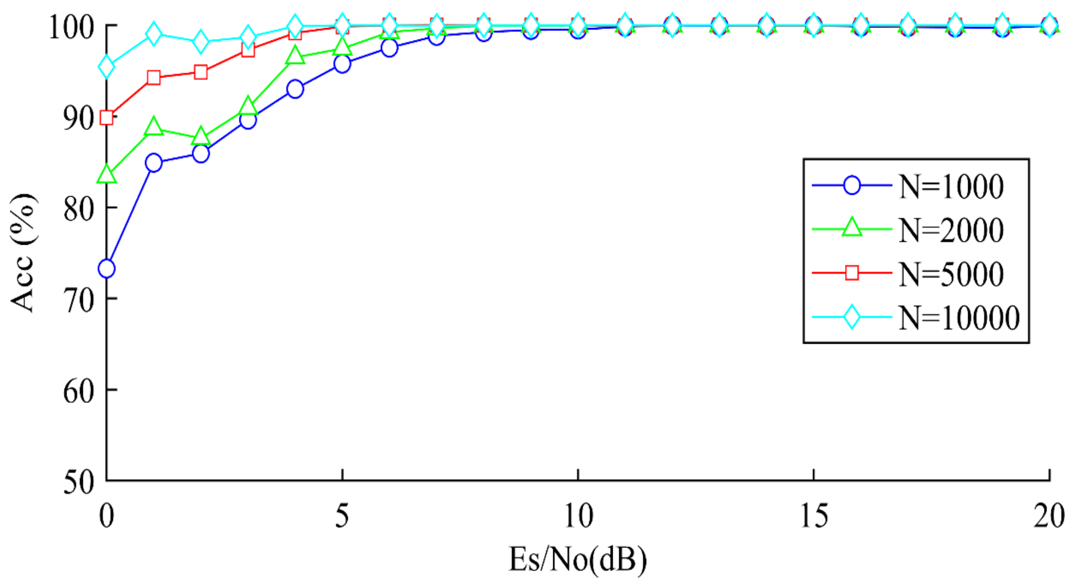

Figure 5.7 Classification accuracy for different quantities of symbols.

The influence of using different lengths of signal symbols per data block on the classification accuracy is shown in Figure 5.7. Using a long row of data symbols to extract the classification features enhances the correct classification rate. For example, when using N = 5000 symbols leads to an improvement in classification accuracy nearly exceeds 98% at an SNR of 5dB compared to N = 1000 symbols. The results in Figure 5.7 also suggest that the classification accuracy rate is a function of the SNR of the channel and the number of symbols in the signal. This relationship is due to the fluctuation in the extracted feature values based on these parameters, which may suggest that misclassification increases with lower SNR and smaller block lengths.

In our evaluation of the APSK classifier over different channels, we set the sample length to 512*4 and the SNR between 0 ~ 30 dB. For the simulation scenarios, the phase and frequency offset are assumed to be constant, and the classifier performance is investigated in AWGN-only, multi-path, and unknown channel conditions with a symbol rate of 20 MHz, fading variables, average path gains of 0, -15, and -20 dB, path delays of 0, $1 * 10^{-7}$, and $2 * 10^{-7}$ seconds, a factor k = 3 dB, and maximum Doppler shift of 15.5 Hz.

Figure 5.8 depicts the classification accuracy rate at N = 512*4 with three different channel scenarios. For this test, the maximum Doppler shift and the SNR of the channel are known at the receiver site, and these limitations are used to train the classifier. The accuracy of classification is good for AWGN-only channels compared to multi-path fading channels due to the existence of a strong signal attributable to the line of sight component. Also, an increasing SNR is seen to results in better classification accuracy. The classifier performance under unknown channel noise provides a significantly high correct classification rate reaching 95%.

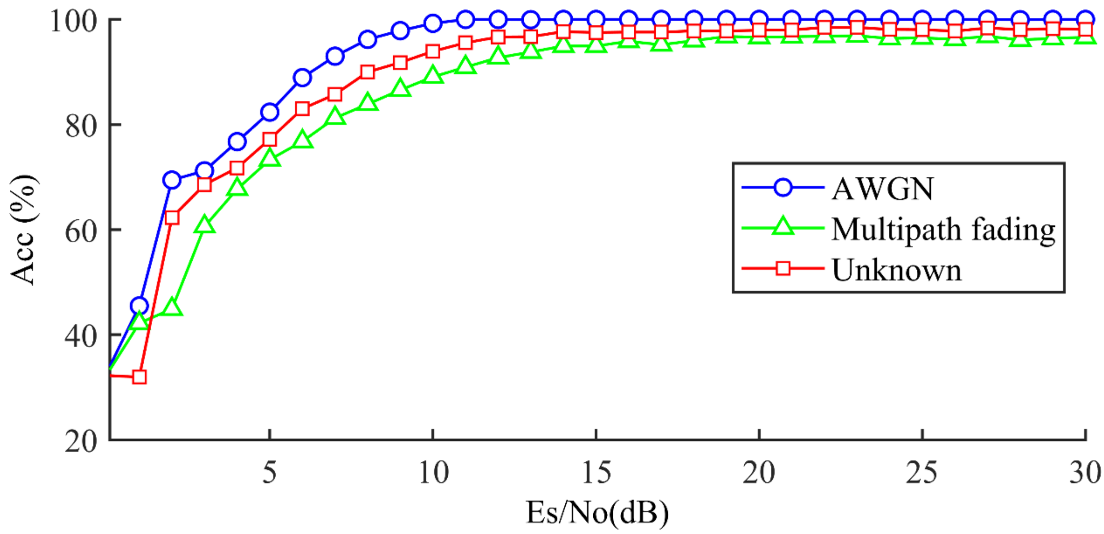

Figure 5.8 The accuracy of classification for different channels environments.

5.7.2 Flat-fading channel with phase and frequency offset

In the flat-fading channel, we set the signal length at 512×4 symbols and SNR 0 to 20 dB. The signal realizations of the 720 samples were tested for each class. The phase noise and frequency offset were considered separately. For phase offset, we used five angles $(0^{\circ}, 5^{\circ}, 10^{\circ}, 20^{\circ}, 30^{\circ})$. In the simulation, a relative frequency f_o (computed as the ratio between the carrier frequency and the symbol sampling frequency) has been utilised to indicate different levels of frequency offsets.

It was limited by reduction ratios $(0\%, 1\%, 2\%, 3\%, 6\%)$ of the actual carrier frequency offset f_c.The results are presented in Figures 5.9 and 5.10. In the case of the phase offset, Figure 5.9 shows that the phase offset has a small effect on the classifier performance at SNR levels below 5dB. However, it had almost no significant influence at SNR>6 dB levels. The reason for the superior performance of the APSK-classifier under the phase offset could be attributed to the powerful capability of the k^{th} power of the magnitude of signal to derive the features that have a high discrimination between modulation signals.

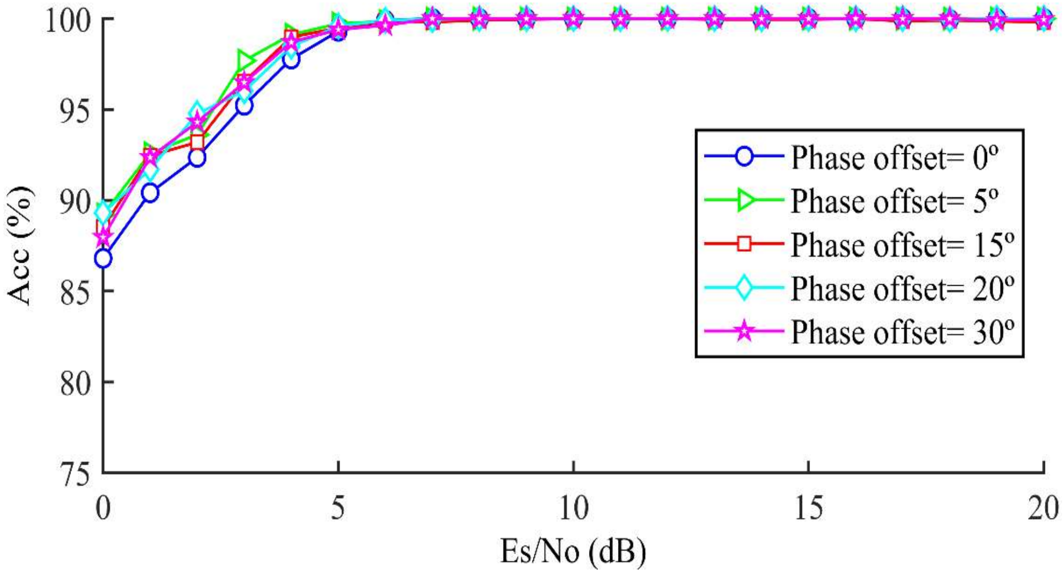

Figure 5.9 Accuracy of correct classification versus SNR for different values of phase offset.

In the case of the frequency offset, Figures. 5.10 shows that the frequency offset has an influence on classifier performance, particularly when SNR is below 5dB. At SNR>5 dB, the effect ratios of 1%f_c , 2%f_c, and 3%f_c showed a slightly better performance than the effect ratio 6%f_c. At SNR> 7dB, the performance gaps become nearly equal.

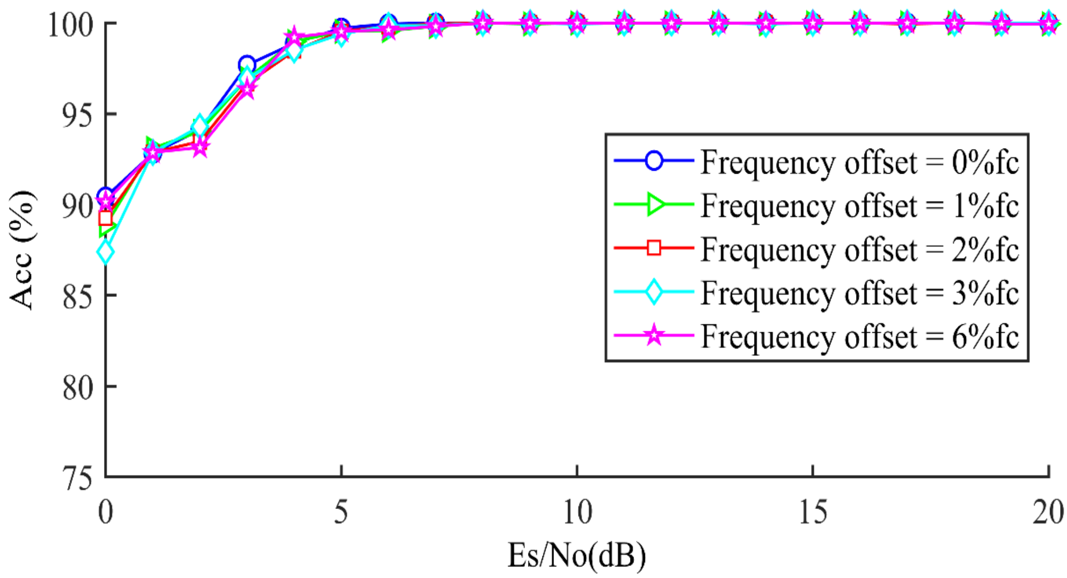

Figure 5.10 Accuracy of correct classification versus SNR for different values of frequency offset.

5.8 Comparison with an Existing Method

To ensure a flexible comparison, the simulation scenario is performed by applying the same parameters used in [171]. Specifically, we use the same modulation schemes in our comparison of the three M-APSK types of 16-APSK, 32-APSK, and 64-APSK with a data length of 1000 symbols per signal. Figure 5.11 compares the accuracy of classification of a template matching the classification of MAPSK [171] with the proposed APSK classifier. The proposed classifier provides a correct classification accuracy of nearly 100% at an SNR > 5 dB. At the same time, the classifier with the template matching delivers a classification accuracy near 100% at an SNR > 8 dB. So, the proposed APSK classifier exceeds the template matching classifier in terms of the correct classification rate. However, the accuracy of the correct classification is not the only factor for favouring one classifier over another. Other important aspects include the intricacy of the system and the order of computations involved in making the classificatory decision.

Because modulation classification is a real-time practical problem, systems with simple structures and low complexity are more attractive. The APSK classifier includes simple signal processing operations, such as the operation for computation of the magnitude of the Fourier transform, squared magnitude of signals, and other conventional mathematical operations like multiplication and addition.

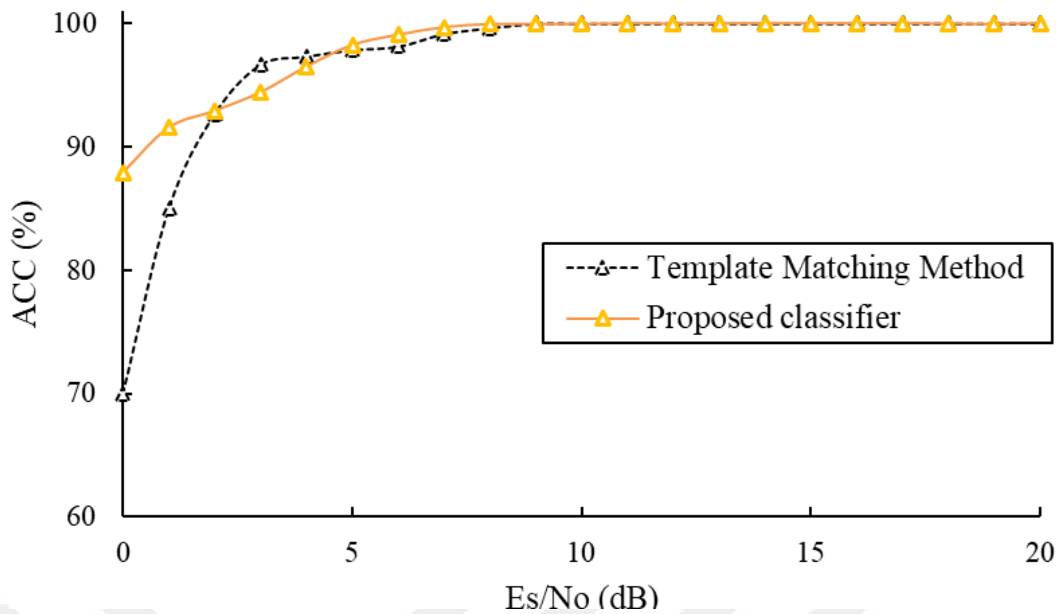

Figure 5.11 Comparison of the APSK classifier with the template matching recognition method.

5.9 The Complexity of the Training

We conduct two stages of experiments to concentrate on the effects of the training samples on the classification accuracy of the proposed APSK classifier. In the first set of experiments, we focus on the classification accuracy of the proposed APSK classifier by varying the SNR, which has been the prime criteria for measuring the performance of an AMC system. We set the signal length at 512*4 symbols, and the SNR varies between 0 to 20 dB. Following this, the modulated signals are segmented into 240, 360, 480, 720, and 1080 samples to form the training dataset while the testing dataset contains 720 samples.

The results presented in Figures 5.12 the best performance is achieved when using L = 720 for each signal generated. However, this performance advantage is highest between 6 to 20 dB. The performance curves for L = 240, 480, 360, and 1080 signal samples show nearly equal accuracy in the range of SNR from 5 to 20 dB. As expected, for a low SNR below 5dB, the difference between the trained and tested data becomes more prominent, so the classifier accuracy deteriorates. However, by increasing the SNR, the performance curve improves considerably, especially with larger signal samples. Furthermore, the classification accuracy curve is better for L = 240, 480, and 720 signal samples.

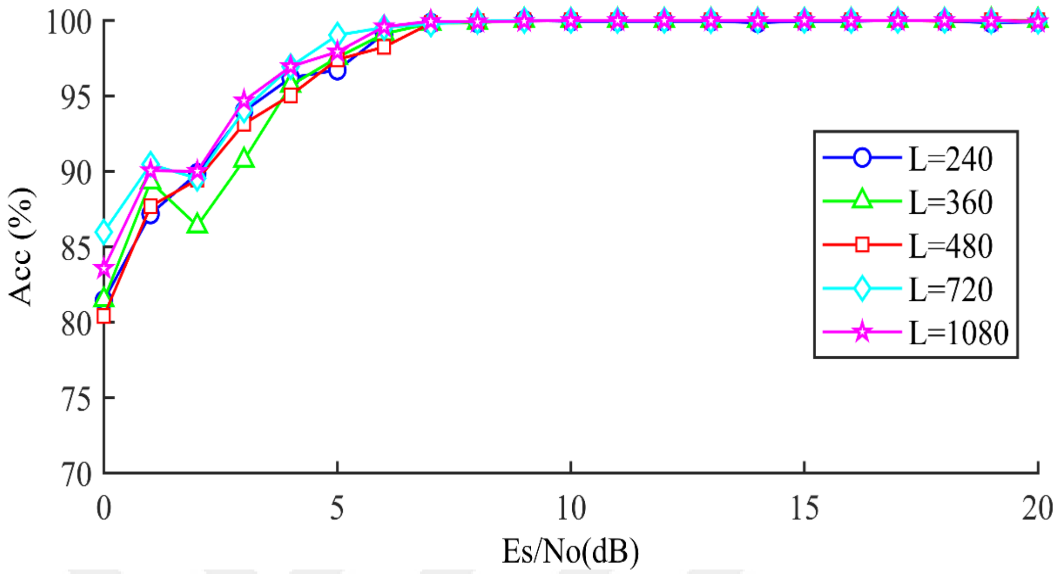

Figure 5.12 Accuracy of correct classification vs SNR for different numbers of training samples while testing with 720 signal realisations from 16-APSK, 32-APSK, and 64-APSK. Each consists of a signal length N = 512*4 under the AWGN channel.

The second set of experiments focuses on the influence of testing signal sample length to the classification accuracy of the proposed APSK classifier. In this scenario, similar settings are applied as before, except the testing signal includes 1080*2 samples for each APSK class. The performance curves are seen in Figure 5. 13, and, again, the APSK classifier outperforms for a training length of L = 720 samples. However, the proposed APSK classifier shows nearly equally superior and robust accuracies for the training samples with length L = 240, 360, 480, and 1080. These results prove the enhanced ability of the proposed APSK classifier to show robustness with only a few training signal samples, which is important for good AMC classification.

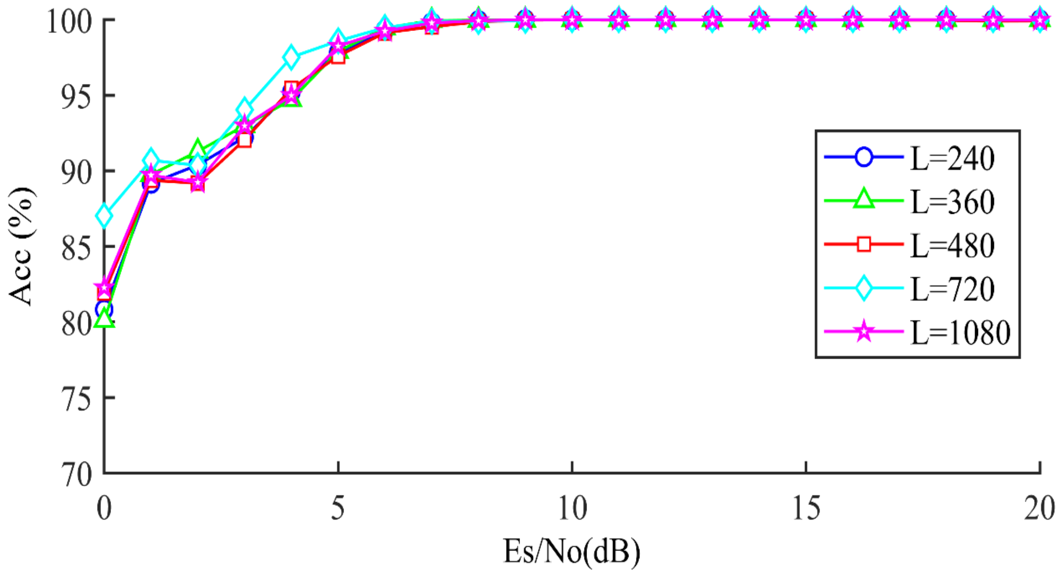

Figure 5.13 Accuracy of correct classification vs the SNR for different numbers of training samples while testing 1080 *2 signal realisations from 16-APSK, 32-APSK, and 64-APSK. Each consists of a signal length N = 512*4 under the AWGN channel.

5.10 Performance on an Unknown Channel SNR

Next, we evaluate the robustness of our proposed APSK classifier based on the MLP network by training our signal samples at a different SNR range than the test signal. In this test, we only focus on the AWGN channel for a better understanding of the performance with an unknown SNR at the receiver. First, the training dataset is uniformly distributed in two ranges of SNR from 0 to 15 dB padded by 2 and from 0 to 20 dB with a step of 1. Next, the test dataset is created with an SNR range from 0 to 20 dB. A signal realisation of 1080 samples is used for training while testing on 720 samples, and each modulation scheme in both datasets is comprised of the same 512*4 symbols. The performance curves are seen in Figure 5.14 showing that the data trained at a range of SNR from 0 to 20 dB with a step of 2 dB has an advantage of around 5% over the data trained at a range of SNR from 0 to 15 dB. This result can be attributed to the data generated to train and test the APSK classifier at range of SNR from 0 to 20 dB padded by 2 dB are in close proximity. The gap between the two curves decreases to 5 dB SNR, after which the performance becomes equivalent. Also, the classifier trained at a range of SNR from 0 to 15 dB maintains high accuracy even when the test data is generated at a high SNR of 15 dB.

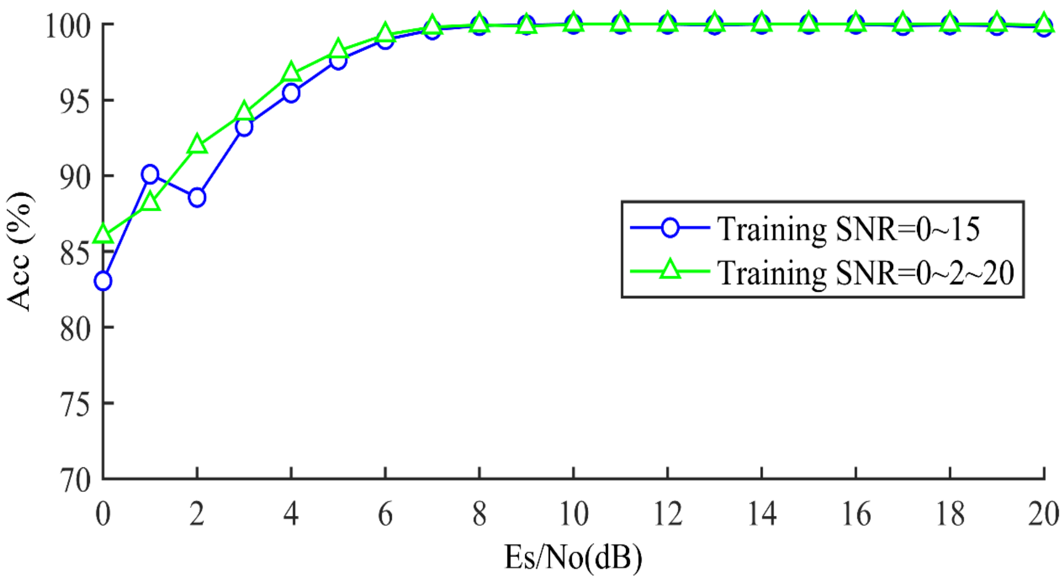

Figure 5.14 The classification accuracy rate vs unknown SNR conditions with 720 testing signal samples for each modulation scheme containing 512*4 symbols.

5.11 Discussion

While the presented work does not provide a final solution, we highlight a promising line of research for automatic modulation recognition algorithms Due to the complexity of this issue, an increasing demand exists for the use of automatic digital radio signals for a variety of applications. Nevertheless, this work provides interesting results with the development of a novel method to recognise DVB-S2X standard-specific to the MAPSK modulation type. An APSK classifier is introduced by using an MLP-based neural network architecture and kth order spectrum features. However, better results could be accomplished by performing the training and testing on larger input datasets, so future work should include additional datasets to provide new insight. Further options for future work could use other machine learning methods, such as SVM or decision tree, in connection with the proposed features sets to create a hybrid classifier.

5.12 Conclusion

A novel algorithm for an AMC is presented using an MLP neural network architecture. In addition to sharing the advantages of a conventional neural network architecture, the combination with the MLP network structure and instantaneous signal features provide further merits.

1. Four spectrum ratios are extracted, which reduce the complexity of the learning algorithm.
2. Five training dataset inputs are utilised for the classification of the APSK schemes using the MLP neural network structure.
3. Results show that even training the signal sample at different values of the SNR compared to the test signal samples, the classifier provides good results.

Also, the simulation results show that the performance of the proposed recognition method significantly outperforms existing methods. The proposed APSK classification method is not influenced by the frequency offset and can be used with an AWGN channel and multi-path fading channel while also offering good accuracy with unknown channel parameters. Finally, to the best of our knowledge, there exists little work in the literature on APSK modulation classification using conventional MLP neural network architecture. Thus, we demonstrate the significant potential for MLP networks in APSK signal identification.

5.13 Chapter Summary

In this chapter, the focus was on the classification of DVB-S2 specified for {16,32, and 64}-APSK which are mostly used in the system of satellite broadcasting standards. In here the classification algorithm imitated with the conception of the pattern recognition method. New instantaneous features set have been extracted. The MLP feedforward neural network classifier comprises four neurons in the input layer and three in the output layer. The performance evolution of the proposed classifier has shown significance robustness and accurate at a noise channel.

CHAPTER SIX

CONCLUSIONS AND SUGGESTIONS FOR FUTURE WORKS

6.1 Introduction

In this dissertation, the study was divided into two tasks to develop an attractive algorithm for automatic modulation classification.

- The first task sought to develop an algorithm for the classification of high-order M-QAM schemes that included:

1. Enhancement of the extracted statistical features by using the properties of a logarithmic function.

2. The conventional threshold-decision classifier was developed into a hybrid-type threshold-decision classifier called a logarithmic-threshold classifier.

3. The multiple trees of the logarithmic-threshold decision classifier could provide further merits, including an extension for future modulation schemes.

4. The performance evaluation confirmed that the presented algorithm performs better than the previously presented methods.

- In the second task, a novel attractive classifier to recognise the DVB-S2X APSK modulation standard was presented. The proposed system is able to meet high-performance satellite digital broadcasting standards by accomplishing the following:

1. A novel instantaneous feature set for classification of APSK signals is presented.

2. An efficient automatic-modulation scheme for the DVB-S2X 16-, 32-, and 64-APSK modulation classifications is obtained.

3. The combination of extracted features and a neural network results in an improved ability to distinguish signals.

4. The performance evaluation demonstrates the merits of the proposed algorithm in noisy channels.

In this dissertation, a novel feature generation method is proposed, which is a crucial part of any pattern-recognition system. An overview of modulation signals is presented in Chapter 3. Modified higher-order cumulants using the characteristic of a logarithmic function were developed and have been reported in Chapter 4. Further, in Chapter 5, higher-order spectral features are used to create a classification algorithm based on neural-network properties to deal with modulation-recognition problems specified in the M-APSK DVB-S2X modulation signals standard. These novel features are combined with some conventional classification strategies to describe signal-classification problems more realistically. In this chapter, an outline of the contributions of this study is initially addressed. Subsequently, some recommendations for future directions are listed.

6.2 Discussion and Observations for Task One

In this section, some modifications are suggested to mitigate the disadvantages of the conventional high-order cumulant method for modulation-identification problems. Further, some crucial changes made to HOCs will be highlighted to facilitate their application in M-QAM recognition.

6.2.1 Creation of logarithmic cumulants' features

The goal of the first task in this work was to improve higher-order cumulants and make them suitable for the modulation recognition of M-QAM signals. Feature modification is performed using a natural logarithmic function, which normalises the selected features and improves sample distribution in a single step. The advantage of using the logarithmic function for HOC improvement is that it does not demand any information about the size of the signal samples. Moreover, the level-logarithmic cumulant is limited to a certain level and never goes above that level. By estimating the logarithmic cumulants in an AWGN channel, class-overlapping is significantly reduced and only the selected class contributes to the solution. The logarithmic cumulant is developed to generate a feature (referred to as a statistical-logarithmic feature) by creating nonlinear successions of the input cumulant. This can be defined as a particular case of magnitude reduction, which is the result of a significant number with a small-dimension value. Logarithmic cumulant features can be applied with linear or nonlinear classifiers and have proved to be excellent input features for linear classifiers.

6.3 Discussion and Observations for Task Two

This aims of the second task were to design a DVB-S2X 16-, 32-, and 64-APSK modulation-signal classifier using PR criteria and new sets of instantaneous parameters. In this task, an intelligent scheme was designed to recognise MAPSK modulation signals. A neural-network multilayer perceptron (MLP) architecture, with the maximum value of power-spectral density and a set of high-order spectral densities, could provide further advantages and excellent classification accuracy when classifying high-order APSK signals. Further, an MLP gives a reasonable recognition rate even at an SNR = 0 dB.

In total, the classification of behaviour into three DVB-S2X modulation standards, i.e., 16, 32, and 64-APSK, are presented in this task. The datasets of signals had random row data that were generated to evaluate their overall performance. This work showed that combining different sets of instantaneous features and MLPs to create APSK classifiers significantly enhanced the correct classification rate of the classifier, even at low noise ratios. It is also shown that the proposed classifier could provide a classification accuracy of up to 99.66% at an SNR of more than 1 dB. At an SNR of greater than 5 dB, the accuracy increased to 99.8%.

In addition, this classifier had a high-speed process for classification with few training samples. Furthermore, it did not show high computational complexity.

6.4 Summary and General Remarks

The feature-based method of classifying modulation signals was split into two subsystems, the feature extraction subsystem and the decision-making subsystem (classifier). In this work, the ANN classifier is a good candidate for identifying (DVB-S2/S2X/SH) standard-specified 16-, 32-, and 64-APSK modulated signals, although it has certain limitations. However, the logarithmic DT classifier is proposed as a new generation of hybrid decision-tree classifiers and, in this dissertation, logarithmic DT-classifiers are used to recognise high-order M-QAM modulated signals. The feature-extraction subsystem is selected, which is convenient for certain types of modulated signals and is appropriate for hybrid, multiple logarithmic DT classifiers. Hence, the proposed classifier modules are divided into two categories: one system for the recognition of MPSK and M-QAM signals and a smart classifier used for the recognition of 16-, 32-, and 64-APSK signals.

Importantly, the following conclusions can be drawn:

1. This thesis does not propose a final solution but instead a highly efficient algorithm to overcome the weak points of traditional AMC algorithms, which are based on statistical features and PR criteria in the first task. In the second task, higher-order spectral features are combined with MLP classifiers.

2. The M-QAM classifier module is advantageous in terms of its accuracy and computational complexity relative to those used in other studies. It had especially high efficiency when the proposed recogniser module utilised only six pre-selected features.

3. The limitations of the two proposed systems are discussed sufficiently at the end of their respective chapters.

6.5 Suggestions and Recommendations for Future Work

The following is recommended for future work.

- The classification system for MAPSK signals can be extended to cover more modulation schemes of MPSK signals, which may require more features to be extracted.

- Logarithmic-cumulants features, along with LDT and RBF classifiers, for the modulation classification, can be extended for distinguishing other modulation schemes that are not covered in this thesis, such as MASK signals, MSK signals, etc.

- Evaluating the performances of all classification systems when the digitally modulated signals are passed through various multipath, fading, and time-varying communication channels.

- Feature extraction can be performed using the optimisation approaches of soft-computing techniques, such as particle-swarm optimisation (PSO) or the genetic algorithm (GA).

- A hardware implementation for the classification system using three nodes in the field-programmable gate array (FPGA) board (Zed–Board) with an AD9361/9364 RF transceiver and omnidirectional antenna should be attempted.

- **Some substantial title related to these recommendations**
  - New Trends on Automatic Digital Modulation Identification.
  - New Trends on Automatic Digital Modulation Classification.
  - Linear and Nonlinear Classification of Quadrature Modulation Signals.
  - Classification of Quadrature Modulation Signals Using Linear and Nonlinear Classifier.

- **List of related publications**

Journal Papers with Abstracting and Indexing: “Science Citation Index Expanded”

1. **Ali, A. K., & Erçelebi, E. (2020).** Algorithm for automatic recognition of PSK and QAM with unique classifier based on features and threshold levels. ISA transactions.

2. **Ali, A. K., & Erçelebi, E. (2020).** Automatic modulation recognition of DVB-S2X standard-specific with an APSK-based neural network classifier. Measurement, 151, 107257.

3. Ali, A. K., & Erçelebi, E. (2019). An M-QAM Signal Modulation Recognition Algorithm in AWGN Channel. Scientific Programming, 2019.

4. **Ali, A. K., & Erçelebi, E. (2020).** Automatic Modulation Classification by A Novel Hybrid Neural Network Architecture. Computer Communications."under-review"

REFERENCES

[1] Dobre, O.A., Abdi, A., Bar-Ness, Y., Su, W. (2007). Survey of Automatic Modulation Classification Techniques: Classical Approaches and New Trends, *IET Communications*, **1** (**2**), 137-156.

[2] Weber, C., Peter, M., Felhauer, T. (2015). Automatic Modulation Classification Technique for Radio Monitoring, *Electronics Letters*, **51** (**10**), 794–796.

[3] Puengnim, A., Thomas, N., Tourneret, J., Vidal, J. (2010). Classification of Linear and Non-Linear Modulations Using the Baum – Welch Algorithm and MCMC Methods, *Signal Processing*, **90** (**12**), 3242–3255.

[4] ETSI (2009). *Digital Video Broadcasting (DVB); modulation systems for Broadcasting , other broadband satellite applications (DVB-S2).*

[5] Chugg, K.M., Long, C., Polydoros, A. (1996). Combined Likelihood Power Estimation and Multiple Hypothesis Modulation Classification, 1137–1141.

[6] Wei, W., Mendel, J.M. (2000). Maximum-Likelihood Classification for Digital Amplitude-Phase Modulations, **48** (**2**), 189–193.

[7] Tang, Z.B., Pattipati, K.R., Kleinman, D.L. (1991). An Algorithm for Determining the Decision Thresholds in a Distributed Detection Problem, *IEEE Transactions on Systems, Man and Cybernetics*, **21** (**1**), 231–237.

[8] Chen, Y., Czylwik, A. (2010). Automatic Modulation Classi Fi Cation Methods for Wireless OFDM Systems in TDD Mode, **58** (**9**), 2480–2485.

[9] Dennis Wong, M.L., Nandi, A.K. (2008). Semi-Blind Algorithms for Automatic Classification of Digital Modulation Schemes, *Digital Signal Processing*, **18** (**2**), 209–227.

[10] Xu, J.L., Su, W., Zhou, M. (2010). Software-Defined Radio Equipped With Rapid Modulation Recognition, *Transactons on Vechicular Technology*, **59** (**4**), 1659–1667.

[11] Fehske, A., Gaeddert, J., Reed, J.H. (2005). A new approach to signal classification using spectral correlation and neural networks. in: First IEEE Int. Symp. New Front. Dyn. Spectr. Access Networks, 2005. DySPAN 2005., pp. 144–150.

[12] Ebrahimzadeh, A., Ghazalian, R. (2011). Blind Digital Modulation Classification in Software Radio Using the Optimized Classifier and Feature Subset Selection, *Engineering Applications of Artificial Intelligence*, **24** (**1**), 50–59.

[13] Zhu, Z., Nandi, A.K. (2015). *Automatic Modulation Classification Principles Algorithms and Applications*. First edit John Wiley & Sons:United Kingdom.

[14] Abdelmutalab, A., Assaleh, K., El-Tarhuni, M. (2016). Automatic modulation classification using hierarchical polynomial classifier and stepwise regression. in: IEEE Wirel. Commun. Netw. Conf. WCNC, IEEE:Doha, Qatar.pp. 0–4

[15] An, N., Li, B., Huang, M. (2010). Modulation Classification of Higher Order MQAM Signals using Mixed-Order Moments and Fisher Criterion. in: Int. Conf. Comput. Autom. Eng., IEEE:pp. 150–153.

[16] Swami, A., Sadler, B.M. (2000). Hierarchical Digital Modulation Classification Using Cumulants, *IEEE Transactions on Communications*, **48** (**3**), 416–429.

[17] Zhu, Z., Waqar, M.A., Nandi, A.K. (2014). Genetic Algorithm Optimized Distribution Sampling Test for M-QAM Modulation Classification, *Signal Processing*, **94** (**1**), 264–277.

[18] Nandi, A.K., Azzouz, E.E. (1998). Algorithms for Automatic Modulation Recognition of Communication Signals, *IEEE Transactions on Communications*, **46** (**4**), 431–436.

[19] Zhou, L., Man, H. (2013). Wavelet cyclic feature based automatic modulation recognition using nonuniform compressive samples. in: IEEE 78th Veh. Technol. Conf. (VTC Fall), IEEE:Las Vegas, NV, USA.pp. 1–6.

[20] Muller, F.C.B.F., Cardoso, C., Klautau, A. (2011). A Front End for Discriminative Learning in Automatic Modulation Classification, *IEEE Communications Letters*, **15** (**4**), 443–445.

[21] Abdelmutalab, A., Assaleh, K., El-Tarhuni, M. (2016). Automatic Modulation Classification Based on High Order Cumulants and Hierarchical Polynomial Classifiers, *Physical Communication*, **21** (**December 2016**), 10–18.

[22] Boiteau, D., Martret, C. Le (1996). Classification of linear modulations by mean of a fourth-order cumulant. in: 8th Eur. Signal Process. Conf. (EUSIPCO 1996), IEEE:Trieste, Italy, Italy.pp. 1–4.

[23] Norouzi, S., Jamshidi, A., Zolghadrasli, A.R. (2016). Adaptive Modulation Recognition Based on the Evolutionary Algorithms, *Applied Soft Computing*, **43** 312–319.

[24] Sarieddeen, H., Dawy, Z. (2016). On the blind classification of parametric quadrature amplitude modulations. in: 3rd Int. Conf. Adv. Comput. Tools Eng. Appl. ACTEA 2016, IEEE:Beirut, Lebanon.pp. 190–194.

[25] Ali, A., Yangyu, F. (2017). Unsupervised Feature Learning and Automatic Modulation Classification Using Deep Learning Model, *Physical Communication*, **25** 75–84.

[26] Ho, K.M., Vaz, C., Daut, D.G. (2010). Automatic classification of amplitude, frequency, and phase shift keyed signals in the wavelet domain. in: IEEE Sarnoff Symp., pp. 1–6.

[27] Zhang, W. (2014). Automatic Modulation Classification Based on Statistical Features and Support Vector Machine. in: XXXIth URSI Gen. Assem. Sci. Symp. (URSI GASS), IEEE:Beijing, China.pp. 1–4.

[28] Hazza, A., Shoaib, M., Alshebeili, S.A., Fahad, A. (2013). An overview of feature-based methods for digital modulation classification. in: 1st Int. Conf. Commun. Signal Process. Their Appl., IEEE:Sharjah, United Arab Emirates.pp. 1–6.

[29] Sun, X., Su, S., Huang, Z., Zuo, Z., Guo, X., Wei, J. (2019). Blind Modulation Format Identification Using Decision Tree Twin Support Vector Machine in Optical Communication System, *Optics Communications*, **438** 67–77.

[30] Wang, C., Du, J., Chen, G., Wang, H., Sun, L., … He, Z. (2019). QAM Classification Methods by SVM Machine Learning for Improved Optical Interconnection, *Optics Communications*, **444** (**2019**), 1–8.

[31] Jordanov, I., Petrov, N., Petrozziello, A. (2016). Supervised radar signal classification. in: Int. Jt. Conf. Neural Networks, IEEE:Vancouver, BC, Canada.pp. 1464–1471.

[32] Mobasseri, B.G. (2000). Digital Modulation Classification Using Constellation Shape, *Signal Processing*, **80** (**2**), 251–277.

[33] Kharbech, S., Dayoub, I., Zwingelstein-colin, M., Simon, E.P. (2016). On Classifiers for Blind Feature-Based Automatic Modulation Classification Over Multiple-Input–Multiple-Output Channels, *IET Communications*, **10** (**7**), 1–16.

[34] Alain, G., Bengio, Y. (2014). What Regularized Auto-Encoders Learn from the Data-Generating Distribution Guillaume, *Journal of Machine Learning Research*, **15** (**1**), 3563–3593.

[35] Scherer, D., Andreas, M., Behnke, S. (2010). Evaluation of Pooling Operations in Convolutional Architectures for Object Recognition. in: Int. Conf. Artif. Neural Networks, Springer, Berlin, Heidelberg:Thessaloniki, Greece.pp. 92–101.

[36] Dulek, B., Ozdemir, O., Varshney, P.K., Su, W. (2014). A Novel Approach to Dictionary Construction for Automatic Modulation Classification, *Journal of the Franklin Institute*, **351** (**5**), 2991–3012.

[37] Sim, K., Yoon, W. (2014). Automatic Recognition Algorithm for Linearly Modulated Signals Under Non-Coherent Asynchronous Condition, *Journal of the Korea Institute of Information and Communication Engineering*, **18** (**10**), 2409–2416.

[38] Cheng, L., Liu, J. (2014). An Optimized Neural Network Classifier for Automatic Modulation Recognition, *TELKOMNIKA Indonesian Journal of Electrical Engineering*, **12** (**2**), 1343–1352.

[39] Azzouz, E.E., Nandi, A.K. (1995). Automatic Identification of Digital Modulation Types, *Signal Processing*, **47** (**1**), 55–69.

[40] Zhinan, X., Wenle, B. (2009). A novel blind recognition algorithm for modulated m-qam signals. in: WRI Int. Conf. Commun. Mob. Comput., IEEE:Yunnan, China.pp. 461–465.

[41] M.P. DeSimio ; G.E. Prescott, V (1988). Adaptive generation of decision functions for classification of digitally modulated signals. in: Proc. IEEE 1988 Natl. Aerosp. Electron. Conf., IEEE:Dayton, OH, USA, USA.pp. 1010–1014.

[42] Ho, K.C., Prokopiw, W., Chan, Y. (2000). Modulation Identification of Digital Signals by the Wavelet Transform, *IEE Proceedings-Radar, Sonar and Navigation*, **147** (**4**), 169–176.

[43] Ramakomar, V., Habibi, D., Bouzerdoum, A. (1999). Automatic recognition of digitally modulated communications signals. in: ISSPA 1999 - Proc. 5th Int. Symp. Signal Process. Its Appl., IEEE:Brisbane, Queensland, Australia, Australia.pp. 753–756.

[44] Mirarab, M.R., Sobhani, M.A. (2007). Robust Modulation Classification for PSK / QAM / ASK Using Higher-order Cumulants. in: 6th Int. Conf. Information, Commun. Signal Process., IEEE:Singapore, Singapore.pp. 1–4.

[45] Wei, W., Mendel, J.M. (1999). A Fuzzy Logic Method for Modulation Classification in Nonideal Environments, *IEEE Transactions on Fuzzy Systems*, **7** (**3**), 333–344.

[46] Pedzisz, M., Mansour, A. (2005). Automatic Modulation Recognition of MPSK Signals Using Constellation Rotation and Its 4th Order Cumulant, *Digital Signal Processing*, **15** (**3**), 295–304.

[47] Gulati, S., Bhattacharjee, R. (2006). Automatic Blind Recognition of noisy and faded digitally modulated MQAM signals. in: Annu. IEEE India Conf., IEEE:New Delhi, India.pp. 1–6.

[48] Le Guen, D., Mansour, A. (2003). Automatic recognition algorithm for digitally modulated signals based on statistical approach in time-frequency domain. in: Proc. SPC 2003.

[49] Richterova, M. (2005). Signal Modulation Recognizer Based on Method of Artificial Neural Networks, *IEICE Transactions on Communications*, **E89-B** (**8**), 2245–2248.

[50] Li, J., He, C., Chen, J., Wang, D. (2006). Automatic Digital Modulation Recognition Based on Euclidean Distance in Hyperspace, *IEICE Transactions on Communications*, **89** (**8**), 2245–2248.

[51] Li, J., Wang, J., Fan, X., Zhang, Y. (2008). Automatic digital modulation recognition using feature subset selection. in: Prog. Electromagn. Res. Symp., p. 171.

[52] Hu, Y.-Q., Juan, L., Tan, X. (2010). Digital Modulation Recognition Based on Instantaneous Information, *The Journal of China Universities of Posts and Telecommunications*, **17** (**3**), 5259–5290.

[53] Su, W., Lei, Z., Li, H., Han, T. (2010). The research of modulation recognition algorithm base on softwore radio. in: 2nd Int. Conf. Comput. Eng. Technol., Chengdu, China.pp. 308–312.

[54] Kubankova, A., Kubanek, D. (2011). Extended Method of Digital Modulation Recognition and Its Testing, *Radioengineering*, **20** (**1**), 25–30.

[55] Y. Haiying, S.X. and L.H. (2013). The Modulation Recognition Based on Decision-Making Mechanism and Neural Network Integrated Classifier, *High Technology Letters*, **19** (**2**), 132--136.

[56] Cheng, L., Liu, J. (2013). Automatic Modulation Classifier Using Artificial Neural Network Trained by PSO Algorithm, *Journal of Communications*, **8** (**5**), 322–329.

[57] Popoola, J., Olst, R. (2011). A Novel Modulation-Sensing Method, *IEEE Vehicular Technology Magazine*, **6** (**3**), 60–69.

[58] Liu, Y., Liang, G., Xu, X., Li, X. (2008). The methods of recognition for common used M-ary digital modulations. in: Int. Conf. Wirel. Commun. Netw. Mob. Comput. WiCOM 2008, IEEE:Dalian, China.pp. 1–4.

[59] Popoola, J.J., Olst, R. V. (2011). Automatic classification of combined analog and digital modulation schemes using feedforward neural network. in: Ieee Africon, IEEE:Livingstone, Zambia.pp. 13–15.

[60] Fu-qing, H., Zhi-ming, Z., Yi-tao, X.U., Guo-chun, R.E.N. (2008). Modulation Recognition of Symbol Shaped Digital Signals. in: Int. Conf. Commun. Circuits Syst., IEEE:Fujian, China.pp. 328–332.

[61] De Vito, L., Rapuano, S., Villanacci, M. (2010). Prototype of an Automatic Digital Modulation Classifier Embedded in a Real-Time Spectrum Analyzer, *IEEE Transactions on Instrumentation and Measurement*, **59** (**10**), 2639–2651.

[62] Xu, Y., Ge, L., Wang, B. (2009). Digital modulation recognition method based on tree-structured neural networks. in: Int. Conf. Commun. Softw. Networks, IEEE:Macau, China.pp. 708–712.

[63] Ghani, N., Lamontagne, R. (2002). Neural networks applied to the classification of spectral features for automatic modulation recognition. in: Proc. MILCOM '93 - IEEE Mil. Commun. Conf., IEEE:Boston, MA, USA, USA.pp. 111–115.

[64] Alharbi, H., Mobien, S., Alshebeili, S., Alturki, F. (2012). Automatic Modulation Classification of Digital Modulations in Presence of HF Noise, *EURASIP Journal on Advances in Signal Processing*, **2012** (**1**), 238.

[65] Hazza, A., Shoaib, M., Saleh, A., Fahd, A. (2011). Robustness of Digitally Modulated Signal Features against Variation in HF Noise Model, *Eurasip Journal on Wireless Communications and Networking*, **2011** (**1**), 1–12.

[66] Yin, C., Li, B., Li, Y. (2010). Modulation classification of MQAM signals from their constellation using clustering. in: 2nd Int. Conf. Commun. Softw. Networks, ICCSN 2010, IEEE:Singapore, Singapore.pp. 303–306.

[67] Kubankova, A., Kubanek, D. (2010). Algorithms of Digital Modulation Classification and Their Verification, *WSEAS Transactions on Communications*, **9** (**9**), 563–572.

[68] Geisinger, N.P. (2010). Classification of Digital Modulation Schemes Using Linear and Nonlinear Classifiers, NAVAL POSTGRADUATE SCHOOL, 2010.

[69] Kubankova, A., Kubanek, D. (2011). Digital modulation recognition based on feature, spectrum and phase analysis and its testing with disturbed signals. in: Proc. 10th WSEAS Int. Conf. Telecommun. Informatics Microelectron. Nanoelectron. Optoelectron. WSEAS Int. Conf. Signal Process., pp. 162–166.

[70] Ali, A.K., Erçelebi, E. (2019). Automatic Modulation Recognition of DVB-S2X Standard-Specific with an APSK-Based Neural Network Classifier, *Measurement*, **151** 244–257.

[71] Makhlasawy, R.M. Al (2013). Automatic Modulation Recognition in OFDM Systems Using Cepstral Analysis and Support Vector Machines, *Journal of Telecommunications System & Management*, **01** (**03**), 1–7.

[72] Schreyogg, C., Kittel, K., Kressel, U., Ag, D., Ag, D.A. (1997). Robust classification of modulation types using spectral features applied to HMM. in: MILCOM 97 MILCOM 97 Proc., IEEE:Monterey, CA, USA, USA.pp. 1377–1381.

[73] Abdelmutalab, A.E. (2015). Learning-Based Automatic Modulation Classification, American University of Sharjah, 2015.

[74] Madheswaran, M. (2009). Modulation Identification Algorithm for Adaptive Demodulator in Software Defined Radios Using Wavelet Transform, *International Journal of Signal Processing*, **5** (**1**), 74–81.

[75] Dan, W., Xuemai, G., Qing, G. (2005). A new scheme of automatic modulation classification using wavelet and WSVM. in: IEE Mobil. Conf. 2005. Second Int. Conf. Mob. Technol. Appl. Syst., IEEE:Guangzhou, China.pp. 132–132.

[76] Meng, L.L., Si, X.J. (2008). An improved algorithm of modulation classification for digital communication signals based on wavelet transform. in: Int. Conf. Wavelet Anal. Pattern Recognit., IEEE:Beijing, China.pp. 1226–1231.

[77] Hong, L., Ho, K.C. (1999). Identification of digital modulation types using the wavelet transform. in: Mil. Commun. Conf., IEEE:Atlantic City, NJ, USA, USA.pp. 427–431.

[78] SALIVENDRA SUBRAHMANYA SASTRY1, D.M.C.S. (2016). Automatic Digital Modulation Classification Signals Using Statistical Parameters with Neural Networks and Fuzzy Logic, *IJSETR*, **5** (**49**), 10029–10033.

[79] Park, C.-S., Choi, J.-H., Nah, S.-P., Jang, W., Kim, D.Y. (2008). Automatic Modulation Recognition of Digital Signals using Wavelet Features and SVM. in: 10th Int. Conf. Adv. Commun. Technol., IEEE:Gangwon-Do, South Korea.pp. 387–390.

[80] Valipour, M.H., Homayounpour, M.M., Mehralian, M.A. (2012). Automatic digital modulation recognition in presence of noise using SVM and PSO. in: 6th Int. Symp. Telecommun. IST 2012, IEEE:Tehran, Iran.pp. 378–382.

[81] Keshk, M.E.M., Elrabie, E., El-samie, F.E.A., El-naby, M.A. (2013). Blind Modulation Recognition in Wireless MC-CDMA Systems Using a Support Vector Machine Classifier, *Wireless Engineering and Technology*, **2013** (**3**), 145–153.

[82] Keshk, M.E., Asami, K. (2017). FPGA-based Automatic Modulation Recognition System for Small Satellite Conference on Small Satellites. in: SSC17-XII-06, pp. 1–8.

[83] Prakasam, P., Madheswaran, M. (2008). Digital Modulation Identification Model Using Wavelet Transform and Statistical Parameters, *Journal of Computer Systems, Networks, and Communications*, **2008.**

[84] Sadkhan, S.B. (2010). A proposed digital modulated signal identification based on pattern recognition. in: Syst. Signals Devices (SSD), 7th Int. Multi-Conference, Amman, Jordan.pp. 1–6.

[85] Faek, F.K. (2010). Digital Modulation Classification Using Wavelet Transform and Artificial Neural Network, *Journal of ZankoySulaimani*, **13** (**1**), 59–70.

[86] Maliatsos, K., Vassaki, S., Constantinou, P. (2007). Interclass and Intraclass Modulation Recognition Using the Wavelet Transform, *IEEE International Symposium on Personal, Indoor and Mobile Radio Communications, PIMRC*, (**3**).

[87] Ma, Y.L. and C. (2012). Automatic Modulation Recognition for Digital Communication Signals, **10** (**2**), 110–114.

[88] Hassanpour, S., Pezeshk, A.M., Behnia, F. (2016). Automatic Digital Modulation Recognition Based on Novel Features and Support Vector Machine, *2016 12th International Conference on Signal-Image Technology & Internet-Based Systems (SITIS)*, 172–177.

[89] Hassan, K., Dayoub, I., Hamouda, W., & Berbineau, M. (2009). Automatic modulation recognition using wavelet transform and neural network. in: 9th Int. Conf. Intell. Transp. Syst. Telecommun., Lille, France.pp. 234–238.

[90] Ali, A.., Ergun, E. (2019). An M-QAM Signal Modulation Recognition Algorithm in AWGN-Channel, *Scientific Programming*, 17.

[91] Xiong, X., Feng, J., Jiang, L. (2015). Automatic Digital Modulation Classification for ORS Satellite Relay Communication, *2015 International Conference on Wireless Communications and Signal Processing, WCSP 2015*,

[92] Wang, L., Guo, S., Jia, C. (2017). Recognition of Digital Modulation Signals Based on Wavelet Amplitude Difference, *Proceedings of the IEEE International Conference on Software Engineering and Service Sciences, ICSESS*, 627–630.

[93] Chang, D.-C., Shih, P.-K. (2015). Cumulants-Based Modulation Classification Technique in Multipath Fading Channels, *IET Communications*, **9** (**6**), 828–835.

[94] Bouchou, M., Wang, H., Lakhdari, M.E.H. (2018). Automatic Digital Modulation Recognition Based on Stacked Sparse Autoencoder, *International Conference on Communication Technology Proceedings, ICCT*, **2017-Octob** 28–32.

[95] Li, P., Wang, F., Wang, Z. (2007). Algorithm for Modulation Recognition Based on High-Order Cumulants and Subspace Decomposition, *International Conference on Signal Processing Proceedings, ICSP*, **3** (**2**), 0–3.

[96] Li, P.H., Zhang, H.X., Wang, X.Y., Xu, N., Xu, Y.Y. (2012). Modulation Recognition of Communication Signals Based on High Order Cumulants and Support Vector Machine, *Journal of China Universities of Posts and Telecommunications*, **19** (**SUPPL. 1**), 61–65.

[97] Li, S.P., Chen, F.C., Wang, L. (2012). Modulation Recognition Algorithm of Digital Signal Based on Support Vector Machine, *Proceedings of the 24th Chinese Control and Decision Conference, CCDC 2012*, 3326–3330.

[98] Zhou, S., Wu, Z., Yin, Z., Yang, Z. (2018). Noise-Robust Feature Combination Method for Modulation Classification Under Fading Channels, *2018 IEEE 88th Vehicular Technology Conference (VTC-Fall)*, 1–5.

[99] Ali, A., Yangyu, F., Liu, S. (2017). Automatic Modulation Classification of Digital Modulation Signals with Stacked Autoencoders, *Digital Signal Processing: A Review Journal*, **71** 108–116.

[100] ZHOU, X., WU, Y., YANG, B. (2010). Signal Classification Method Based on Support Vector Machine and High-Order Cumulants, *Wireless Sensor Network*, **02** (**01**), 48–52.

[101] Xu, B., Wen, X., Wang, X. (2019). Research on Modulation Recognition Technology Based on Machine Learning, *International Journal of Computer Applications Technology and Research*, **8** (**4**), 102–106.

[102] Ji, B., Wang, Y., Gao, Y. (2019). An Algorithm to Recognize Digital Modulated Signals Based on High Order Cumulants. in: Signal Process. Syst., Springer Singapore:pp. 1967–1974.

[103] Hashim, I.A., Abdul Sadah, J.W., Saeed, T.R., Ali, J.K. (2015). Recognition of QAM Signals with Low SNR Using a Combined Threshold Algorithm, *IETE Journal of Research*, **61** (**1**), 65–71.

[104] Zhe Xing1, Y.G. (2018). Method to Reduce the Signal-to-Noise Ratio Required for Modulation Recognition Based on Logarithmic Properties, *IET Communications*, **12** (**11**), 1360–1366.

[105] Ahmadi, N. (2011). Modulation Recognition Based on Constellation Shape Using TTSAS Algorithm and Template Matching, *Journal of Pattern Recognition Research*, **1** (**1**), 43–55.

[106] Chou, Z., Jiang, W., Xiang, C., Li, M. (2013). Modulation Recognition Based on Constellation Diagram for M-QAM Signals, *Proceedings Of11th International Conference on Electronic Measurement and Instruments, ICEMI 2013*, **1** 70–74.

[107] Daponte, P., Grimaldi, D., Molinaro, A., Sergeyev, Y.D. (1996). Fast Detection of the First Zero-Crossing in a Measurement Signal Set, *Measurement*, **19** (**1**), 29–39.

[108] Hsue, S.-Z., Soliman, S.S. (1990). Automatic modulation classification using zero crossing. in: IEE Proc. F (Radar Signal Process., pp. 459–464.

[109] De Vito, L., Rapuano, S. (2009). Validating a Method for Classifying Digitally Modulated Signals, *Measurement: Journal of the International Measurement Confederation*, **42** (**3**), 427–435.

[110] Fangjuan, X., Chisheng, L., Guojin, W. (2008). An efficient and simple method of MPSK modulation classification. in: 2008 Int. Conf. Wirel. Commun. Netw. Mob. Comput. WiCOM 2008, pp. 1–3.

[111] Guan, H.B., Ye, C.Z., Li, X.Y. (2004). Modulation Classification Based on Spectrogram, *Proceedings of International Conference on Machine Learning and Cybernetics*, **6** (**August**), 3551–3556.

[112] Ma, J., Qiu, T. (2018). Automatic Modulation Classification Using Cyclic Correntropy Spectrum in Impulsive Noise, *Communications Letters*, **2337** 1–4.

[113] Fontes, A.I.R., De M. Martins, A., Silveira, L.F.Q., Principe, J.C. (2015). Performance Evaluation of the Correntropy Coefficient in Automatic Modulation Classification, *Expert Systems with Applications*, **42** (**1**), 1–8.

[114] Jiang, Y., Zhang, Z.Y., Qiu, P.L. (2004). Modulation Classification of Communication Signals, *Proceedings - IEEE Military Communications Conference MILCOM*, **3** 1470–1476.

[115] Chirov, D.S., Vynogradov, A.N., Vorobyova, E.O. (2018). Application of the Decision Trees to Recognize the Types of Digital Modulation of Radio Signals in Cognitive Systems of HF Communication, *Systems of Signal Synchronization, Generating and Processing in Telecommunications (SYNCHROINFO)*, 1–6.

[116] Prakasam, P., Madheswaran, M. (2008). Digital Modulation Identification Model Using Wavelet Transform and Statistical Parameters, *Journal of Computer Systems, Networks, and Communications*, **2008** 1–8.

[117] Wang, H., Zhang, B., Wu, J., Han, Y., Wu, X., Jia, R. (2010). A Research on Automatic Modulation Recognition with the Combination of the Rough Sets and Neural Network. in: A Res. Autom. Modul. Recognit. with Comb. Rough Sets Neural Netw., pp. 2–5.

[118] Hamouda, W., Hassan, K., Dayoub, I., Berbineau, M. (2010). Automatic Modulation Recognition Using Wavelet Transform and Neural Networks in Wireless Systems, *Eurasip Journal on Advances in Signal Processing*, **2010.**

[119] Gang, H., Jiandong, L., Donghua, L. (2004). Study of Modulation Recognition Based on HOCs and SVM, *Vehicular Technology Conference, 2004. VTC 2004-Spring. 2004 IEEE 59th*, **2** ((**IEEE Cat. No. 04CH37514**)), 898–902.

[120] Aslam, M.W., Member, S., Zhu, Z., Member, S. (2012). Automatic Modulation Classification Using Combination of Genetic Programming and KNN, **11** (**8**), 2742–2750.

[121] Avci, E. (2009). Selecting of the Optimal Feature Subset and Kernel Parameters in Digital Modulation Classification by Using Hybrid Genetic Algorithm-Support Vector Machines: HGASVM, *Expert Systems with Applications*, **36** (**2 PART 1**), 1391–1402.

[122] Zhilu Wu, Xuexia Wang, Z.G. and G.R. (2005). Automatic digital modulation recognition based on support vector machines. in: 2005 Int. Conf. Neural Networks Brain, IEEE:Beijing, China.pp. 1025–1028.

[123] Mustafa, H., Doroslovacki, M. (2004). Digital Modulation Recognition Using Support Vector Machine Classifier, *Conference Record of the Thirty-Eighth Asilomar Conference on Signals, Systems and Computers, 2004.*, **2** 2238–2242.

[124] Abrahamzadeh, A., Seyedin, S.A., Dehghan, M. (2007). Digital-Signal-Type Identification Using an Efficient Identifier, *Eurasip Journal on Advances in Signal Processing*, **2007.**

[125] Zhang, G.P. (2000). Neural Networks for Classification: A Survey, *Transactions on System*, **30** (**4**), 451–462.

[126] Azzouz, E.E., Nandi, A.K. (1997). Automatic Modulation Recognition—I, *Journal of the Franklin Institute*, **334** (**2**), 275–305.

[127] Wong, M.L.D., Nandi, A.K. (2004). Automatic Digital Modulation Recognition Using Artificial Neural Network and Genetic Algorithm, *Signal Processing*, **84** (**2**), 351–365.

[128] Avci, E., Avci, D. (2008). The Performance Comparison of Discrete Wavelet Neural Network and Discrete Wavelet Adaptive Network Based Fuzzy Inference System for Digital Modulation Recognition, *Expert Systems with Applications*, **35** (**1–2**), 90–101.

[129] E. E. Azzouz and A. K. Nandi (1995). *Modulation, Automatic of Recognition Communication Signals*. Springer Science & Business Media:New York.

[130] Chou, Z., Jiang, W., Xiang, C., Li, M. (2013). Modulation recognition based on constellation diagram for M-QAM signals. in: Proc. 11th Int. Conf. Electron. Meas. Instruments, ICEMI 2013, pp. 70–74.

[131] Park, C.S., Jang, W., Nah, S.P., Kim, D.Y. (2007). Automatic Modulation Recognition Using Support Vector Machine in Software Radio Applications, *International Conference on Advanced Communication Technology, ICACT*, **1** 9–12.

[132] Boutte, David, and B.S. (2009). A Hybrid ICA-SVM Approach to Continuous Phase Modulation Recognition, *Signal Processing Letters*, **16** (**5**), 402–405.

[133] Shermeh, A.E., Azimi, H. (2010). Blind Signal-Type Classification Using a Novel Robust Feature Subset Selection Method and Neural Network Classifier, *Annals of Telecommunications - Annales Des Télécommunications*, **65** (**9–10**), 625–633.

[134] Dobre, O.A., Abdi, A., Bar-Ness, Y., Su, W. (2010). Cyclostationarity-Based Modulation Classification of Linear Digital Modulations in Flat Fading Channels, *Wireless Personal Communications*, **54** (**4**), 699–717.

[135] Hsue, S., Soliman, S. (1990). Automatic Modulation Classification Using Zero Crossing, *IEE Proceedings F (Radar and Signal Processing)*, **1** (**i**), 459–464.

[136] Yu, Z., Shi, Y.Q., Su, W. (2003). M-Ary Frequency Shift Keying Signal Classification Based-on Discrete Fourier Transform, *Proceedings - IEEE Military Communications Conference MILCOM*, **2** 1167–1172.

[137] Dobre, O.A., Öner, M., Rajan, S., Inkol, R. (2012). Cyclostationarity-Based Robust Algorithms for QAM Signal Identification, *IEEE Communications Letters*, **16** (**1**), 12–15.

[138] Lathi, B.P., Ding, Z. (2010). *MODERN DIGITAL AND ANALOG COMMUNICATION SYSTEMS*. Fourth Edi OXFORD UNIVERSITY PRESS:New York.

[139] Jajoo, G., Kumar, Y., Yadav, S.K., Adhikari, B., Kumar, A. (2017). Blind Signal Modulation Recognition through Clustering Analysis of Constellation Signature, *Expert Systems with Applications*, **90** 13–22.

[140] Haykin, S., Moher, M. (1989). *Analog & Digital Communications*.

[141] Forouzan, B.A. (2007). *Data Communications and Networking*. 4thEdition ed. MeGraw-Hill:New York.

[142] Solso, R.L., MacLin, O.H., MacLin, M.K. (2014). *Advanced Electronic Communications Systems*. Sixth Edit Pearson Education Limited:London.

[143] Goleman, D., Boyatzis, R., Mckee, A. (2007). *Digital Satellite Communications*. New York.

[144] Zaishuang Liu, Qiuliang Xie, Kewu Peng, and Z.Y. (2011). APSK Constellation with Gray Mapping, **15** (**12**), 1271–1273.

[145] Sklar, B. (1999). *Rayleigh Fading Channels*. CRC Press LLC:Boca Raton, Florida.

[146] Parhi, D.R., Kumar, B. (1997). Rayleigh Fading Channels in Mobile Digital Communication Systems PartI, **21** (**3**), 295–316.

[147] Bertoni, H.L. (2000). *Radio Propagation for Modern Wireless Systems*. 1st Editio Prentice Hall:New York.

[148] HAYKIN, S., MOHER, M. (2005). *Modern Wireless communications*. Pearson In Pearson Prentice Hall:United States of America.

[149] Han, J., Kamber, M., Pei, J. (2012). *Classification: Basic Concepts 8*. Third Edit Elsevier, Morgan Kaufmann:United States of America.

[150] Azarbad, M., Hakimi, S., Ebrahimzadeh, A. (2012). Automatic Recognition of Digital Communication Signal, *International Journal of Energy, Information and Communications*, **3** (**4**), 21–34.

[151] Grus, J. (2015). *Data Science from Scratch*. First Edit O'Reilly Media:United States of America. Published.

[152] Songnan Xi and Hsiao-Chun Wu (2006). Robust automatic modulation classification using cumulant features in the presence of fading channels. in: IEEE Wirel. Commun. Netw. Conf. 2006. WCNC 2006., pp. 2094–2099

[153] Dobre, O.A., Bar-Ness, Y., Wei Su (2003). Higher-Order Cyclic Cumulants for High Order Modulation Classification, *IEEE Military Communications Conference, 2003. MILCOM 2003.*, **1** (**C**), 112–117.

[154] Ahmadi, N., Berangi, R. (2008). Modulation Classification of QAM and PSK from Their Constellation Using Genetic Algorithm and Hierarchical Clustering, *2008 3rd International Conference on Information and Communication Technologies: From Theory to Applications, ICTTA*, (**11670**),

[155] Alsharif, M.H., Nordin, R. (2017). Evolution towards Fifth Generation (5G) Wireless Networks: Current Trends and Challenges in the Deployment of Millimetre Wave, Massive MIMO, and Small Cells, *Telecommunication Systems*, **64** (**4**), 617–637.

[156] Ahmadi, N. (2010). Using Fuzzy Clustering and TTSAS Algorithm for Modulation Classification Based on Constellation Diagram, *Engineering Applications of Artificial Intelligence*, **23** (**3**), 357–370.

[157] Zhou, L., Sun, Z., Wang, W. (2017). Learning to Short-Time Fourier Transform in Spectrum Sensing, *Physical Communication*, **25** 420–425.

[158] Yabo Yuan, Peng Zhao,BoWang, B. (2016). Hybrid Maximum Likelihood Modulation Classification for Continuous Phase Modulations, *IEEE Communications Letters*, **20** (**3**), 450–453.

[159] Molisch, A.F., Balakrishnan, K., Cassioli, D., Chong, C., Emami, S., … Siwiak, K. (2005). IEEE 802 .15 .4a Channel Model - Final Report, *Environments*, 1–40.

[160] Mashor, M.Y. (1999). Some Properties of RBF Network with Applications to System Identification, **7** (**1**), 1–37.

[161] Ghauri, S.A., Qureshi, I.M., Aziz, A., Cheema, T.A. (2014). Classification of Digital Modulated Signals Using Linear Discriminant Analysis on Faded Channel, *World Applied Sciences Journal*, **29** (**10**), 1220–1227.

[162] Lin, Y., Ibob, C.J. (1997). Classification of Quadrature Amplitude Modulated (QAM) Signals via Sequential Probability Ratio Test (SPRT), *Processing*, **1684** (**97**).

[163] Su, W. (2013). Feature Space Analysis of Modulation Classification Using Very High-Order Statistics, *IEEE Communications Letters*, **17** (**9**), 1688–1691.

[164] Bagga, J., Tripathi, N. (2013). Automatic Modulation Classification Using Statistical Features in Fading Environment, *International Journal of Advanced Research in Electrical, Electronics and Instrumentation Engineering*, **2** (**8**), 3701–3709.

[165] Ciblat, P., Ghogho, M. (2006). Blind NLLS Carrier Frequency-Offset Estimation for QAM, PSK, and PAM Modulations: Performance at Low SNR, **54** (**10**), 1725–1730.

[166] Mobasseri, B.G. (1999). Constellation Shape as a Robust Signature for Digital Modulation Recognition, *Military Communications Conference Proceedings, 1999. MILCOM 1999. IEEE*, **00** (**c**), 442–446.

[167] Yin, C., Li, B., Li, Y., Lan, B. (2010). Modulation Classification of MQAM Signals Based on Density Spectrum of the Constellations, *Proceedings of the 2010 2nd International Conference on Future Computer and Communication, ICFCC 2010*, **3** 57–61.

[168] Tanc, Y.H., Akan, A. (2013). Modulation Identification of Digital M-Ary QAM Signals by Hilbert-Huang Transform, *Proceedings of the IEEE International Conference on Electronics, Circuits, and Systems*, 678–681.

[169] Hsieh, W.W., Sci-, O. (1999). *Neural Networks and Learning Machines*. 3rd ed. Pearson Prentice Hall:Ontario,Canada.

[170] Riedmiller, M. (1994). Advanced Supervised Learning in Multi-Layer Perceptrons — From Backpropagation to Adaptive Learning Algorithms, *Computer Standards & Interfaces 16*, **16**

[171] Deng, Y., Wang, Z. (2014). Modulation Recognition of MAPSK Signals Using Template Matching, **50** (**25**), 1986–1988.

CURRICULUM VITAE

Name / Surname	Ahmed Khalid Ali
Nationality	Iraqi
Birth place / Date	28.11.1989
Mariel status	Single
E-Mails	engineer28ahmed@gmail.com
ResearchGATE scientific network	https://www.researchgate.net/profile/Ahmed_Ali118
Google	https://scholar.google.com/citations?user=--RX14MAAAAJ&hl=ar&authuser=1
General information	Received B.Sc. Degree in Electrical Engineering from faculty of engineering at AL Mustansiriyah University, Baghdad, Iraq 2012, and a Master degree 2016 in electrical and electronics engineering from the University of Gaziantep. He is currently a PhD candidate. His research interests digital signal processing, pattern recognition. Moreover, power electronics, modelling and simulation, renewable energy resources. He has good experience in information technology (IT) and network security.
Disciplines	Control Systems Engineering, Electronic Engineering
Skills and expertise	Finite Element Method, FEM Simulation, MATLAB Simulation, Information and Communication Technology Pattern Recognition, Renewable Energy Technologies, Signal Processing, Power Electronics, Advanced Machine Learning, Automation & Robotics.
Membership	Iraqi Engineers Association. Federation of Arab Engineers.
Languages	Arabic English and Good comments in French

Reviewer for Journal

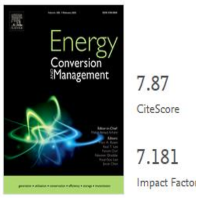

https://www.journals.elsevier.com/energy-conversion-and-management

Energy Conversion and Management.

PUBLICATIONS

1. **Ali, A. K.,** & Erçelebi, E. (2020). Automatic modulation recognition of DVB-S2X standard-specific with an APSK-based neural network classifier. *Measurement*, ***151***, 107257.

2. **Ali, A. K.,** & Erçelebi, E. (2020). Algorithm for Automatic Recognition of PSK and QAM with Unique Classifier Based on Features and Threshold Levels. ISA transactions, ***accepted for published***.

3. **Ali, A. K**., & Erçelebi, E. (2019). An M-QAM Signal Modulation Recognition Algorithm in AWGN Channel. *Scientific Programming*, *2019*.

4. **Ali, A. K.,** & Erçelebi, E.(20xx). Automatic Modulation Classification using Different Neural Network and PCA Combinations. Expert Systems with Applications, "**Under review** ".

5. **Ahmed K. Ali** and Ergun Erçelebi, "Simulation and Study of SVPWM Inverter for (VFD) Applications," International Journal of Electronics and Electrical Engineering (ijeee), Vol. **5**, No. **2**, pp. 158-170, April 2017. doi: 10.18178/ijeee.5.2.158-170

6. **Ali, A. K.,** and Erçelebi, E. (2018). A Low-cost modelling of the variable frequency drive optimum in industrial applications. Journal of Energy Systems, **2**(**1**), 2842.